Estimating wet season-lowland rice production using remote sensing techniques: a case study in Lao PDR

By

Vilon Viphongxay

Thesis
Submitted to Flinders University
for partial fulfilment for the degree of

Master of Geospatial Information Science

College of Science and Engineering
19 October 2020

TABLE OF CONTENTS

LIST OF ABBREVIATIONS

AEZ	Agro-Ecological Zone
AVHRR	Advanced Very High-Resolution Radiometer
ALOS	Advanced Land Observing Satellite
AOI	Areas of Interest
CCI-LC	Climate Change Initiative- Land Cover
CTIF	Conditional Temporal Interpolation Filtering
DEM	Digital Elevation Model
EDM	Empirical Decomposition Model
EMR	Electromagnetic Radiation
EVI	Enhance Vegetation Index
FAO	Food Agriculture Organization
Fmask	Function of Mask
GDR	Ground Range Detection
GoL	Government of Lao PDR
GPS	Global Positioning System
IRRI	International Rice Research Institute
ISODATA	Iterative Self-Organizing Data Analysis Technique
LAI	Leaf Area Index
Lao PDR	Lao's People Democratic Republic
LPDAAC	Land Processes Distributed Active Archive Centre
LSB	Lao Statistics Bureau
LSWI	Land Surface Water Index
MAE	Mean Absolute Error
MODIS	Moderate Resolution Imaging Spectroradiometer
NASA	National Aeronautics and Space Administration
NDVI	Normalised Difference Vegetation Index
NIR	Near Infrared
OBIA	Object-based image analysis
OLI	Operational Land Imager
OLS	Ordinary Least Square
PALSAR	Phased Array-type L-band SAR
RADAR	Radio Detecting and Ranging
RF	Random Forest
RMSE	Root Mean Square Error
SAR	Synthetic Aperture RADAR
SLC	Single Look Complex
SRTM	Shuttle RADAR Topography Mission
SVM	Support Vector Machine
SWIR	Short Wave Infrared
TOA	Top of Atmosphere
UN	United Nations
UXO	Unexploded Ordnance
VH	Vertically polarised transmit and horizontally polarised receive
VV	Vertically polarised transmit and vertically polarised receive
WFP	World Food Programme

ABSTRACT

Rice is an important crop that feeds more than half of the global population. Rice demand remains high, however, population growth, climate change, limited suitable land areas, and a lack of water challenge its availability. Access to fast and accurate information about rice production at lower spatial units, such as the district-level and lower, is crucial. This study explores the usefulness of freely available satellite images for mapping the extent of rice which, in turn, can be used to forecast rice production at lower spatial units.

This study uses satellite imagery from Moderate Resolution Imaging Spectroradiometer (MODIS). Specifically, MOD09A1, the MODIS 8-day composite product that developed by selecting the least cloud contaminated data from the daily images, was used. All available imagery was downloaded from the Land Processes Distributed Active Archive Centre (LPDAAC) within the 2016 growing season, totalling 138 tiles (3 tiles by 46 time-slices). Additionally, Landsat 8 level-1 data, with a higher, 30-metre spatial resolution was used to spot-check the trend of the NDVI and LSWI in some key Agro-Ecological Zones.

In pre-data processing step, the MODIS data was calibrated with the scaling factor provided with the manual and followed by the additional cloud removal. Atmospheric corrections and the exclusion of cloud cover and its shadow layers were carried out with the Landsat 8 level-1 data. The algorithm uses the NDVI, EVI, and LSWI to detect moisture levels in soil and vegetation at the time when rice crops were temporarily flooded. After that, all the irrelevant areas such as permanent water, forest, and steeply sloping layers were excluded. Then a phenology analysis of potential rice crops was carried out using the EVI to estimate the potential number of rice pixels. Finally, the study estimates district-level rice production using Simple Linear Regression while the Dasymetric mapping technique was used to interpolate rice yield at the district level.

The study found that there were both over- and underestimations of the extent of rice crop areas in different locations within the study area when compared with the official figures. Underestimated rice crop area data was found in the Northern and Eastern upland provinces and this signals a limitation of the method. However, those provinces that have a relatively large scale of rice cultivation have an error of less than 10%, and these are located in low and flat land areas. Overall, the RMSE is 15,000 Ha, and the R^2 value is 0.95.

Keywords: **Lowland rice, MODIS, NDVI, EVI, LSWI, Dasymetric, Lao PDR**

DECLARATION

I certify that this thesis does not incorporate without acknowledgment any material previously submitted for a degree or diploma in any university; and that to the best of my knowledge and belief it does not contain any material previously published or written by another person except where due reference is made in the text.

Signed.....

Date.....19 Oct 2020.....

ACKNOWLEDGEMENTS

I would like to express my sincere thanks to the Australian Government with regard to its Australia Award Scholarship (AAS) program for supporting my education in both Australia and the Lao PDR. This support has helped me advance my education in Geospatial Information Science. I would also like to thank all the concerned agencies such as International Student Services (ISS) at Flinders University, the Lao Australia Institute (LAI), Vientiane College (VC), and the Government of Lao PDR for facilitating all the necessary processes, for instance, the academic preparation, travel, and the opportunity to live in South Australia throughout the duration of my education.

My sincere thank goes to Flinders University, especially the College of Science and Engineering, for admitting me into the Master of Geospatial Information Science program. On this note, my deep gratitude goes to all the staff and teachers, but I would also like to single out a specific few herein. Firstly, David Bruce, Associate Professor and Lecturer in Remote Sensing, for the overall guidance he provided me with this thesis topic and also while teaching a number of the Remote Sensing topics. Secondly, Dr Tessa Lane, a Lecturer in GIS who taught and supervised my thesis project through to the end. Without their kind support, I would not be able to complete this thesis and my Master's degree.

Also, I would like to thank my parents, relatives, and family for their support, understanding, help, and motivation which they provided throughout my two years of living in South Australia. Without their support and encouragement, I would not be able to complete my studies.

LIST OF FIGURES

LIST OF TABLES

LIST OF EQUATIONS

CHAPTER ONE: INTRODUCTION

1.1 Problem statement and rationale

Rice is an essential crop for billions of people around the world. In Lao PDR, rice is not only a staple food crop for most of the country's citizens, but it is an essential means to sustain the livelihoods of the poor (Armstrong & Ramasawmy 2012; Eliste & Santos 2012; Manivong, Cramb & Newby 2014; Mohanty, Wailes & Chavez 2010). Because of the significance of rice as a food staple and its current status for food security, access to on-time and accurate information about rice production, especially at the district level, is crucial. Currently, the Lao Government relies on two monitoring systems for rice production data, with these being the Lao Census of Agriculture and the reporting system. While the agricultural census provides accurate data down to the lowest spatial units like a village, the intensive cost for this method of data collection and its prolonged intervals of 10 years between census dates are demotivating factors for investment into this method of data collection (Pozhamkandath, Nampanya & Ishihara 2014; Sun, H-s et al. 2009). Furthermore, results from the census and other household surveys are not georeferenced, which limits spatial analysis (Dong & Xiao 2016). Similar to the census method of data collection, the reporting system that authorities from each administration unit use to manually compile information and report on figures also provides detailed data down to the district level. Although the reporting system is inexpensive, it lacks any consensus on the methodology for the reporting of data, suffers delays in the reporting of data, and the reliability of the data being accurate is low (GoL & FAO 2013). It is essential for information about rice production to be current and timely, not only for agricultural and environmental management but also for disaster management (Bouapao et al. 2016; Peng et al. 2011; Saysompheng 2018).

In recent decades, there have been many success stories with the use of remote-sensing technology, especially in mapping the extent of rice crops in a study area. Active remote-sensing provides the promising capacity to collect aerial imagery regardless of weather conditions (Shao et al. 2001; Torbick et al. 2017; Zhang, Y et al. 2009; Zhang, Y et al. 2020). These sensors are suitable to map the extent of rice farming because rice crops are grown in monsoonal areas where cloud cover often obscures the observation of rice crops using optical imagery (Clauss et al. 2018; Nelson et al. 2014; Nguyen, DB, Gruber & Wagner 2016). Specifically, the recently launched Sentinel-1 satellite provides free access to Synthetic Aperture RADAR (SAR) imagery with a high revisit rate of 12 days, while also resolving some previous RADAR issues (Tian et al. 2018). However, constraints associated with RADAR imagery still exist. For instance, brightness can cause a speckled effect, thereby degrading the quality of the data received (Mosleh, MK, Hassan, QK & Chowdhury, EH 2015). Besides this, the available C-band from Sentinel-1A/B SAR images appears to present limitations when detecting inundated water hidden under the cover of the rice

canopy (Liu et al. 2019; Slagter et al. 2020; Torbick et al. 2017). Also, access to the long wavelength of RADAR imagery is difficult because of the cost involved (Zhang, Y et al. 2009).

Passive remote-sensing depends on electromagnetic radiation (EMR) from the sun as the primary source of energy to record information. The onboard sensor records the EMR emitted and reflected from objects on the Earth's surface to produce aerial imagery (Khorram et al. 2012; Khorram et al. 2016). This type of sensor is unable to collect information at night, and also when cloud cover blocks the objects being observed (Chen, C et al. 2011; Mosleh, M, Hassan, Q & Chowdhury, E 2015). A range of different passive sensors produce satellite images with different spatial, spectral, and temporal resolutions, but most of them encounter cloud contamination issues. However, some sensors can be used to resolve and address such issues in different ways. The MODIS 8-day composite image provides a trade-off between spatial resolution and the obscurity caused by cloud cover. This data has been experimented with in mapping the extent of rice production in the region and at the country-level with favourable accuracy rates (Sun, H-s et al. 2009; Vermote, EF, Roger & Ray 2015; Xiao et al. 2006; Xiao et al. 2005). Specifically, access to this imagery at no monetary cost is essential for the extensive monitoring of rice crops. Therefore, this remote sensing technique is of interest for further experimentation with country-specific data.

1.2 Study aim and objectives

This study aims to explore the capacity of passive remote-sensing techniques and the freely available satellite imagery for the mapping of lowland, rainfed rice fields. The expected outcome of this research aims to find a solution to address the information gap mentioned above.

Specifically, the study's objectives are to:

- Estimate the extent of wet season, lowland, rainfed rice farming for the entire country of Lao PDR,
- Interpolate the zonal yield statistics of smaller spatial units than the provincial level, so the data retrieved better supports the program target and problem monitoring,
- Provide recommendations to the concerned authorities on the application of remote sensing and GIS techniques to fill the information gap in the extent of rice farming and production.

1.3 Research question

Can optical satellite low-cost remote-sensing provide reliable estimates for the extent of rice farming and yield on multiple scales for Lao PDR?

1.4 Study area

This study apportions the whole country of the Lao People's Democratic Republic (Lao PDR) as the targeted area for the study. Figure 1 illustrates the true colour (Red, Green, and Blue bands) of the map of the study area. Lao PDR is situated in the middle of the Indochinese Peninsula between the latitudes of 13˚45ˈN and 22˚ 41ˈN, the longitudes of 100˚09ˈE and 107˚45ˈE, and with no access to the sea (Kanemaru, Muhammad & Hirota 2014). Lao PDR shares its border with five countries – China, Vietnam, Cambodia, Thailand, and Myanmar – and has a total land area of approximately 238,600 square kilometres (Kittikhoun 2009). Along its western border, the Mekong River flows down the length of the country and becomes a significant supply source for water to various crops, including rice. Also, the geographic characteristics of the country from the north to the south range from flat land to mountainous and this is favourable to different types of crops, including different rice crops (Hurni, Hett, Heinimann, et al. 2013).

Figure 1. Map of the study area

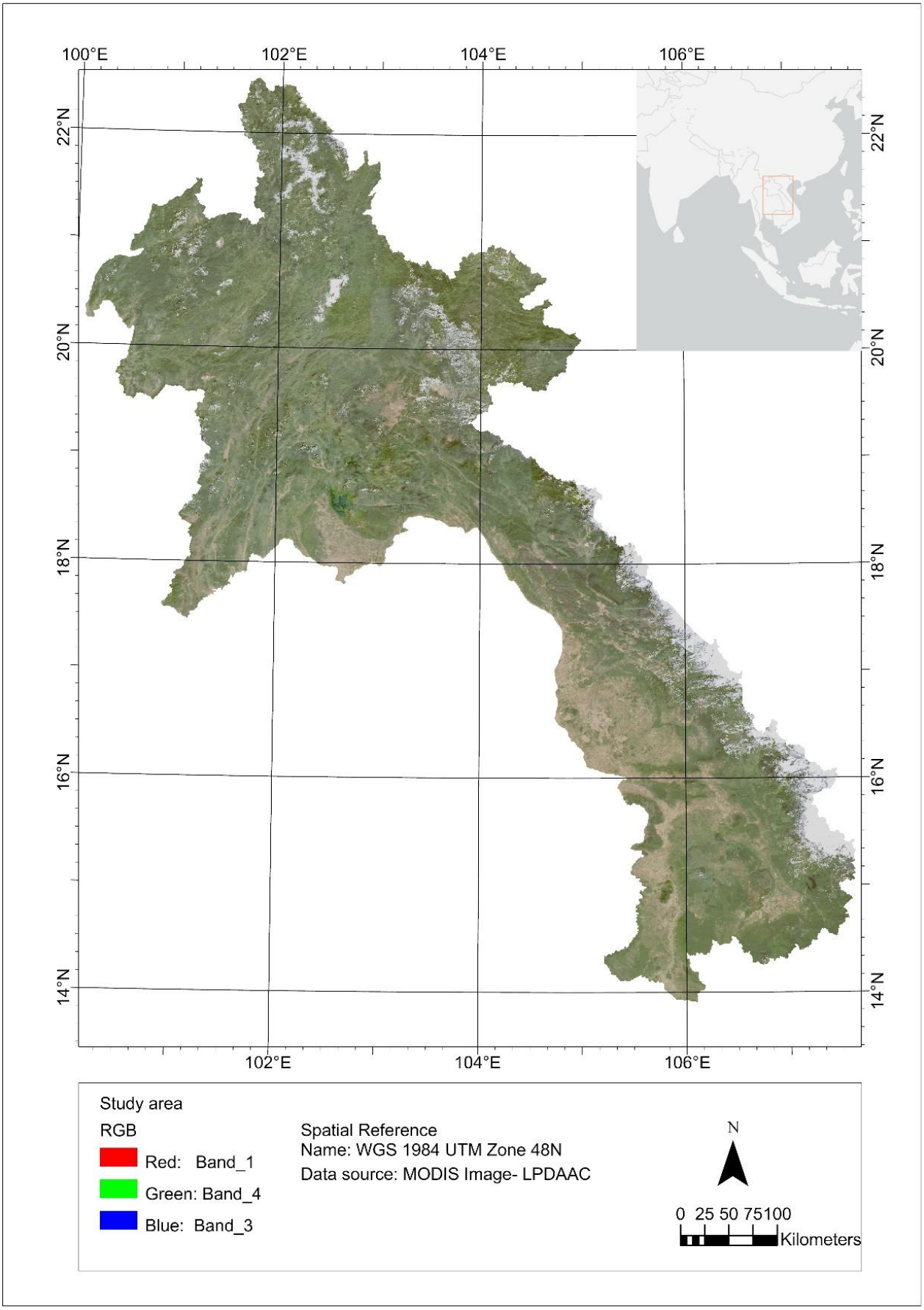

Lao PDR has a tropical, monsoonal climate with two seasons – hot and wet versus hot and dry (FAO 2020). The wet or monsoon season runs from May to late October while the dry season runs from November to April the following year. The maximum temperature ranges from 28˚C to 35˚C while the variation between the maximum and minimum temperatures is sometimes less than 10 ˚C. However, the temperature remains above 30 ˚C throughout the monsoon season, which is favourable for rice growing and especially the germination of rice seeds (Basnayake et al. 2006). Furthermore, the average rainfall of Lao PDR varies from the north to the south of the country. The northern part of the country is more likely to receive less rainfall than the central and southern parts of the country (Krishnamurthy, Chong & Poungprom 2015). Annually, the northern provinces receive approximately 1,566 millimetres of rain, the southern provinces around 2,237 millimetres, and the central provinces about 3,200 millimetres (Basnayake et al. 2006).

In Lao PDR, there are 18 provinces and 148 districts with a population of 7 million (LSB 2019) . Rice has been the main priority of the National Socio-economic Development Plan since the early 1990s (Eliste & Santos 2012). As a result, farmers converted any possible land into the rice-growing areas, however, rainfed rice plantations covering the majority of the agricultural land(Linquist et al. 2006). Different ethnic groups engage in different rice production systems; for instance, the Lao-Tai ethnic group engages mostly in rainfed paddy rice farming. In contrast, other smaller groups who live in the north and at higher altitudes rely on slash and burn cultivation in those upland areas (Schiller et al. 2006). Also, please see Appendix 1 which provides further information on the administration level of the provinces and district of the country.

Overall, agricultural activities can be divided into six Agro-Ecological Zones (AEZ) which is displayed in Appendix 2. The dominant lowland rice production is largely grown along the Mekong Corridor Zone (Li, El Solh & Siddique 2019; WFP 2013). According to the United Nations WFP (2013), the Mekong Corridor consists of a flat area that has an altitude ranging from 100-200 metres above sea level with an annual rainfall of 1,500-2,000mm. Given the suitability of this landscape and its immediate water source, the main livelihood in this AEZ is lowland rainfed rice cultivation. Consequently, lowland paddy rice fields are predominantly distributed in this AEZ more than the other Agro-Ecological Zones.

In contrast, the Northern Highlands AEZ in the north of the country has an altitude range of 500-2,500 metres, with the livelihood of citizens in this zone being predominantly associated with cash crops and livestock rearing (Li, El Solh & Siddique 2019). Also, the upland AEZs in the eastern part of the country, especially the Central and Southern Highlands, are limited in terms of lowland rice cultivation. The reason for this is due to topographic characteristics in which the mountains are

contaminated with unexploded ordnances (UXO) resulting in limited agricultural opportunities (GoL & FAO 2013; Saysompheng 2018). See Appendix 2 for further information on AEZ.

1.5 Significance of the research

This research provides a solution to address the current information gap in rice production. The efficiency of the methodology is crucial for any governmental consideration about how to further improve its monitoring of rice production. This study takes advantage of remote-sensing techniques and free, archived, optical satellite imagery to estimate the area of wet season, lowland rice paddies. It shows how the government could forecast rice production before the harvest period with low cost and minimal resources. Also, it shows how to use current crop statistics to interpolate a more accurate visualisation of the problem. Consequently, this early information is provided to planners in the earliest possible, timely manner. In the meantime, other sectors of the economy and government can also use these figures to evaluate their respective program outcomes. For example, those who manage food security can benefit from this early release of information so they are better informed to proactively take action in advance of any previously unexpected risk. The research results of this study are not only useful to the technical level officers who practically engage in producing such data, but also the high-ranking officers who make decisions based on that data. Technically, staff from concerned ministries could use the results of this study as a reference to improve their current techniques, and perhaps this input can be used to develop a proposal for the funding of a similar project. Also, at the decision-making level, this study could be used to improve the understanding of techniques which use current geospatial information technologies and their application to the agricultural sector and for the Lao Statistics Bureau.

1.6 Outline of the thesis structure

This thesis consists of six chapters which explain relevant issues and solutions to mapping the extent of paddy rice as well as appropriate techniques to estimate rice production at lower spatial units. Chapter one introduces the problem, background, objective of the research, and the description of the study area. Chapter two contains the critical literature that is relevant to the demand for rice, rice growth, and the different techniques of rice mapping. Chapter three covers the respective processes necessary to estimate the extent of rice farming and production. Chapter four presents all the key outputs yielded by each method. Chapter five provides a discussion of the main findings, for instance, the issues and opportunities associated with the methodology used. Finally, chapter six offers a conclusion and recommendations for future research.

CHAPTER TWO: LITERATURE REVIEW

2.1 Rice production in Lao PDR

2.1.1 Factors influencing the demand for rice

Rice is an essential food crop that feeds more than half of the global population. The demand for rice may shift or decline due to changes in consumer behaviour. However, even though changing consumer behaviour and the presence of volatile factors which can contribute to a scarcity of rice production (such as water for irrigation and suitable land for farming rice), rice remains the primary crop to meet the food demands of the poor and the world's increasing population overall (Mohanty, Wailes & Chavez 2010). In Lao PDR, several factors maintain rice's position as the nation's most critical crop. First, since most people rely on rice as their staple food, the significance of rice will remain high well into the future. This picture is reflected in the food consumption behaviour of the population where more than eighty per cent of each household's daily energy needs are derived from rice consumption (Armstrong & Ramasawmy 2012). Furthermore, environmental factors such as the unavailability of suitable land for rice farming are expected in the future. This problem arises from the continued growth of the population and urbanisation; meaning there will be more people to feed while urban expansion will reduce the amount of suitable land available to grow rice (Eliste & Santos 2012).

Other factors that fuel the rise of the significance of the rice crop are national vulnerabilities and the status of food security for the country. Although at the country level a rice deficit appears to be less concerning, the issue becomes worse when considered at the nation's regional and community levels, especially among some ethnic groups (Schiller et al. 2006). Furthermore, with a poverty rate of about twenty per cent, a high correlating rate of malnutrition makes a rice-deficit situation alarming (Boupha 2020; LSB & UNICEF 2018). Thus, if rice crops do not perform well or yield highly, the status of food security and nutrition can be worsened as a direct result of the main livelihood of the poor being rice farming (Manivong, Cramb & Newby 2014). Similarly, the risk of natural disasters such as flooding, drought, and crop disease make food security even more worrisome. Lao PDR has a long history of severe, natural disasters. For example, in 1966, the country experienced the most devasting flooding in its history (Schiller et al. 2006). However, another severe bout of flooding occurred in 2018 when one of the nation's hydropower dams collapsed as a result of the tropical storm Son Tinh (UN 2019). Also, drought is another climate risk event which threatens food security in Lao PDR (FAO 2020). All these are contributory factors which keep the need for a high supply of rice.

2.1.2 Rice ecosystems

Overall, rice production across Lao PDR comprises of three distinct systems. They include irrigated rice production in the dry season, lowland rice production in the wet season, and upland

rice production in the wet season also. First, irrigated rice accounts for about thirteen per cent of the nation's total rice production. This rice is generally grown between December and May in the flat and lowland areas where irrigation systems dominate (Eliste & Santos 2012; Linquist et al. 2006). Irrigated and lowland rice production are similar in terms of crop ecology where some flooding and standing water is required. The only difference between the two systems is the timing of the farming and the water source. Irrigated rice is located in the same area as lowland rice, but only in those specific locations which are near to a water source and where irrigation systems exist. Lowland rice production is most prominent in the Savannakhet, Khammuane, Salavan, and Vientiane provinces as well as Vientiane Capital (Linquist et al. 2006). This ecosystem of rice is the majority of all rice production in Lao PDR and represents about seventy-seven per cent of the nation's total rice production (Eliste & Santos 2012). In general, lowland rice production begins in June and runs through to early November using rainfall as the primary source of water. In the rainy season there is more flexibility than during the dry season. Thus, farmers can grow rice more widely and even in the highlands or upland areas where it is suitable to do so. As a result, lowland rice cultivation is also common in high-altitude and mountainous areas as well as along the Mekong Valley (Linquist et al. 2006).

Unlike rainfed rice and irrigated rice, upland rice does not need seedling preparation because farmers sow the rice seeds directly into the soil at the beginning of the rainy season (IRRI 1975). The upland rice crop is generally grown in rice fields where water is quickly drained following rainfall (Gupta & O'Toole 1986). According to Ahmadi et al. (2004), such a rice system emerges in response to the poverty and the need of a cereal staple food, especially in the area where lowland or flat land surfaces are limited. In Lao PDR, upland rice paddy cultivation covers approximately ten per cent of the total rice production around the nation but uses the slash and burn cultivation technique. The upland rice cycle runs from late April to early October and is mostly in the northern and eastern parts of the country, the mountainous areas (Eliste & Santos 2012; Linquist et al. 2006). A significant proportion of the population, especially the poor who live in rural and remote communities, relies on upland rice farming for a subsistent living (Heinimann et al. 2013). Also, upland rice includes the rotary and slash-and-burn practices, with the largest proportion of upland rice cultivation being in the northern part of the country (Saito et al. 2006).

2.1.3 Key constraints of rice production

Pest and crop disease are two serious issues for rice production. However, based on the generic risk profile of the country in terms of its vulnerability to natural disasters, flood and drought are the most frequently registered risks (Saysompheng 2018). Despite damage to infrastructure and the humanitarian aspect, agriculture is another sector that is severely impacted when extreme climatic events occur. According to Schiller et al. (2001), since 1966 Lao PDR has experienced flooding or drought in at least some part of the country almost every year. This accounted for a loss of 20-30 per cent in arable land areas between 1991 and 1999, while the general loss in rice crop

production as a result of flooding or drought was estimated to be at 15 per cent in 2018 (Saysompheng 2018). The effect of natural disasters substantially influences the whole cycle of rice growing. Specifically, if drought occurs at the beginning of the growing season, the remaining cycle is affected. Since water is the primary means to initiate rice growing, farmers need water with the appropriate temperature to facilitate the germination of rice seeds (Linquist et al. 2006). When a drought occurs, the transplanting of rice is most likely delayed and eventually the following stages, the most critical determinants for rice productivity, are also delayed in turn (Fukai 1999; Ishimaru et al. 2016). The current constraints may be hard to address since there is the anomaly with the onset of the rainy season. According to Krishnamurthy, Chong and Poungprom (2015), the variation of seasonality fluctuates by about ten days. The high uncertainty of rainfall remains and it may be hard for farmers to adapt year-by-year. In some years, farmers start the transplanting of rice seedlings as late as August (Ikeura et al. 2016). These are the main constraints that farmers have been facing in the last decade, where farmers need to adapt to the climatic situation.

2.1.4 Rice growth and its development

Rice is an annual grass and its life cycle can be divided into three main phases: vegetative, reproductive, and ripening or maturing. Within these three main phases there are substantial growth stages. According to Kuenzer and Knauer (2013), there are about ten stages which could be categorised in the rice growth cycle. Figure 2 illustrates the broad picture of rice growth starting from the initial rice seed through to when the rice is harvested. Referring to this illustration, the first step is to germinate the rice seed before preparing the seedlings for transplantation. After the rice seedlings have been transplanted into the rice field, the rice starts tillering with stems and leaves. In this stage, more shoots are added to the main shoot. The vegetative phase ends with a maximisation of tillering before an elongation of the stems begin. In this stage, no more stems are added to the current rice tillers. Next is the reproductive phase. Moldenhauer and Slaton (2001) explain that the reproductive phase involves six critical stages starting from the formation of rice panicles to rice ‘headings’, which is when the panicles begin to emerge from their ‘boots’ before rice flowers start to bloom. Finally, there is the ripening or maturing phase, which includes starch grain development. Starch will form into grain but remain soft at first before hardening and becoming ready for harvest (Moldenhauer & Slaton 2001). The entire process of rice growth takes about 110-120 days in a tropical region. By comparison, the same process can take up to 150 days in temperate weather regions (Le Toan et al. 1997). However, these timeframes also depend on the variety of rice planted (Moldenhauer & Slaton 2001).

Figure 2. Rice growth cycle. Image sourced from the International Rice Research Institute (IRRI)-Rice Knowledge Bank (Nelson et al. 2014, CC-BY)

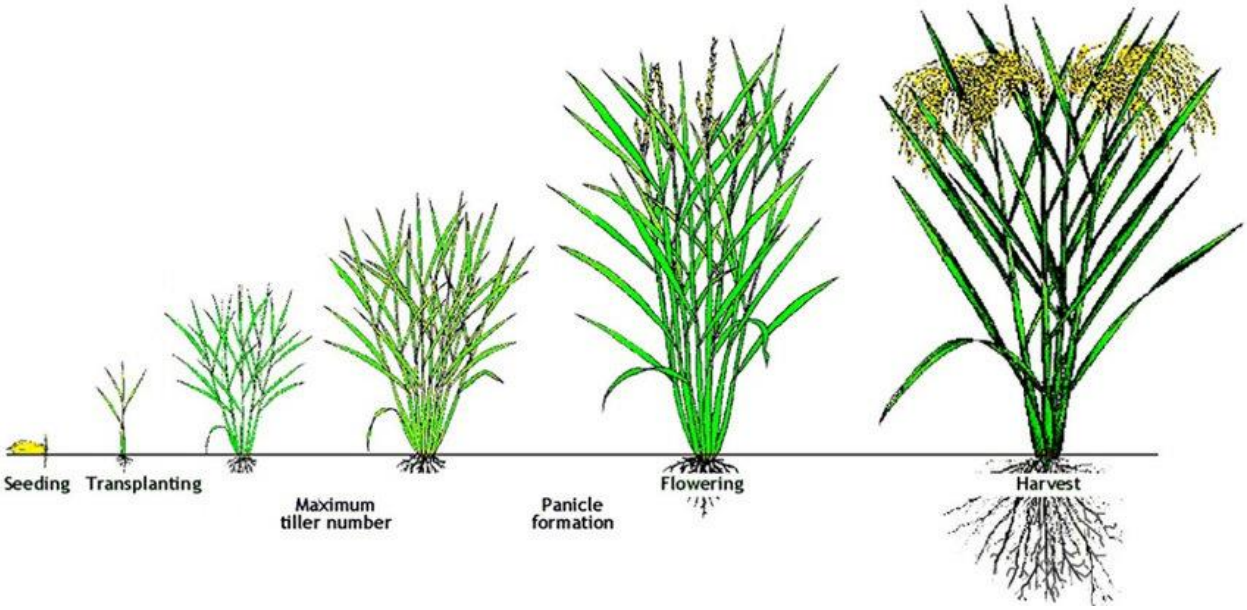

2.2 Mapping the extent of rice farming with low spatial resolution optical imagery

2.2.1 Vegetation indices-based approach

In the literature regarding remote sensing, the pixel-based approach is one of the most popular approaches applied to delineate paddy rice fields from other landscapes. There are two critical elements for this approach: multispectral band imagery and knowledge of how rice grows. These two elements are combined into one algorithm and used to detect rice fields. Xiao et al. (2006); (Xiao et al. 2005) developed this algorithm based on three vegetation and water indices. These indices are the outputs of the differentiation between the visible wavelength, Near-infrared band, and Short-wave infrared band wavelengths of the optical satellite. The Normalised Difference Vegetation Index, the Enhanced Vegetation Index, and the Land Surface Water Index are the most common indices used in this approach, while knowledge of rice growth is another essential element. As mentioned above, a rice crop has three phases in its life cycle. However, the most critical phase for mapping the extent of rice cropping in a study area is the transplanting period. According to Xiao et al. (2005), the rice calendar is essential because the algorithm needs to run according to the time when farmers transplant their rice crops, so the temporary flooding is detected. This algorithm has been used ever since, with Xiao et al. (2006) applying this assumption with MODIS data and mapping the extent of rice farming for the whole South East Asian region. Some studies have even modified and enhanced this algorithm by applying specific techniques to meet their unique objectives. For example, instead of mapping rice in general, some studies modify the algorithm using specific knowledge of different rice species so they can differentiate the different ecosystems of rice (Sun, H-s et al. 2009).

2.2.4 Advantages and disadvantages of vegetation-based mapping with low-resolution imagery

Low and moderate spatial resolution imagery like MODIS and AVHRR imagery provide high temporal resolution and a swath width which are appropriate for the large scale monitoring of vegetation (Xiao et al. 2006; Xiao et al. 2005). These characteristics are necessary when there is a need to monitor vegetation on an extensive scale. At the nation's regional and whole country levels, it is essential to have data which allows such large-scale monitoring, while a high temporal resolution is also crucial for monitoring purposes because the rice crop is highly dynamic (Bridhikitti & Overcamp 2012; Sun, P et al. 2017). Despite the advantages of low and moderate spatial resolution imagery, there are some challenges that different users may encounter during the data analysis. Low spatial resolution imagery yields larger pixel sizes, for instance, 250 metre x 250 metre, 500 metre x 500 metre, and 1,000 metre x 1,000 metre pixels. At this spatial resolution, it is challenging to differentiate rice fields that are grown on small parcels of land and where there is a high diversity of land cover (Mosleh, M, Hassan, Q & Chowdhury, E 2015; Tingting & Chuang 2010; Xiao et al. 2006). These are, therefore, both advantages and disadvantages of using this mapping approach with low and moderate spatial resolution.

2.3 Mapping the extent of rice farming with medium to very high-resolution imagery

2.3.1 Object-based image analysis

Object-based image analysis (OBIA) is another method which is extensively applied when mapping rice. In most cases, this method is chosen in response to limitations of the pixel base, which is quite common with low-spatial resolution imagery (Peña-Barragán et al. 2011; Singha, Wu & Zhang 2016). The object-based analysis comprises of two steps of image segmentation, where the image is divided into sub-homogenous pixel groups before the classification method is implemented (Wulder et al. 2008). The difference between a pixel-based versus an object-based approach is the way it identifies the objects. While the pixel-based approach focusses on the individual pixel values, the object-based approach gives priority to the homogeneity of the pixels (Singha, Wu & Zhang 2016). This means the object-based approach clusters or groups pixels according to their similarities before a statistical method is applied in the classification process.

2.3.2 Benefits and drawbacks of applying object-based image analysis

Classification of objects in highly topographical areas and with varying land cover classifications can be challenging. However, the object-based image analysis (OBIA) approach is capable of classifying objects in highly heterogeneous areas where the variability of each land cover classification is small (Dong & Xiao 2016; Kim & Yeom 2014). OBIA advantageously applies various statistical parameters to analyse pixel values when segmenting the image, thereby increasing the accuracy of the rice mapping process (Dao & Liou 2015). However, this approach

needs a high spatial resolution image. Although Landsat and Sentinel-2 data is freely available to download, other high resolution imagery like Rapid-EYE and SPOT-6/7 can be costly to acquire, especially for extensive or large scale mapping (Bridhikitti & Overcamp 2012; Sozzi et al. 2018). Besides, it is difficult to find a cloud-free image with high spatial resolution imagery during the wet season. Also, high spatial resolution imagery has a narrow swath width which challenges the timing and other resources of the mapping project.

2.4 Mapping the extent of rice farming with RADAR imagery

2.4.1 Mapping of the temporary inundation of rice paddies with RADAR imagery

The inundation and transplanting periods for rice paddies are essential, even when using active remote sensing (Kuenzer & Knauer 2013). When mapping rice using RADAR as the data source, the analysis unit is called the "backscatter coefficient" instead of “pixels” (the unit used in optical image analysis). Like the optical image-based approach, to distinguish rice paddies from other features, the rice-growing calendar and other information about rice growing phases are fundamental. Thus, with a temporal analysis of the backscatter coefficient, the unique feature of rice transplanting and temporary flooding is detected. Torbick et al. (2017) used C-band from Sentinel-1 to conduct a temporal analysis of backscatter compared to the seasons and rice calendar to classify rice paddy areas in Myanmar. Their temporal analysis found that a low rate of backscatter was observed initially but this was then followed by an immediate increase of backscatter at the beginning of the rice growing season. This behaviour was considered a sign of the temporary inundation of rice fields (Mansaray et al. 2017).

2.4.2 Classification of rice crops with RADAR imagery using polarimetric analysis

Despite the successful analysis of the temporary flooding areas of rice paddies using the methods above, other methods can also be employed for classification procedures. Regarding the range of classification methods, the literature indicates several algorithms have been developed and tested. Often, the classification schema involves collecting samples from the objects and field missions. Zhang, Y et al. (2009) experimented with the classification technique by adopting the support vector machine (SVM) to classify rice paddy areas using Phased Array type L-band SAR or PALSAR. SVM is the optimal classifier that finds the best representation of the class (Tan et al. 2007). SVM is applicable in other types of data too, for example, in optical imagery like Landsat and Sentinel-2. This approach can yield an accuracy of up to 80 per cent. Furthermore, Mansaray et al. (2019) conducted a comparative study of the accuracy across the classifications of SVM and Random Forest (RF) on rice mapping from three different datasets including SAR from Sentinel-1A. Their results indicated that SVM is more accurate than RF in all datasets. Also, another classifier is called the Neural Net Classifier and this is available as commercial software used to classify rice paddies, using ground truth data from the field (Shao et al. 2001). However, not all studies can involve field missions and this method exploits any contrasts in variations over time of

SAR images to distinguish rice paddies from other land features (Le Toan et al. 1997). These are some of the most effective classification approaches which have been applied in rice paddy mapping using RADAR imagery.

2.4.3 RADAR imagery sources and applications in rice mapping

Many kinds of RADAR images have been produced and made available since its launch in the late 1990s. Some of those satellites which have been used for mapping agriculture are ERS-1 and 2, ALOS-1 and 2, RADARSAT-1 and 2, and Sentinel-1A and 1B. Some of these sensors have recently concluded their missions while others remain in orbit. The Advanced Land Observing Satellite (ALOS-1) was the largest satellite ever launched by Japan. Developed in Japan and launched in 2006, it completed its mission in 2011 (Rosenqvist et al. 2007). The subsequent ALOS-2 launched in 2014, however, and remains available to analysts (Reiche et al. 2018). The Phased Array type L-band SAR (PALSAR) onboard the ALOS-2 can capture images with a spatial resolution of 6.25 to 50 metres, with swath widths ranging from 70 to 360 kilometres. Zhang, Y et al. (2009) experimented with PALSAR images to map rice paddies, while Shao et al. (2001) applied multi-temporal data from RADARSAT to map rice paddies and achieved over 90 per cent accuracy. Another sensor that provides C-band data in SAR imagery, especially since this data is comparable with SAR imagery produced by RADARSAT, is ERS-1 (Le Toan et al. 1997).

Furthermore, the most recently launched satellite offering RADAR imagery is from the European Space Agency Copernicus program. The onboard Sentinel-1A/B has four acquisition modes and each method provides Synthesis Aperture RADAR (SAR) produced in four levels. Of these, it is Level 1-GDR, or the ground detection range, which is commonly applied when mapping rice plantations (Mansaray et al. 2017). The bands in SAR imagery are called Amplitude and Intensity, and they have dual polarisations in terms of vertically transmitted and vertically received (VV), or vertically transmitted and horizontally received (VH). The product has three levels, with Level 0 being the foundation level from which Levels 1 and 2 are generated from. However, the ground detection range that is typically applied in agriculture monitoring (ESA 2000-2020; Mansaray et al. 2017; Mansaray et al. 2019).

2.4.4 Opportunities and challenges when applying RADAR imagery to rice mapping

While microwave remote sensing or the application of the RADAR sensor is weather independent, data availability and data structure remain a challenge. The limitation for rice mapping is cloud cover and long rainy days in the tropical regions where rice production is most prevalent. RADAR is, therefore, the only mapping option that can collect the phenological changes during the monsoon season (Le Toan et al. 1997; Shao et al. 2001; Zhang, Y et al. 2009). The other advantage of RADAR is its high geometric resolution and the wide swath width of the image. However, the spatial resolution depends on the polarisation type. For instance, a single-look image provides higher spatial resolution than a multiple-looks image. ALOSPALSAR is capable of

providing ground resolution at 10 to 20 metres with a high swath width of up to 360 kilometres (Rosenqvist et al. 2007). Furthermore, the high temporal resolution allows for better observation of changes in crops, especially crop phenology. In terms of temporal resolution, PALSAR has a repetitive rate of 46 days, while Sentinel-1 A and B can revisit the same location every six days. This is even better than the previous C-band SAR images (Clauss et al. 2018; Mansaray et al. 2017). Furthermore, SAR images from Sentinel-1 A and B are archived and freely available from the European Space Agency's platform (Clauss, Ottinger & Künzer 2017).

By contrast, the structure of SAR data is complicated and may need specific software to convert it to a format suitable for analysis. With RADAR imagery, it is a complicated process converting SAR amplitude to the sigma naught (σ°) backscatter coefficient (Sun, C et al. 2019). To do this, different analysts apply different algorithms to achieve the best representative dataset. The data in Sentinel-1A is converted into the backscatter coefficient with a tool called SNAP and by using a specific equation (Mansaray et al. 2017), while a different calibration method is required for SAR images from RADARSAT (Shao et al. 2001). Sometimes, a RADAR image loses spatial resolution from such pre-processing steps. For instance, an SLC RADAR image has a higher spatial resolution than multiple-look images but due to necessary noise filtering, the quality of the representation of the Earth's surface is negatively affected (Torbick et al. 2017). Another constraint of SAR is associated with the availability of the data. Due to the limited capacity of data storage, RADAR images are not available everywhere and archiving of data is not provided for larger areas (Clauss et al. 2018). In addition, the cost to access the specific wavelength of SAR for more accurate mapping is limited because it is expensive to acquire (Mosleh, M, Hassan, Q & Chowdhury, E 2015). In terms of constraints for rice classification, SAR images can be confusing or difficult to separate or distinguish crops with a similar shape to rice, potentially causing misclassification (Forkuor et al. 2014). Also, there is a higher degree of uncertainty when mapping steep rises in highly topographical areas, where rice fields are smaller, and also in the areas around the edges or border of images (Zhang, Y et al. 2009). So, these are some essential factors which need to be considered when using RADAR imagery.

2.5 Rice yield estimation approach with different sensors

2.5.1 Rice yield estimate indices and heading stage identification

The Normalised Difference Vegetation Index (NDVI) is a traditional vegetation index which many studies have proven successfully correlates to crop yields (Chang, Shen & Lo 2005; Huang et al. 2013; Skakun et al. 2017). Some studies have used the NDVI as the primary indicator while also combining it with other vegetation indices to forecast rice yields (Cai & Sharma 2010; Huang et al. 2013). However, the NDVI has several limitations when representing crop phenology. This is especially true in areas with a high coverage of vegetation present, as the NDVI value becomes saturated with increased green biomass and lacks the reliability to measure the productivity or

yields of rice crops (Huete, Alfredo et al. 2002). Consequently, some studies avoid using the NDVI for crop yield forecasts. For example, Son et al. (2013) chose the enhanced vegetation index (EVI) and the leaf area index (LAI) instead of the NDVI to forecast rice yield. In crop yield studies, the leaf area index for rice paddy areas plays an essential role in providing phenological value. LAI has a strong relationship to vegetation indices and rice productivity, thereby making it suitable for yield forecasts (Xiao, He, et al. 2002). Furthermore, another critical element of rice yield estimation is the identification of heading dates when the panicle begins to emerge from the boot, with this usually taking about 10-14 days (Moldenhauer & Slaton 2001). While some studies define the heading stage as 80 days after the rice is transplanted (Oza, Panigrahy & Parihar 2008), other studies define the heading stage as 30 days before the harvest (Son et al. 2013). Nevertheless, the determination of the heading stage needs to refer to the rice crop calendar as well as information from the relevant local authorities (Xiao et al. 2005). These are two essential stages that data analysts must consider before they conduct the analysis.

2.5.2 Methods of rice yield estimation with optical imagery

Once the paddy rice areas have been mapped, it is possible to estimate crop yields or crop production. There are several assumptions and methods which can be applied, however, these methods are based on census and remotely-sensed data to forecast yield. These methods assume that the official statistical yields represent the advancement of technologies, fertiliser, and other improvements to farming methods. By contrast, the remotely-sensed yield represents natural influences, for instance, precipitation, temperature, disease, and soil. The yields from an official census are converted into raster format to allow for production estimates after the planted area and the key indicator have been applied, for example, when the NDVI, EVI, or LAI has been computed. So, to forecast rice yield, it is essential to have an estimated extent of rice crop area before the remotely-sensed yield is derived from the heading stage. Once the average and individual rice yields are available, it is merely a matter of multiplying the official rice yield by the remotely-sensed rice yield (Cai & Sharma 2010; Huang et al. 2013).

Another approach is to forecast the rice yield using a regression model. This method assumes that the official rice yield is the dependent variable and the vegetation indices are the rice yield predictors (Groten 1993; Noureldin et al. 2013). Son et al. (2013) used the EVI instead of the NDVI together with the LAI to predict the rice yield with a multiple regression model. Thus, results from the regression model provided predicted yields with associated errors, which is useful to assess the robustness of the results. Also, there is one crucial detail to be aware of when forecasting rice yields. Any pixel usually mixes with a non-rice background in the same pixel. It is essential, therefore, to extract only those pixels that have at least more than 90% of rice (Son et al. 2013). These are the methods and techniques used to forecast rice yields with optical imagery as well as official statistical figures.

2.5.3 Forecasting rice yields using RADAR images

Once the rice area is delineated, the production of rice can be estimated based on the backscatter coefficient value. This means the value of the backscatter coefficient, especially the median from the VH polarisation of C-Band SAR images, will be used to estimate rice yields further. This follows the simple concept of forecasting crop yield by multiplying the planted area by the yield per unit of area (Clauss, Ottinger & Künzer 2017). As a result, the overall production will be a summation of the production of all the planted areas. Clauss et al. (2018) used the C-Band SAR images from Sentinel-1A to classify the rice paddy areas in the Mekong Delta with super-pixel segmentation. The area was divided into three groups according to the local rice varieties, with the median backscatter from each variety multiplied by the area for that rice variety's production.

On the other hand, instead of using a backscatter coefficient value as the yield, Lao Statistics Bureau sometimes records details of historical rice yields by rice variety as well as their life span, and this data can be used to forecast rice production in turn. For example, Shao et al. (2001) forecasted the rice yield of different rice varieties using a multi-temporal analysis of rice backscatter behaviour from the rice growth cycle with RADARSAT. They estimated the remotely-sensed area according to the official, historical yields of rice varieties. Thus, the simple mathematical model to calculate rice production is to multiply the estimated area of rice by the yield per unit of area from the census.

2.6 Noise and eliminating strategies for each sensor

2.6.1 Noise of low spatial imagery and solutions

The main issues associated with low spatial resolution optical imagery of cloud, shadow, and aerosol scatter, as well as several algorithms available for noise filtering, have all been discussed in the literature analysis. The moderate and low spatial resolution refers to MODIS and AVHRR imagery. MODIS products are tested with a cloud mask that was developed using all 36 bands of the imagery to maximise the reliability of the product (Ackerman et al. 1998). Even if the image vendors apply noise filters before the release of the products, some noise will still be present, especially with regard to the remaining cloud cover (Xiao et al. 2006). An additional cloud mask is essential for all MODIS data before the data analysis (Sun, H-s et al. 2009). The impact on the image is serious because information about key objects is lost or missing when cloud or shadow block the sensor. Different studies have applied several additional measures to MODIS data. Sun, H-s et al. (2009) adopted the CTIF, which stands for conditional temporal interpolation filtering, to reduce haze. This method addresses the issue while retaining the best data, with the pixels exhibiting the most scatter being removed (Groten 1993). Furthermore, another technique to address cloud contamination in addition to the cloud flag provided with the product is the removal of all Blue band reflectance at 0.2 and above (Sakamoto et al. 2006; Xiao et al. 2006; Xiao et al. 2005). Since the Blue band is sensitive to atmospheric scattering, the high reflectance of this band

is considered an error. Son et al. (2013) adopted the empirical mode decomposition (EDM) to filter out thin cloud and remove any contaminated pixels. However, the missing value was treated with a time series profile using a linear interpolation method. EDM is the most efficient filter to address noise from the cloud in the NDVI time-series(Chen, CF et al. 2011). Overall, it is difficult to find cloud-free images during the monsoon season but selecting the best technique to minimise the impact of cloud contamination of the data is necessary.

2.6.2 Noise and noise-addressing strategies for medium to high-resolution imagery

High spatial resolution optical imagery encounters similar noise to that of low and moderate spatial resolution imagery, however, the solution applied to resolve the problem is slightly different. According to Gao, B et al. (2002), cloud and cloud shadow have a significant, negative effect on remote-sensing studies, especially with data analysis. For example, it influences the true reflection of the Earth's surface and creates a bias in the NDVI and other indices. Detection of cloud is generally more straightforward than of cloud shadow. While the shadow from thick clouds may be easier to detect, identification of shadow from thin clouds is more complicated. This is due to the reflectance of cloud shadow appearing differently on different backgrounds. For instance, the reflection of cloud shadow on a bright background is different from that on a dark background (Zhu & Woodcock 2012). In dealing with cloud cover and its shadow, Kontgis, Schneider and Ozdogan (2015) applied Fmask, which is an algorithm explicitly developed to filter out cloud cover and cloud shadow contamination in Landsat imagery. This cloud mask is not only applied to Landsat imagery, it is also applicable to other high spatial resolution images like that of Sentinel-2 (Zhu, Wang & Woodcock 2015). The general cloud mask discusses how to remove cloud but pays less attention to filling in the missing pixels. Thus, Cheng et al. (2014) propose an algorithm called Spatio-temporal Markov Random Field. This algorithm was developed to support the cloud removal process while concurrently replacing the omitted pixels with the most represented pixels from another window or auxiliary time series.

2.6.3 RADAR imagery-related noise and how to address it

The most frequently reported noise found in RADAR images, especially in Synthetic Aperture RADAR (SAR) images, is the speckle effect. Speckle is the disorder of the SAR image which results from multiple reflection points combining in the same pixel, which ultimately leads to having many bright and dark pixels in the image (Bruniquel & Lopes 1997). Another effect caused by speckling is a rougher image, meaning the image is not as smooth as an optical image (Shao et al. 2001). Speckle reduces the accuracy of identifying different objects, while also affecting the change detection analysis. Le Toan et al. (1997) claim that change detection analysis is sensitive to the speckle effect. Thus, in response to this issue, a number of algorithms have been developed for different assumptions. According to Lopes, Touzi and Nezry (1990), four speckle filters have been developed. However, based on the literature studied, the most extensively applied filter to address the speckle effect is the Lee filter (Shao et al. 2001; Tan et al. 2007; Zhang, Y et al.

2009). Furthermore, there are other schema which have been reported as effective, for example, Multilook (L-looks) and the Gamma-Gamma MAP (Bruniquel & Lopes 1997; Lopes et al. 1993). In addition, there is another technique which uses pixel segmentation to spatially average the backscatter time series and this also minimises the effect of speckle (Clauss, Ottinger & Künzer 2017). Also, for Sentinel-1A SAR data, this issue can be addressed by using SNAP that includes several spatial filters including Lee filter (Sun, C et al. 2019). It is essential to understand the effects of speckle on RADAR imagery and solve the issue for a better representation of the data before further data analysis is conducted.

2.7 Accuracy assessment and validation of rice mapping

2.7.1 Validation of rice mapping in low and moderate resolution imagery

Validation of the studies that apply low and moderate spatial resolution imagery is more likely to rely on the comparison of the estimated rice extent and with census figures. The technique applied to compare data may vary, however, the most common method to compare the estimation to the actual data is using simple linear regression. This means taking the actual data as the dependent variable and the remotely-sensed results as an independent variable. The root means square error (RMSE) and the r-square value are then assessed. This method is proposed by Xiao et al. (2006), who used moderate spatial resolution time-series data from the MODIS sensor to map rice paddies across the whole South East Asian region, including Lao PDR. From their studies, they compiled official statistics regarding rice production, including the planted area from national statistics offices of 13 countries, to compare with their estimated extent of rice farming. This similar method of assessing accuracy has been applied in many studies (Bridhikitti & Overcamp 2012; Sun, H-s et al. 2009; Xiao et al. 2005). By contrast, other studies choose only the root mean square error as a means to validate their results. According to Son et al. (2013), who conducted rice mapping using MODIS data to monitor rice paddies in the Mekong Delta, they computed RMSE to assess the accuracy of their estimate with the actual rice production figures. These techniques offer a range of options where field missions to collect ground truth data is unfeasible.

2.7.2 Accuracy assessment of rice mapping in high spatial resolution images

In studies that use high spatial resolution imagery, the method for the assessment of accuracy is slightly different from that of low spatial resolution imagery. However, the coverage of the mapped area in high resolution imagery may be significantly lower than at the administrative level. In this case, the method for the accuracy assessment needs to rely on the local statistics approach. The local statistics approach refers to statistical parameters that are available from the data analysis technique, for instance, statistical values from the regression model. In addition, some other figures that could be compiled from the research team can be used for reference purposes, for example, observations from the studied area. Thus, in response to such a situation, Noureldin et al. (2013) relied on both local statistical parameters from their study and their own observations for

validation. In any case, where village or community-level records about crop production are available, it is sensible to use those records as an additional reference. Dao and Liou (2015) conducted a remote-sensing study to investigate the area of rice lost as a result of flooding. In this case, the studied area was much smaller than the zone level, for which crop statistics are provided. So, they used information directly from the villages for verification purposes.

In the worst-case scenario, where other reference data is unavailable, the random sampling technique of different points within the study area from the field can be applied (Mansaray et al. 2017). For this, it is essential for ground truth information from field missions be used to verify the agreement or disagreement of the classification. Also, if fieldwork is unfeasible, another solution is to rely on the auxiliary dataset. This ancillary data can be accessed via Google Earth, the Digital Elevation Model, or a land cover map (Singha, Wu & Zhang 2016). Thus, there are a variety of options to help data analysts validate the output from studies which rely on a high spatial resolution. More importantly, it is necessary to cross-check what is available in the study area and adapt accordingly.

2.7.3 Validation of rice mapping from RADAR image-based studies

Accuracy assessments for RADAR imagery related studies are similar to those for optical image-based studies in that the assessment method used depends on the scale and availability of the reference data. One such validation method is conducted by randomly selecting the sample within the study area and evaluating its classification. Following this, the mean and the confidence interval can be computed, with these being useful to gauge the level of data accuracy (Lasko et al. 2018). Clauss, Ottinger and Künzer (2017) conducted their accuracy assessment using a stratified random sampling technique. For example, they stratified the study area into two classes before randomly selecting approximately 100 labelled points from each class. However, for this technique, a reference image is required. In this case, they used a high-resolution image from the archives of Google Earth and Landsat data as references. Finally, the matching and non-matching points were accounted for and measured as percentages of matching and non-matching data, which offers a representation for the accuracy percentage sought (Zhang, Y et al. 2009). Nevertheless, when fieldwork is feasible, then field visits should be conducted. Field trips provide the opportunity to collect ground truth information at the field level and this is useful to validate the results attained from the remote-sensing studies (Shao et al. 2001). Following this, Clauss et al. (2018) created a database from the field missions where GPS points were marked with the identity of those objects on the ground to resolve any invalidation. Finally, if census data is available, a comparison with official statistics should also be added (Chen, C et al. 2011).

2.8 Summary

In summary, rice is a critical staple food for billions of people around the world, especially among the poor. An increasing population, the risk to food security, the poverty rate and malnutrition of those in poverty, and climate change all make rice even more critical in Lao PDR. Three rice ecosystems are spatially distributed across different Agro-ecological Zones, with the lowland, rainfed rice ecosystem accounting for the majority of all rice production from these three. This rice system is mainly distributed along the Mekong Valley and other suitable areas in the upland or mountainous regions of the country. The main constraints of rice production are flooding and drought, with these two environmental factors having persistently affected the infrastructure and livelihood of the citizens as well. This issue may remain a critical problem to the socio-economic development plan of the Lao Government in the future as climate change is exacerbated.

In order to map the extent of rice farming and forecast rice production, several techniques have been developed and applied. However, from a geospatial perspective, two particular systems – active and passive remote-sensing – have been extensively applied in rice mapping and to forecast rice production. Alternatively, there are a variety of sensors from a different satellite which offer different output products to meet specific scientific research needs. Technically, active remote-sensing, which is otherwise independent of the rice-mapping process, can be used for backscatter analysis. For example, the analysis of rice backscatter behaviour can be used as an input to extract more accurate data about the extent of rice farming in the area studied. By contrast, passive remote-sensing presents the issue of cloud contamination, especially during the monsoon season, requiring the analyst to resort to field missions and the application of various resolution scales. Two main techniques can be applied in pixel-based and object-based mapping procedures, both of which are extensively experimented with.

In general, the remote sensing of rice crops requires knowledge of rice growth and the rice calendar from locals in the farmed study area. In any case, official authorities publish such information in Lao PDR, bearing in mind that climatic conditions and social factors pertaining to rice farmers can impact the currency of such information. Parallel with the knowledge of rice cropping, quality control measures must be implemented before producing any results. Analysts need to understand the specific noise from different sensors and address them accordingly. These noises include geometry-specific noise, speckle or brightness effects from RADAR, and cloud or other atmospheric-associated errors from the optical satellite imagery. These problems require appropriate strategies for effective resolution. Also, the accuracy of the mapped results is critical and different strategies were offered in the literature. However, these strategies depend on the availability of auxiliary data and the context of the study area. Both active and passive remote-sensing are capable of mapping the extent of rice farming for forecasting rice production, however, this depends on the objectives and scale of the mapping exercise.

CHAPTER THREE: METHODS

3.1 Choice of imagery and data collection

3.1.1 Satellite imagery (MODIS)

This study used imagery from the Moderate Resolution Imaging Spectroradiometer (MODIS), the sensor on board the NASA ESO Terra Satellite, launched in 1999. The standard products provided by MODIS are in a tile of 1,200 x 1,200 kilometres. Specifically, MOD09A1, an MODIS 8-day composite product, is developed by selecting the least cloud contaminated data from an 8-day period (Peng et al. 2011). This imagery was chosen as the primary dataset because it is freely available and it minimises the effect of cloud contamination that is a main issue during the monsoon season. Furthermore, this product is atmospherically-corrected and it offers a sound balance between spectral, temporal, and spatial resolution for mapping rice at the country level (Sun, H-s et al. 2009; Xiao et al. 2006; Xiao et al. 2005).

MOD09A1 is a surface reflectance product which is provided with seven spectral bands at a 500-metre spatial resolution and this is useful for mapping rice crops at the country level. All available imagery was downloaded from https://lpdaac.usgs.gov/, the Land Processes Distributed Active Archive Centre (LPDAAC) data sharing platform (Vermote, EF, Roger & Ray 2015). The imagery used amounted to 138 tiles (three tiles by 46 time slices) within the 2016 growing season. Also, MODIS data has the potential to be used for extensive crop monitoring, and the data is regularly updated and archived. Specifically, the daily product is available after two days from capture while the 8-day product is available two weeks after the final capture date (Zhang, P 2007).

3.1.2 Satellite imagery (Landsat-8 OLI)

Landsat-8 OLI offers 16 days of revisits with a 30-metre spatial resolution, which is sufficient to verify trends in the NDVI and LSWI. Two scenes of the Landsat-8 images from path/row 128/48 and 126/50 with eight data points were used, totalling 16 images acquired in the rice-growing area for 2016, and these were downloaded from the US Geological Survey database (https://glovis.usgs.gov/).

3.1.3 Auxiliary datasets

The land cover map used in this study was derived from the European Space Agency Land Cover data-sharing platform: http://www.esa-landcover-cci.org/. This global product is the output of the CCI-LC project and offers a 300-metre spatial resolution. Classifications are based on the Land Cover Classification System from the United Nations Food and Agriculture Organization (Kirches et al. 2017). The dataset was extracted particularly for the study area – the whole country of Lao PDR.

Secondly, the study used the SRTM Digital Elevation Model with a 30-metre spatial resolution to assist in separating rice fields out from the high topographic terrain. 38 tiles covering the whole country were downloaded from the USGS database https://earthexplorer.usgs.gov/. All the scenes captured were mosaicked and generated into a countrywide layer which covered the whole study area.

3.1.4 Vector dataset

The administrative boundaries of provinces and a district were required. These datasets were sourced from the National Geographic Department, Ministry of Home Affairs, Lao PDR.

3.1.5 Crop statistics

Rice crop statistics were downloaded from the website for the Lao Statistics Bureau (LSB) https://laosis.lsb.gov.la/. The LSB is the official national agency empowered by the Lao Government to compile and publish Lao country data pertaining to any required socio-economic information. The Bureau provides technical support to different line agencies with its data collection and the conducting of national surveys, the census, and reporting systems.

3.2 Software used

This study used ArcGIS Pro 2.6/ArcMap10.6.1 to process satellite imagery and spatial data modelling. In contrast, the general simple regression model and other tabulations were processed using Microsoft Excel 2010.

3.3 Data analysis

Figure 3 shows the details and the flow of all the essential processes used for this study. Analysis of the data for this study can be divided into three components. The analysis in the first component focuses on the mapping of rice using MODIS data, auxiliary datasets such as Land Cover Map, and the digital elevation model (DEM). In this process, a spot check of the vegetation index pattern on the potential rice fields was carried out using Landsat-8 OLI with a 30-metre spatial resolution. The objective was to ensure that the indices computed with the MODIS data accurately fluctuate in time with the different periods of the rice-growing season. The next component focused on the process of interpolating the rice yield at the district level. The district rice yield was estimated using the simple regression model based on the provincial rice yield and the remotely sensed rice area run within each specific Agro-Ecological Zone. Finally, validation of the model was conducted using the correlation analysis , the root mean square error (RMSE), and the mean absolute error (MAE). The consistency between the extent of remotely-sensed rice and the official statistics was assessed by Agro-Ecological Zone and by province.

Figure 3. Flow chart of data management and analysis

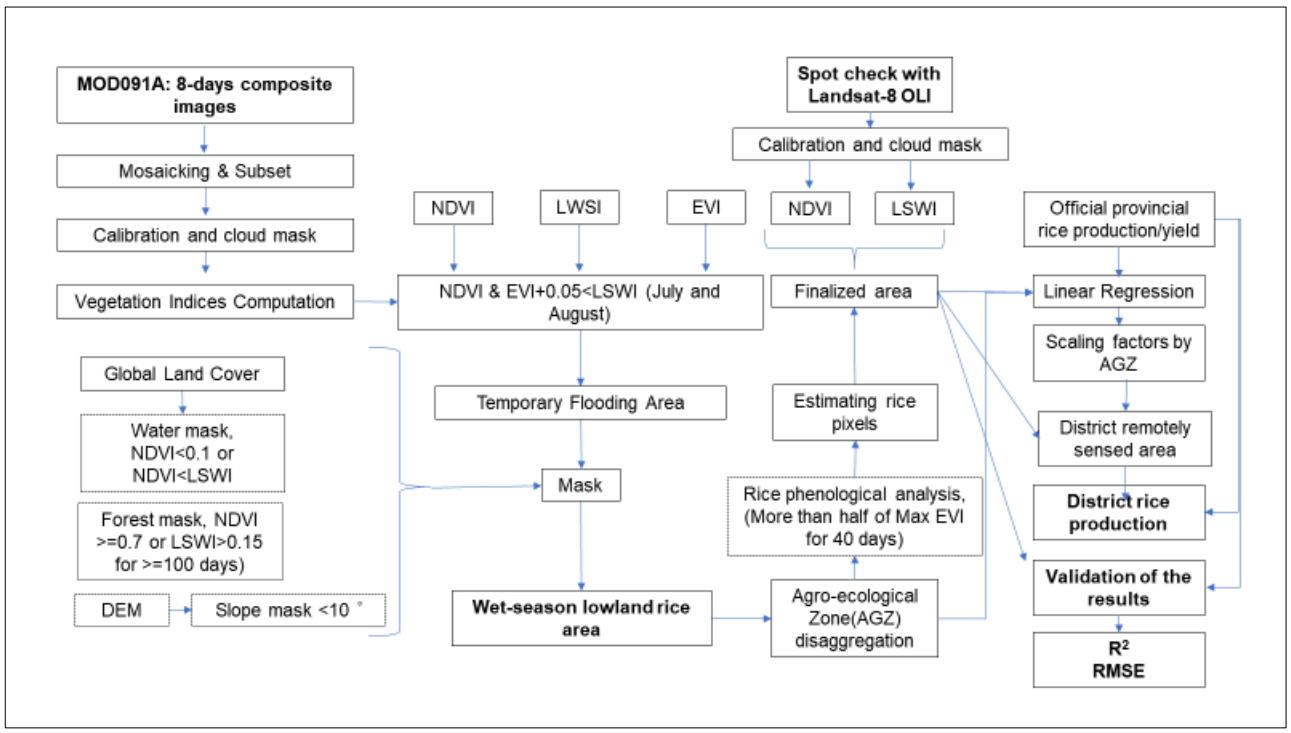

3.4 Pre-data analysis for MODIS images

3.4.1 Image extraction and sub-sets

MOD09A1 is in hierarchical data format (HDF). To extract the data required, a raster dataset was created to accommodate the individual band of the image. MODIS was the primary dataset used in this study to compute the NDVI, EVI, and LSWI. Therefore, the Red (620-670 nm), NIR1 (841-876 nm), Blue (459-479 nm), and SWIR1 (1628-1652nm) bands, or band 1,2,3, and 6, were extracted. The Data Management Tool, Create Raster Dataset, and Mosaic were all used. The specific details of the raster remain as the origin from the raw data such as the cell size of 463 metres x 463 metres, with the pixel type signed as 16 bits. The separated tiles were mosaicked together as one scene before masking that scene with the Data Management Tool, with the provincial administration boundary. Also, the output raster files were re-projected to 'PCS: WGS_1984_UTM Zone 48N' and 'GCS: WGS1984', which are the standard systems for the country (Suepa 2013).

3.4.2 Digital number conversion to reflectance number

The valid range of the digital numbers for MODIS data is -1,00 to 16,000. However, before the data analysis was conducted, the digital numbers were converted to reflectance numbers by adjusting them with a scaling factor of 0.0001, as recommended in the user manual (Vermote, EF, Roger & Ray 2015). The data range then became smaller, more convenient to analyse, and easier to apply any further necessary cut-off points or thresholds (Deus & Gloaguen 2013).

3.4.3 Cloud contamination removal

MOD09A1 offers geometrically corrected surface reflectance imagery with no cloud contamination (Vermote, EF, Roger & Ray 2015). Although the product was designed to avoid contamination from cloud cover, the issue remains. Thus, different studies which use the same products have been applied with a variety of approaches to address the cloud issue. Some studies used the smoothing algorithm such as the conditional temporal interpolation filter (Sun, H-s et al. 2009), while others used the empirical mode decomposition (Son et al. 2013). According to Sun, H-s et al. (2009), a smoothing approach affects the reflectance of the short wave infrared band, and so does the Land Surface Water Index. This study, however, relied on the reflectance of the Blue band, with a threshold of 0.2 and above being excluded (Son et al. 2014; Xiao et al. 2006). This approach was used because the Blue band is sensitive to the atmosphere and cloud cover. Thus, Figure 4(a) shows example where cloud presents, then 4(b) figure shows the cloud mask, and figure 4(c) illustrate an area where cloud was removed from a study area illustrated in 4 (d).

Figure 4. Cloud contaminated scenes

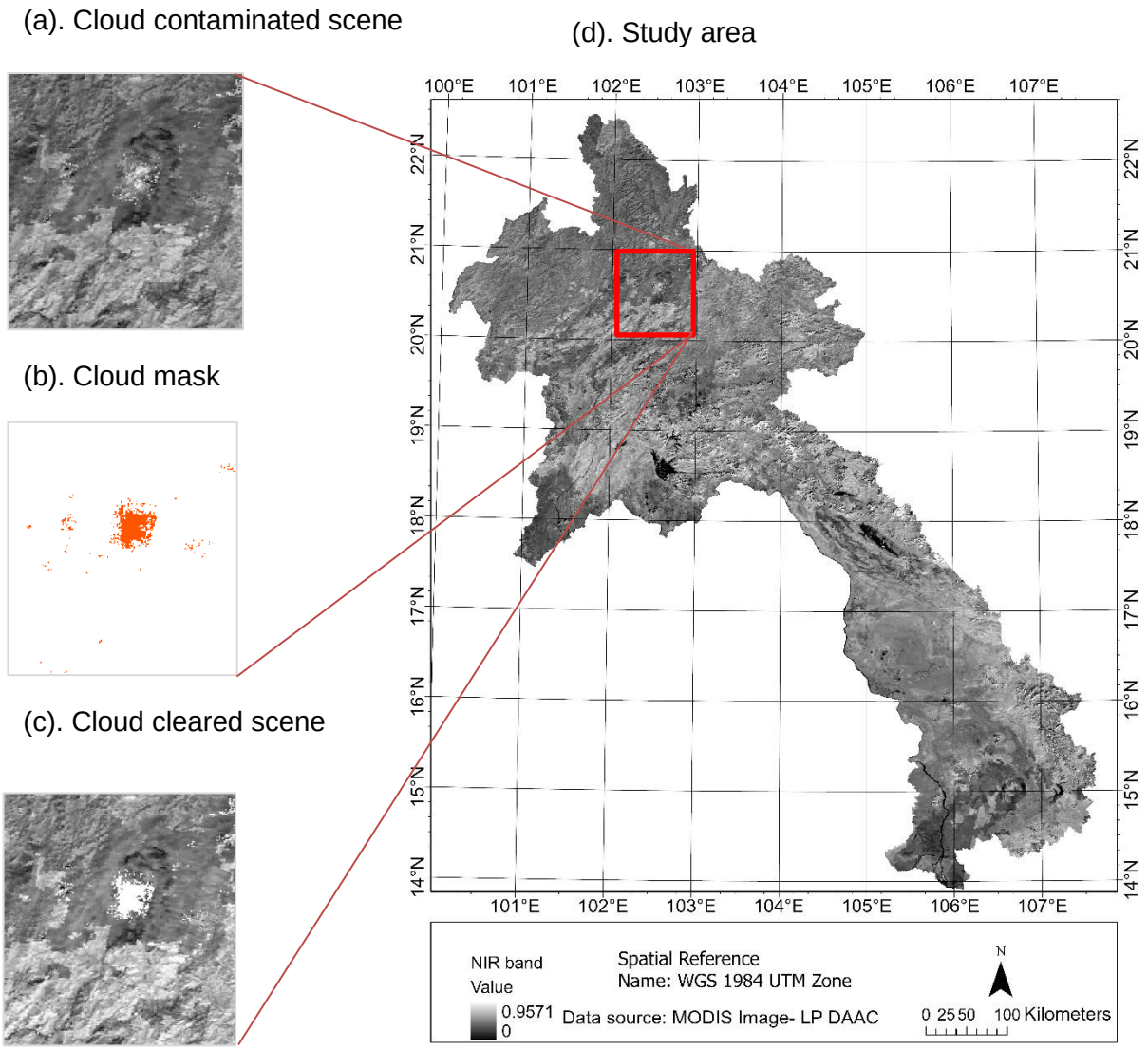

3.5 Pre-data analysis for images attained via Landsat-8 Operational Land Imaging (OLI)

3.5.1 Top of the atmosphere (TOA) reflection

Landsat-8 Operational Land Imaging (OLI) is a multispectral band satellite image that has a 30-metre spatial resolution and a 16-day temporal resolution. This level-1 product is radiometrically and geometrically corrected. It is provided with a high swath width of 190 x 180 kilometres, however, the images need atmospheric correction to calibrate the digital number to the reflectance radiance (Zanter 2016; Zhang, HK et al. 2018). Atmospheric correction helps to minimise the effects of the atmosphere by converting radiometric values into reflectance, so the data correctly represents the earth surface at that specific time and location, thus sun elevation angle was taken into account (González-Márquez et al. 2018; Zhang, HK et al. 2018). Since the purpose of using this imagery was to verify the trends of the NDVI and SLWI, only the relevant bands were extracted and corrected. Therefore, Band 4-Red (640-670 nm), Band 5-NIR (850-880 nm), and Band 6-SWIR1 (1570-1650 nm) were extracted and corrected for further processing. To convert DNS to the reflectance radiance of Landsat-8 OLI, the algorithm illustrated in Equation 3 was run with the additional inputs from the metadata provided with the product (Zhang, HK et al. 2018).

Equation 1. Landsat-8 OLI atmospheric correction adopted from Zanter (2016)

$$p\Lambda = (M_p * Q_{cal} + A_p)/\sin(\theta_{SE})$$

Where:

$p\Lambda$ = TOA reflectance

M_p = Reflectance multiplicative scaling factor for the band

Q_{cal} = Level-1 pixel value in DN

A_p = Reflectance additive scaling factor for the band

$\sin(\theta_{SE})$ = Local elevation angle of the sun

3.5.2 Elimination of cloud and cloud shadow for Landsat-8 OLI imagery

Cloud and cloud shadow severely affect the quality and availability of the optical image, especially during the rainy season. Any pixel contaminated with cloud needs to be eliminated because the cloud creates a bias against the actual reflectance of the object. As a result, the NDVI is lower (Zanter 2016). Fmask was developed to detect the cloud and cloud shadow in Sentinel-2 data as well as Landsat imagery (Zhu, Wang & Woodcock 2015). However, this study used the available cloud classification, or the quality assurance (QA) band, that is available from the Landsat-8 OLI level-1 product (Zhang, HK et al. 2018; Zhou et al. 2016). In order to use it effectively, this study

applied a tool which the USGS team provided. It is the ArcGIS tool which is available for download from this website: https://www.usgs.gov/land-resources/nli/landsat/landsat-quality-assessment-arcgis-toolbox. According to Zanter (2016), the pixel value of 2720 is classified as low cloud cover and cloud shadow, that could be reliable data. Thus, the other pixels, rather than this one, were classified as cloud cover and cloud shadow. Figure 5 (a) depicts the satellite image with cloud while image (b) shows the scene after the cloud is removed. Visually, the cloud effect remains around the edge of the contaminated area even though the well-developed algorithm was executed.

Figure 5. Cloud and cloud shadow elimination

(a) Before cloud exclusion

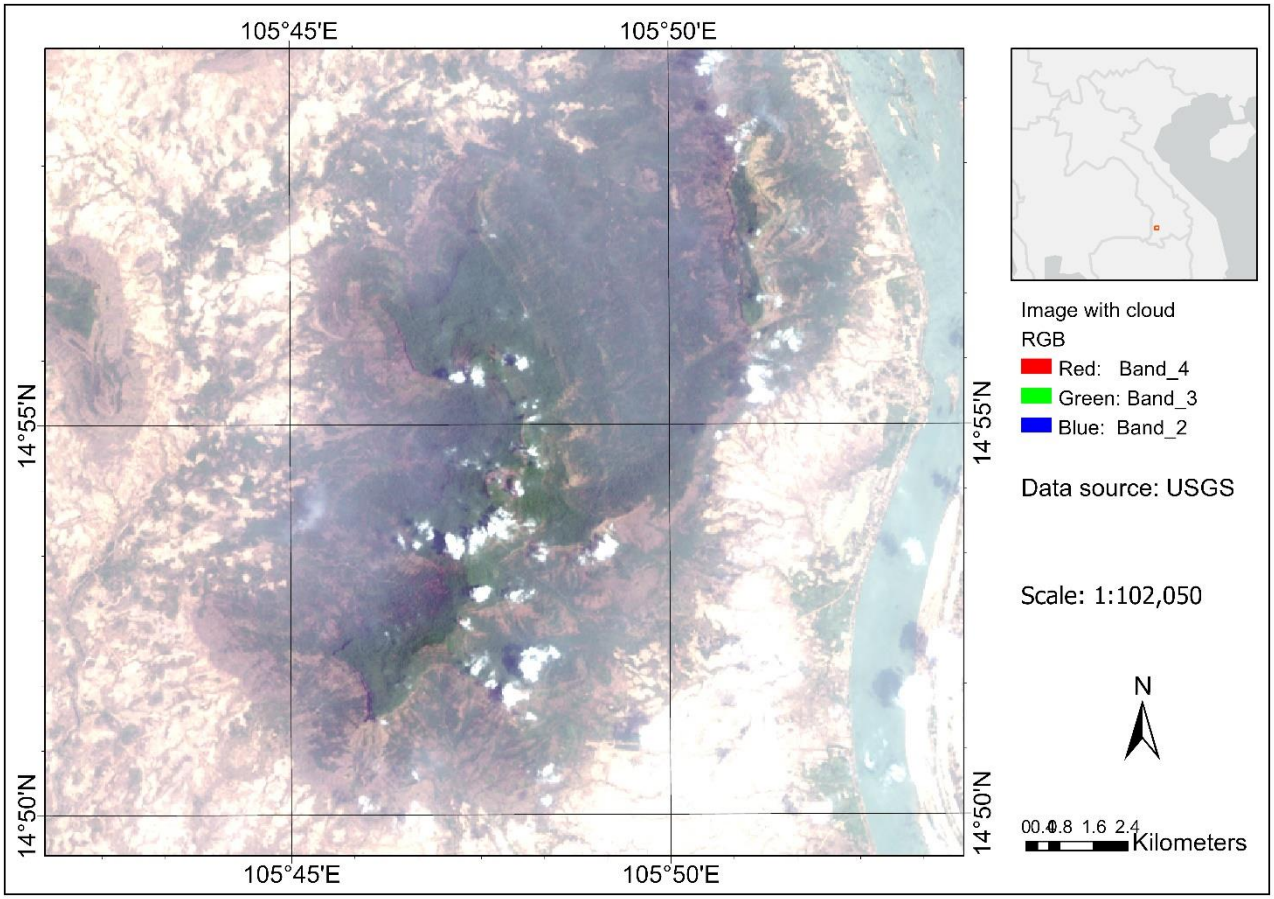

(b) After cloud exclusion

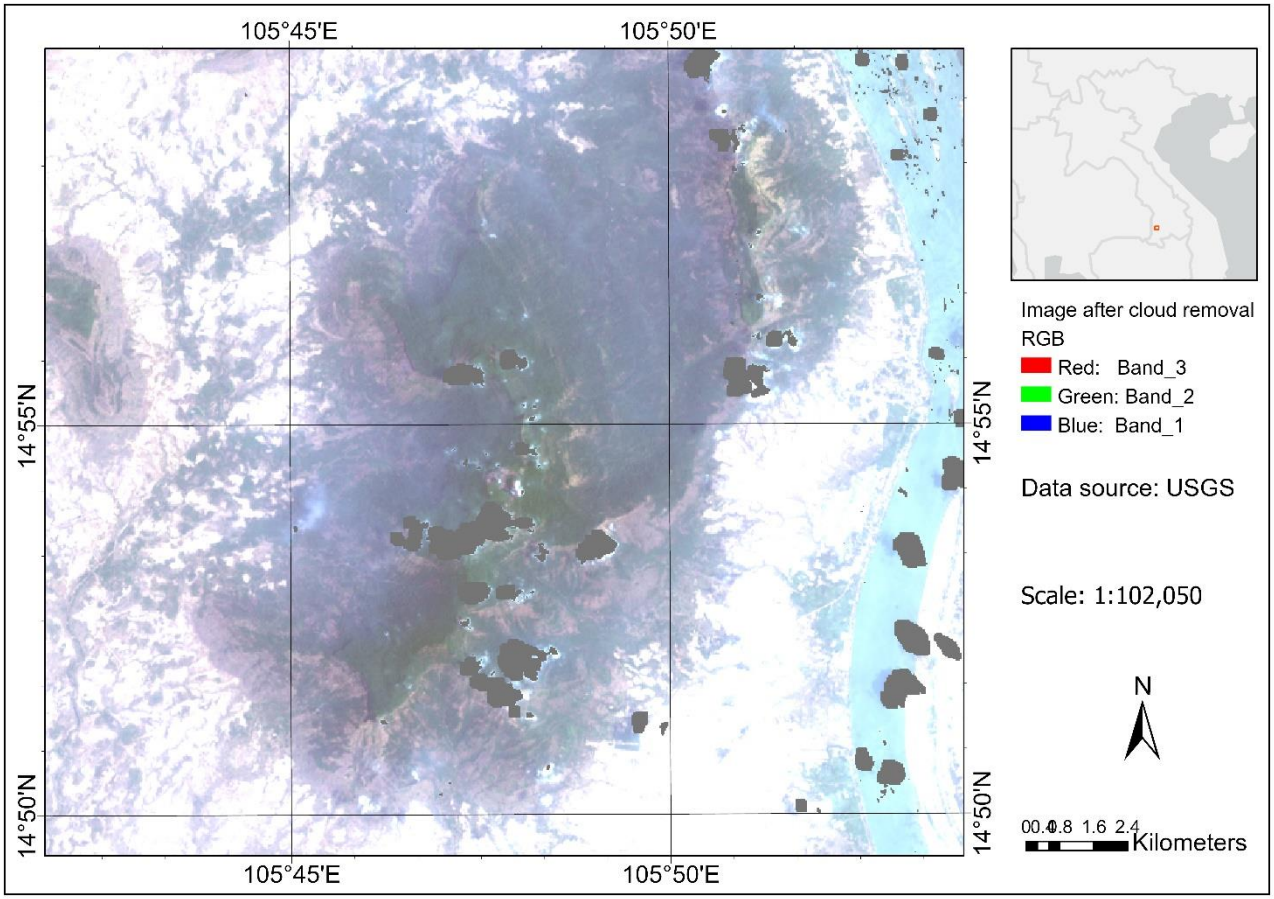

3.6 Algorithm for the detection of temporarily flooded areas using MODIS imagery

3.6.1 Normalised Difference Vegetation Index

The Normalised Difference Vegetation Index (NDVI) is the difference between the Red band, which has a wavelength from 620 to 670 nanometres, and the Near-Infrared band, which has a wavelength of 841 to 876 nanometres. In the process of photosynthesis by vegetation or tree leaves, chlorophyll absorbs visible light while it emits or reflects the Near Infrared energy (Chandrasekar et al. 2010). Thus, healthy vegetation reflects NIR strongly, and so this becomes evident in the NDVI. The NDVI has a high sensitivity to high biomass areas, atmosphere, and the soil background, which all influence the actual reflectance in crop phenology (Huete, AR et al. 1997; Wardlow, Egbert & Kastens 2007). Despite its weakness, the NDVI has a long and successful history in the monitoring of changes in vegetation, including of rice crops when viewed from space (Huang et al. 2013; Jensen 2007; Kogan 1990). However, this study used the NDVI to capture temporarily flooded areas, forest, and surface water, which were used as part of the

algorithm to delineate rice fields (Xiao et al. 2005; Xiao, He, et al. 2002). Please see Equation 2 for an algorithm of the NDVI.

Equation 2. Normalised Difference Vegetation Index algorithm

$$NDVI = \frac{P_{nir} - P_{red}}{P_{nir} + P_{red}}$$

Where:

p_{nir} = Near Infrared Band (841-876 nm)

p_{red} = Red Band (620-670 nm)

3.6.2 Enhanced Vegetation Index

The Enhanced Vegetation Index (EVI) is one of the Vegetation Indices which is used extensively in vegetation studies. The EVI is the improved version of the NDVI. The algorithm illustrated in Equation 3 includes several factors needed to exclude the weakness encountered in the NDVI. For instance, C_1 and C_2 are the coefficients used to prevent the effect of aerosols in the imagery by using the Blue band to adjust the reflectance in the Red band, where G is the gain factor (Wardlow, Egbert & Kastens 2007). Since the EVI minimises the sensitivity to the soil background and the dense canopy of vegetation, it reflects changes in crop phenology more effectively (Huete, Alfredo et al. 2002; Huete, AR et al. 1997). Thus, this study used the EVI as the supplementary variable to the NDVI for detecting rice fields as well as for the phenology trend analysis.

Equation 3. Enhanced Vegetation Index algorithm adopted from Jamali et al. (2011)

$$EVI = G \times \frac{\mathrm{P_{nir}} - \mathrm{P_{red}}}{(P_{nir} + C_1 \times P_{red} - C_2 \times P_{blue} + L)}$$

Where:

p_{nir} = Near Infrared band (841-876 nm)

p_{red}= Red band (620-670 nm)

p_{blue} = Blue band (459-479 nm)

L=1, C1=6, C2=7.5, and G=2.5.

3.6.3 Land Surface Water Index

The land surface water index (LSWI) is the ratio of the Near-Infrared and Short-Wave Infrared bands from the Multispectral band in optical imagery. This term was adopted from the Normalised Difference Water Index (NDWI), which is used for research regarding different types of water, including for detecting the moisture levels of vegetation (Gao, B-C 1996; Mosleh, M, Hassan, Q & Chowdhury, E 2015). While NIR is sensitive to vegetation, SWIR is sensitive to water, and so the moisture of soil and vegetation can be captured from space (Chandrasekar et al. 2010; Gao, B-C 1996; Jackson et al. 2004). Therefore, this study adopted the LSWI as part of the algorithm for detecting temporarily flooded areas during the rice transplanting stage, so that the rice fields can be separated from other terrain (Bridhikitti & Overcamp 2012; Dong & Xiao 2016; Xiao et al. 2006; Xiao et al. 2005). The computation of the LSWI requires the Multispectral band image. In this study, the reflectance values for the Near-Infrared Band, which has a wavelength of 841 to 879 nanometres, and the reflectance radiance for the Shortwave Infrared Band, which has a wavelength of 1628 to 1652 nanometres, were used. Please see algorithm of the index below for more information.

Equation 4. Land and Surface Water Index

$$LSWI = \frac{\mathrm{P_{nir}} - \mathrm{P_{swir}}}{P_{nir} + P_{swir}}$$

Where:

p_{nir} = Near Infrared band (841-876 nm)

p_{swir} = Short wave infrared band (1,628-1,652 nm)

3.6.4 Temporary inundation detection algorithm

While different studies have applied different classification techniques to map the extent of rice cropping, the classification techniques used depended on the type and resolution of the satellite imagery those studies intended to use. This study used Multispectral band satellite imagery with a 500-metre spatial resolution to map the extent of rice farming on a country scale. Thus, a pixel-based temporary flooding analysis of the rice fields is essential (Bridhikitti & Overcamp 2012; Dong & Xiao 2016; Xiao et al. 2006; Xiao et al. 2005). This study applied the algorithm developed by Xiao et al. (2005). It used both the NDVI and the EVI as part of the algorithm to capture the temporarily flooded areas of the rice fields when farmers transplant their rice seedlings. In this algorithm, LSWI is used to estimate the beginning of the rice transplanting, while the NDVI and the EVI are used to understand the ‘greenness’ and changes in the ‘greenness’ of the rice crops (Mosleh, M, Hassan, Q & Chowdhury, E 2015).

The algorithm used in this study was adopted from Xiao et al. (2005), in which it was assumed that there is more water than the rice crop found in the initial stage of the rice-growing cycle (Equation 5). The algorithm, however, involved a parameter of 0.05, which is the global threshold to ease the detection of flooded areas. This parameter varies from study to study, depending on factors such as seasonality, region, aquatic plant, and rice variety. Since these factors influence the reflectance of the LSWI and EVI/DNVI during the rice transplanting stage, this parameter sometimes needs a higher value to ensure rice fields are detected (Peng et al. 2011; Sun, H-s et al. 2009).

Rice transplanting dates are different from one country to the next and even from one Agro-Ecological Zone to the next, making it difficult to define in general terms. In Lao PDR, according to Linquist et al. (2006), farmers generally start transplanting rice in late June to July. This study took the variation of the onset of the rainy season into consideration. Based on the report from the most recent assessment, the variation is about ten days (Krishnamurthy, Chong & Poungprom 2015). Also, some studies emphasise that due to the drought-like conditions in this particular year, the transplanting of rice was delayed until late August (Ikeura et al. 2016). Therefore, the temporal analysis of temporarily inundated areas was conducted from July to August. The date of rice transplanting can be identified from the observation of the vegetation pattern against the water index; for instance, when the NDVI or the EVI is lower than the water index (Xiao et al. 2006; Xiao, Boles, et al. 2002; Xiao et al. 2005).

Equation 5. Temporary flooding algorithm

$$\boldsymbol{TFA = LSWI + P \geq NDVI \; or \; EVI}$$

Where:

$TFA =$ Temporary flooding area

$P =$ Parameter (0.05)

3.7 Non-rice area masking

3.7.1 Permanent water mask

While there are many different techniques to separate water from other features, Xiao et al. (2005) developed a useful algorithm in this regard by assuming that water refers to the condition when the vegetation is lower than the water. Permanent water has long-lasting flooding, so the water is only considered if any pixel is flooded for more than 20 composites, or more than 160 days (Xiao et al. 2006; Xiao et al. 2005). However, this study took into account the time that rice crops can survive while being completely submerged under water. Rice crops can grow well in wet conditions, however, rice crops cannot tolerate continued flooding for more than fourteen days because they need oxygen and the sun's energy to survive (Hattori, Nagai & Ashikari 2011).

Thus, this study considered permanent water as areas which are flooded for more than 16 days (Equation 6). Also, due to the effect of cloud contamination in different MODIS time series, it misses some water bodies. It is essential to find an auxiliary dataset to resolve this issue. Fortunately, the global land cover map was developed at almost the same time as the study and is available for use. The 300-metre spatial resolution Global Land Cover Map from the CCI-LC project provides a crucial contribution in this water mask development. In this study, the Global Land Cover water layer was resampled using the same grid as with MODIS spatial resolution. After that, the study merged the data with the computed water body and used it to exclude water from the potential rice areas. Also, Figure 6 illustrates where computed water and GLC complemented each other.

Equation 6. Surface water algorithm

$$Surface\ Water = NDVI < 0.1\ or\ NDVI < LSWI$$

Figure 6. Contribution of Land Cover Map to the development of the water mask

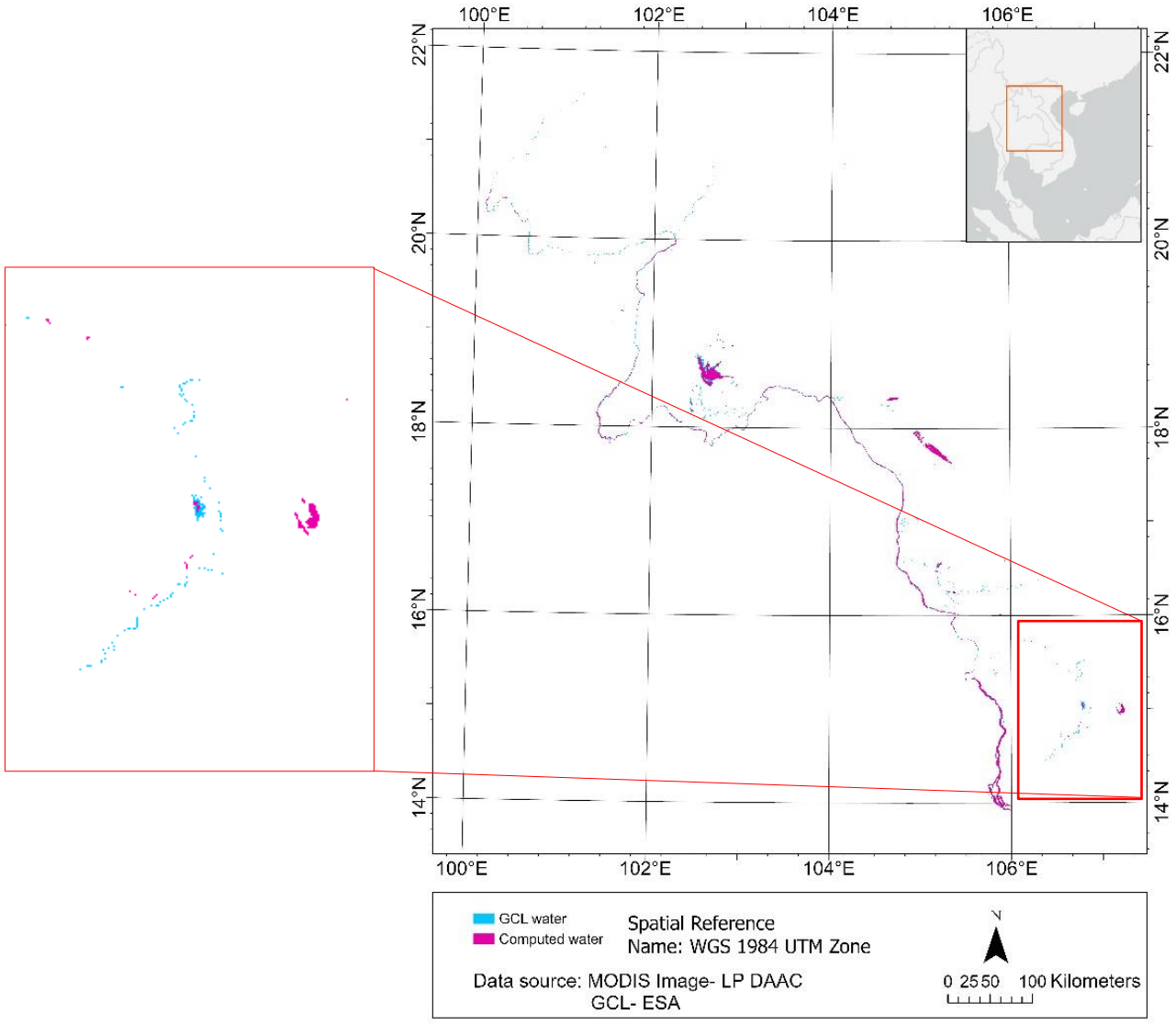

3.7.2 Evergreen forest and shrub mask

The spectral profile of the forest and shrubbery can be confused with one of the rice crops. However, the temporal analysis of the vegetation index is the key to distinguish evergreen forest and even small 'forests' such as shrubs in a rice field. Forest and shrubbery refer to the pixels that have a consistently high NDVI over the years (Peng et al. 2011). Different studies have adopted different thresholds to determine evergreen forests. For instance, the NDVI is more significant than 0.5 (Dao & Liou 2015), while Xiao et al. (2005) assigned any pixel that has an NDVI value equal to or more significant than 0.7, or any pixel that has an LSWI value higher than 0.15 for about 160 days, as a forest mask. This study adopted the 0.7 threshold developed by (Xiao et al. 2005). However, this included more than 80 days (about 50 per cent more) of the temporal data due to some pixels being removed due to cloud contamination. Please see equation 7 below for more information.

Equation 7. Algorithm of evergreen forest and shrubbery adapted from Xiao et al. (2005)

$$Evergreen\ forest\ and\ shrubbery = NDVI \geq 0.7\ or\ LSWI > 0.15$$

3.7.3 Slope masking

The raw data used to compute slope is the SRTM – the digital elevation model (DEM) which was downloaded from the USGS database. Using the Spatial Analyst tool that is available from ArcGISPro, the slope layer was computed. Xiao et al. (2005) eliminated the area above an altitude of 2,000 metres and any areas sloping higher than two degrees out of their study. However, this study found that lowland paddy rice is grown in almost every altitude of elevation where flat land exists (Linquist et al. 2006). Therefore, to maintain the flat area, this study excluded any pixels greater than 10 degrees in slope, regardless of the elevation, because of the associated vertical errors of the SRTM-DEM in the different continental regions which range from 5 metres to 10 metres (Gesch, Muller & Farr 2006).

3.8 Estimation of rice pixels

3.8.1 Extraction of the potential rice area and vegetation indices by Agro-Ecological Zone (AEZ)

Six Agro-Ecological Zones (AEZ) were identified in Lao PDR. They are the Vientiane Plain, the Northern Lowlands, the Northern Highlands, the Mekong Corridor, the Central and Southern Highlands, and the Bolaven Plateau (Li, El Solh & Siddique 2019). In order to estimate the date of rice transplanting and its growth pattern, the potential rice area and vegetation indices were extracted for the individual AGE zones. The data management tool "Extract by mask" in ArGISPro was used to extract potential rice fields and vegetation indices from each Agro-Ecological Zone. However, due to cloud contamination, the Bolevan Plateau AEZ was excluded from the data analysis. Rice phenology change analysis in this study focused on the EVI and LSWI from May to

November for rainfed, lowland rice (Linquist et al. 2006). Since cloud contamination can affect the temporal analysis of rice crops, it is essential to have sufficient pixilation or data to allow for this analysis. However, in this study, any time series that had cloud contamination beyond 50% was excluded before the temporal analysis was performed by using a trend line graph of the EVI and LSWI. Appendix 2 illustrates further information about the AEZs.

3.8.2 Spot check of VIS trend

Verification of the vegetable indices was carried out using Landsat-8 OLI imagery. The intention was to use the higher spatial resolution imagery to double-check if those vegetation indices computed with MODIS data are accurate. Two AEZs, the Vientiane Plain and the Mekong Corridor, were selected. These two zones were selected because they have the highest proportion of rice production. To carry out a spot-check, the area of interest (AOI) was digitised based on the pixel of potential rice area that was already identified using MODIS data. After the AOI within the potential rice fields was created, the NDVI and LSWI were extracted from the indices computed with Landsat-8 OLI imagery. The line plots were created to compare if the trends of the Lansat-8 OLI and MODIS are identical. An AOI area of 103 square kilometres was created in the Vientiane Plain AEZ and an AOI of 137 square kilometres was created in the Mekong Corridor AEZ.

3.8.3 Finalisation of the rice mapping

With MODIS data at a spatial resolution of 500 metres, a pixel can include non-rice areas such as canals and grassland. If this data remains, it can affect the quality of rice yield forecasts where identified rice fields contain no rice. It is essential to ensure that the rice extent contains pixels with rice crops. Some studies which offer better data to cross-check this information, such as field missions, could potentially address this issue. Due to the weakness of the NDVI, for instance, because of the effect of the atmosphere or saturation in areas with high biomass, the EVI was chosen as the indicator to detect vegetation changes in the rice cycle (Sun, H-s et al. 2009). To estimate the number of rice pixels, it was assumed that a rice pixel is a pixel with a potential value of the EVI. Thus, if any pixel has at least more than half of the maximum EVI value in the growing cycle for more than 40 days following the transplanting date, this pixel was assigned as a rice pixel (Bridhikitti & Overcamp 2012; Xiao et al. 2006; Xiao et al. 2005).

3.9 Estimation of district rice production

3.9.1 Scaling factors analysis with simple linear regression

While the provincial rice yield is available, the more useful data is at the district and smaller spatial levels. Thus, it is crucial to estimate rice production at the lowest possible level. In order to estimate rice yield at the district level, the scaling factor of the district yield was required. In order to find the district rice yield, the Linear Regression model in each AEZ was carried out. The study assigned the provincial rice yield as the dependent variable and the remotely sensed rice area as

an independent variable (Son et al. 2013). Different AEZs may result in different yields because each zone has a different climate and soil quality. Within each AEZ, several provinces and districts are part of the zone. However, vice versa, one province may be spread across more than one zone. This study assumed that the subordinated districts has the same yield as of its AEZ. Thus, to estimate the yield of each AEZ, the estimated area was summarised by province using the Zonal Statistics as Table tool from ArcGISpro. The zonal estimated extent of rice was joined into the provincial vector files that have the same format with one of the yields. Then, the provincial rice yield and estimate area were intersected with AEZ. Thus, AEZ had its corresponding province's data. The attribute table was transferred into Excel spread sheet before, the Simple Linear Regression model was run by AEZ to determine the yield of individual AEZs using the equation displayed in Equation 8. Also, Appendices 8 and 9 display zonal rice yield and planted area from Lao Statistics Bureau.

Equation 8. Linear regression model

$$Y = b\,X + a$$

Where:

Y =Yield/scaling factor

X =Remotely sensed area

b =Slope

a =Intercept of Y

With one AEZ being excluded from the analysis, only five regression models were carried out. The Vientiane Plain had four data points for four provinces, the Northern Lowlands model had twelve provinces or points, the Northern Highlands had eleven, the Mekong Corridor six, and the Central and Southern Highland model had six data points also.

3.9.2 Rice yield interpolation with the Dasymetric modelling technique

Once the rice yield or scaling factor of each AEZ becomes available, the process of estimating district rice production becomes possible also. A number of studies have applied the average value of vegetation indices derived from the heading stage, which is the critical stage of rice reproduction as a predictor to estimate rice yield (Cai & Sharma 2010; Huang et al. 2013; Son et al. 2014). This study used the traditional cartographic mapping technique; for instance, 'Dasymetric' Mapping, which is used extensively to address the spatial information gap in population statistics (Su, M-D et al. 2010). The strategy was to apply the available aggregated rice yield statistics at the provincial and AEZ levels into a smaller spatial scale and make small-area estimates using the auxiliary dataset (Petrov 2012). Since the estimated rice extent is spatially

distributed at the pixel level, so this dataset was used as a bridge to interpolate the rice yield for each pixel (Cai & Sharma 2010). First, the process involved summarising the remotely-sensed areas into district levels using the Zonal Statistics as Table tool in ArcGISPro and then merging this information into district boundaries as a vector file. This vector file was then converted to the raster format, which used the same grid as MODIS data at a 500-metre spatial resolution, while keeping all the other parameters the same as the input file. A similar technique was carried out for rice yield at the AEZ level. Thus, the two raster files that were in the grid were available for use. Finally, the rice yield and the estimated extent of rice were further processed to generate district rice production following a formula illustrated in Equation 9 below.

Equation 9. Formula for forecasting rice production

$$P = A * Y$$

Where:

P = Rice production (Tonnes)

A =Remotely sensed area (Ha)

Y =Rice yield (Tonnes/Ha)

3.10 Validation of the results

The credibility assessment of the method is another essential element to help analysts understand how robust the methodology is. Ideally, accuracy assessment involves some field missions and independent images. They can be used as a reference image to make comparisons. However, in absence of such imagery, this thesis adapted the two methods of mean error and root mean square error to determine how accurate the results of the study are (Clauss et al. 2018; Son et al. 2014).

3.10.1 Correlation of the remotely-sensed area and official figures by Agro-Ecological Zone and province

Given the lack of field mission or ground truth data, the accuracy assessment of the results of this study used an alternative method. A comparison of estimated results with available official statistics was applied extensively as the preferred option or in response to the absence of field information (Gumma et al. 2014; Peng et al. 2011; Son et al. 2014). Thus, a scatter plot or linear regression model was applied to evaluate the relationship of the estimate and statistics, so that consistency of the results can be measured (Su, X, Yan & Tsai 2012).

The calculation of this relationship is simple. The remotely-sensed rice area was assigned as the independent variable, while the provincial rice planted area was an independent variable (Dao &

Liou 2015). The squared value and correlation coefficients were assessed to evaluate the robustness of the study methods. The significant relationship of the estimate and results indicate that the method applied to estimate the results are valid (Cai & Sharma 2010; Xiao et al. 2006; Xiao et al. 2005).

Six simple linear regression models were carried out. This included five models for each AEZ and the national model that used all 18 provinces or data points for analysis. Equation 10 illustrates how the analysis was executed.

Equation 10. Linear regression model

$$Y = b\,X + a$$

Where:

Y =Yield/scaling factor

X =Remotely sensed area

b =Slope

a =Intercept of Y

3.10.2 Root Mean Square Error

In this study, the root means square error (RMSE) and the mean absolute error (MAE) were applied to validate the results of the study. Due to the unavailability of rice production at the district level, the provincial land area of rice was therefore used for analysis against the actual data from the official source. It was assumed that if the RMSE and MAE are between 10-20%, the estimated results would be considered reasonable. The study method is indicated as robust when both the RMSE and MAE are less than 10% compared to the actual data (Son et al. 2014). The root mean square error measures the weighted average error of the difference between the estimate and the actual statistic. By contrast, the mean absolute error measures the weighted average of absolute errors. The difference between the two is the sensitivity to the scale of errors. While the MAE is less sensitive to errors, the RMSE aims to detect a large number of errors in the comparison (Willmott & Matsuura 2005). Calculation of these two statistics is simple and the below equation illustrates how to compute them. Equation 11(a) illustrates how the root mean square error was computed, while equation 11(b) shows how the mean square error was calculated.

Equation 11. Algorithm for the Root Mean Square Error

$$(a).\qquad RMSE = \sqrt{\frac{1}{n}\sum_{i=1}^{n}(\widehat{y_i} - y_i)^2}$$

$$(b).\qquad MAE = \frac{1}{n}\sum_{i=1}^{n}(\widehat{y_i} - y_i)$$

Where:

n = Number of provinces,

$\widehat{y_1} =$ Official rice planted area,

$y_i =$ Estimated rice extent

CHAPTER FOUR: RESULTS

4.1 Results of MODIS data pre-processing

4.1.1 Spectral profile investigation results of the MODIS data

MOD09A1 is an atmospherically and geometrically corrected product. However, radiance is converted to the standard reflectance scale of 0 to 1 (Deus & Gloaguen 2013). The data analysis was based on the scale of the corrected image. To ensure the data used in the study correctly represented the Earth's surface, a spectral profile investigation for some key features was carried out. The spectral profile is a measure of reflectance in proportion to an object's response to the sun's energy known as electromagnetic radiation. Objects on the Earth's surface respond to this energy differently depending on the physical and chemical composition of the object. Figure 7 illustrates the spectral profile of vegetation, water, bare soil, and built-up. It found that vegetation has low reflectance in the visible wavelength (Blue, Green, and Red) because the chlorophyll of healthy vegetation absorbs electromagnetic energy while its reflectance is high in the NIR band. Bare soil results in an increasing reflectance where higher wavelengths are needed to detect it, for instance, in the NIR and SWIR bands. This similar behaviour was observed for the built-up. By contrast, water has low reflectance in all wavelengths because it absorbs energy (Jensen 2007; Khorram et al. 2012). However, in this case water was mixed between rivers and wetlands where different quality of water presented and resulted in higher reflectance in some spectral bands.

Figure 7. Spectral profile investigation results

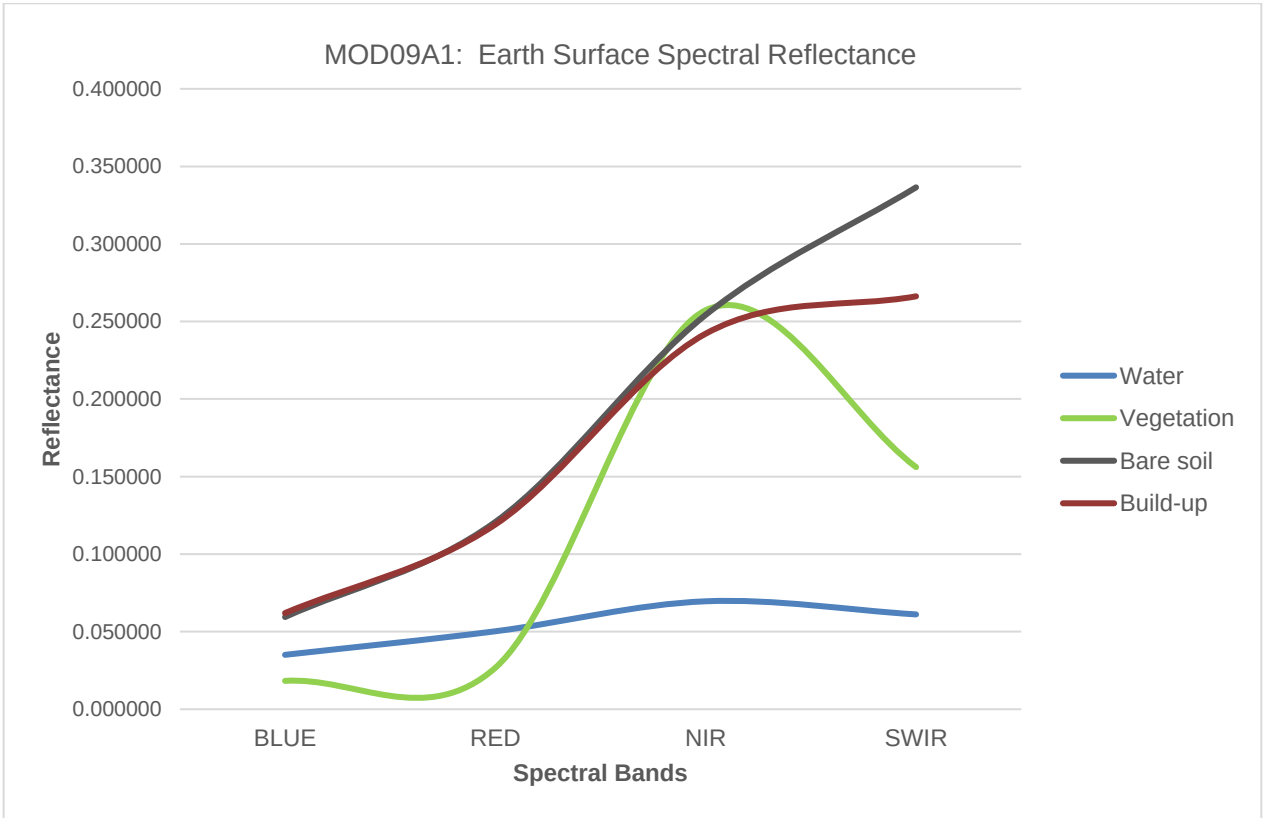

4.1.2 Cloud mask and cloud exclusion

Cloud detection and cloud elimination were carried out on all satellite scenes before data analysis. Based on the analysis of this data, it was discovered that cloud contamination is high during the monsoon season running from mid-May until late September. However, not all time series of this type of imagery were damaged with high amounts of cloud cover. Figure 8 indicates the overall cloud percentage over the whole year with a focus on the monsoon season. It shows that during the non-monsoon season, from November to April, the percentage of cloud cover is lower than 10%. However, during the monsoon season from May to October, some time series were affected by up to 70% cloud contamination.

The time-series analysis of rice crops was carried out by AEZ, and the cloud percentage for each time series in each AEZ is presented in Appendices 11-15. The temporal analysis of the vegetation index of rice fields needs sufficient pixilation to allow for a reliable fluctuation of vegetation in each time series, so imagery with cloud cover above 50% was excluded from the temporal analysis in turn. Appendix 11 illustrates cloud contamination over the Vientiane Pain AEZ. It shows that there are three time series which have cloud cover higher than this threshold; for instance, on May 24, August 12, and September 5.

The percentage of cloud cover in the Northern Highlands AEZ ranges from 1% in the dry months to 64% during some months of the wet season. In this AEZ, there are three time series that were contaminated with cloud cover beyond 50%, being August 12, August 28, and September 5 (see Appendix 12). Furthermore, in the Northern Lowlands AEZ, the percentage of cloud cover is up to 70% during some of the wet months (see Appendix 13). The contamination of cloud cover was even more severe in the Mekong Corridor AEZ, in which some time-series images were damaged by cloud cover as high as 61% on September 5, 70% on June 25, and 81% on August 12 (Appendix 14). Also, the severe effect of cloud cover was observed in the Central and Southern Highlands AEZ, with four time series being affected by more than 50% of cloud cover (Appendix 15).

Figure 8. The overall percentage of cloud contamination during the rice-growing season

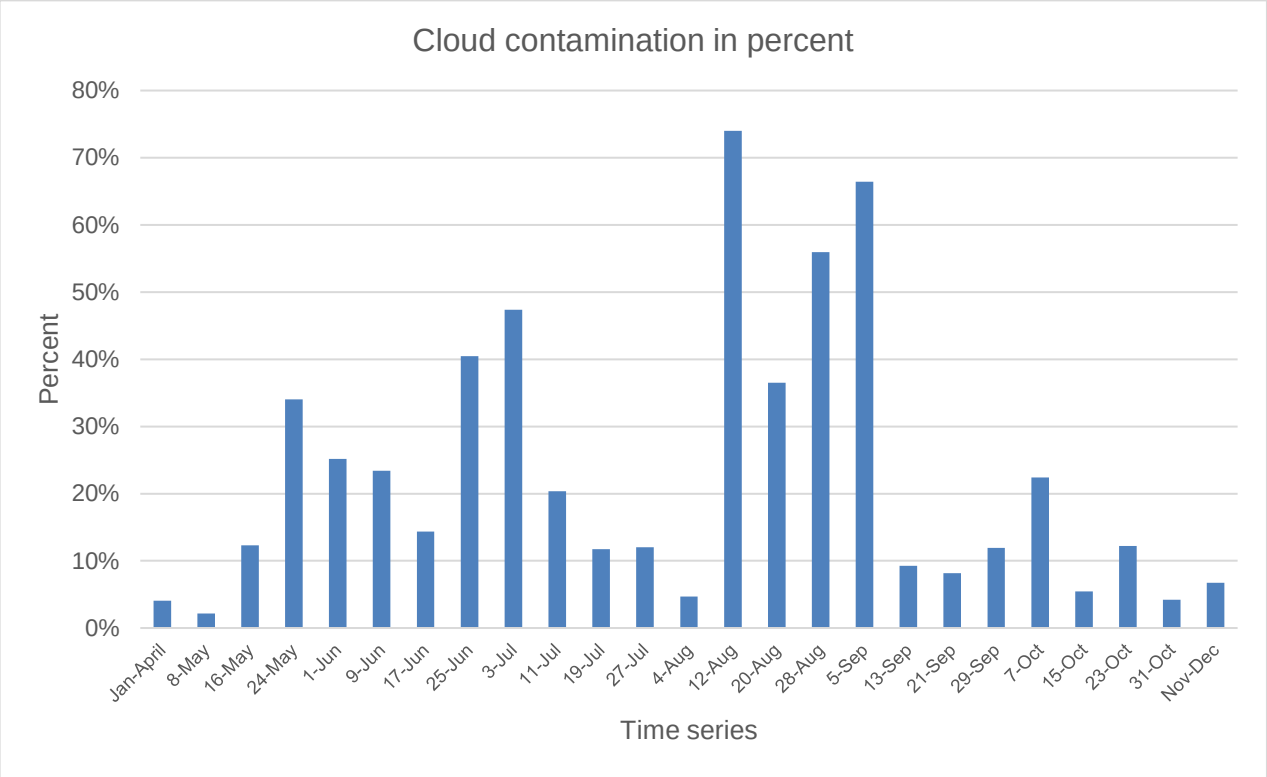

4.2 Results of Landsat-8 OLI data pre-processing

4.2.1 Top of atmosphere reflectance and spectral profile investigation

Similarly, the dataset that was used to verify the results of the vegetation index derived from MODIS needed to be investigated for whether the reflectance is correct. Overall, this investigation found that all the selected features of water, vegetation, bare soil, and build-up are consistent with the other corrected image. Figure 9 shows that vegetation has low reflectance in bands 2, 3, and 4 (Blue, Green, and Red), and high reflectance in band 5 (Near Infrared). This consistency is found also for bare soil, builtt-up, and water.

Figure 9. Spectral profile investigation results

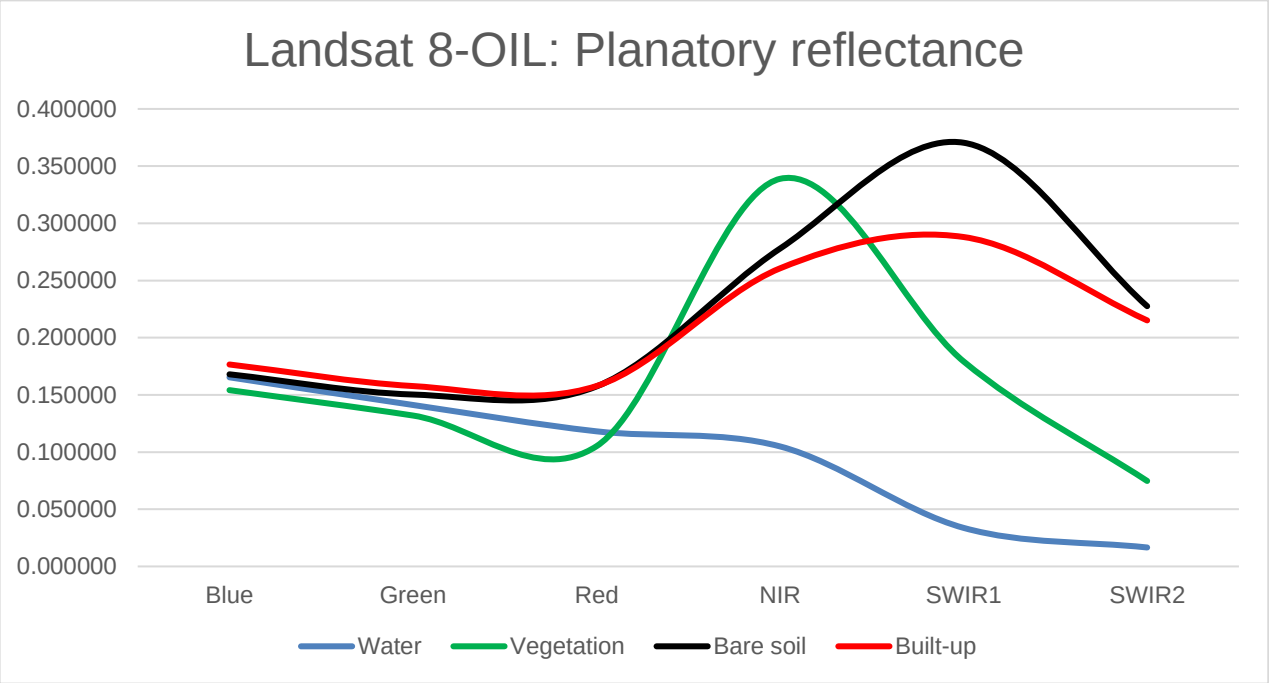

4.2.2 Cloud cover and shadow exclusion in Landsat imagery

Since cloud is a typical issue during the optical time for rice farming, it is difficult to find images with no cloud cover or shadow for an equal period to complete the time-series image. The problem is critical for Landsat imagery that has a lower temporal resolution, for instance, 16 days. However, from the available scenes obtained for this study, the cloud occupies up to 30% of the imagery in scene (a) and nearly 60% in scene (b), as displayed in Figure 10.

Figure 10. Cloud contamination in the spot-check site

(a) Scene 1 - Vientiane Plain

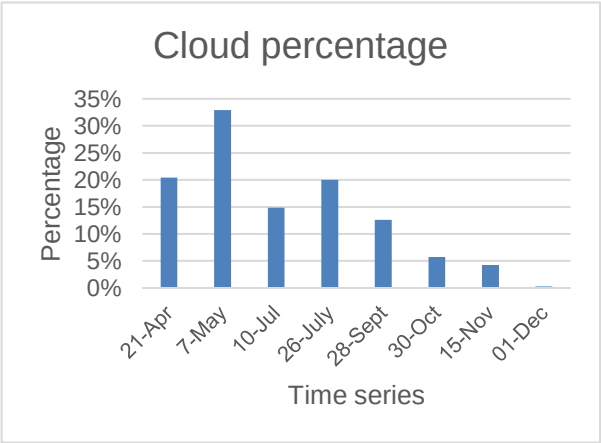

(b) Scene 2 - Mekong Corridor

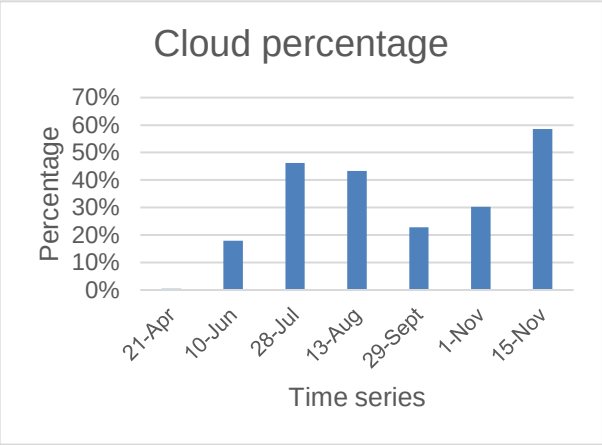

4.3 Results of vegetation and water indices

4.3.1 Normalised Difference Vegetation Index (NDVI)

The Normalised Difference Vegetation Index (NDVI) is a ratio between the Red and NIR bands of the optical image, ranging from -1 to +1. The NDVI measures photosynthesis activity of vegetation on the Earth's surface. A high NDVI refers to the density of 'greenness', indicating healthy vegetation, while a low NDVI indicates the moisture stress that occurs with unhealthy vegetation. Applications of the NDVI vary in science, for instance, it can be used for drought monitoring (Chandrasekar et al. 2010) or including crop yield estimations (Huang et al. 2013). The application of the NDVI in this thesis project was to detect the temporary flooding period of rice crops when farmers transplant their rice. Specifically, the NDVI is useful to estimate bodies of water and forest cover, enabling the process of separating rice fields from other areas (Sun, H-s et al. 2009; Xiao et al. 2006; Xiao et al. 2005). Figure 11(a) shows the satellite image of the base map indicating one part of the study area. The purpose here was to check if the NDVI, which is shown in 11(b), correctly computes and represents different land cover. Thus, Figure 11(b) illustrates how the NDVI represents features of the Earth's surface in one of the time series. In this picture, the green colour refers to areas of vegetation. By contrast, yellow through to red refer to bare soil and bodies of water which lack green vegetation.

Figure 11. NDVI representation of the Earth's surface

(a) The Earth's surface (b) NDVI

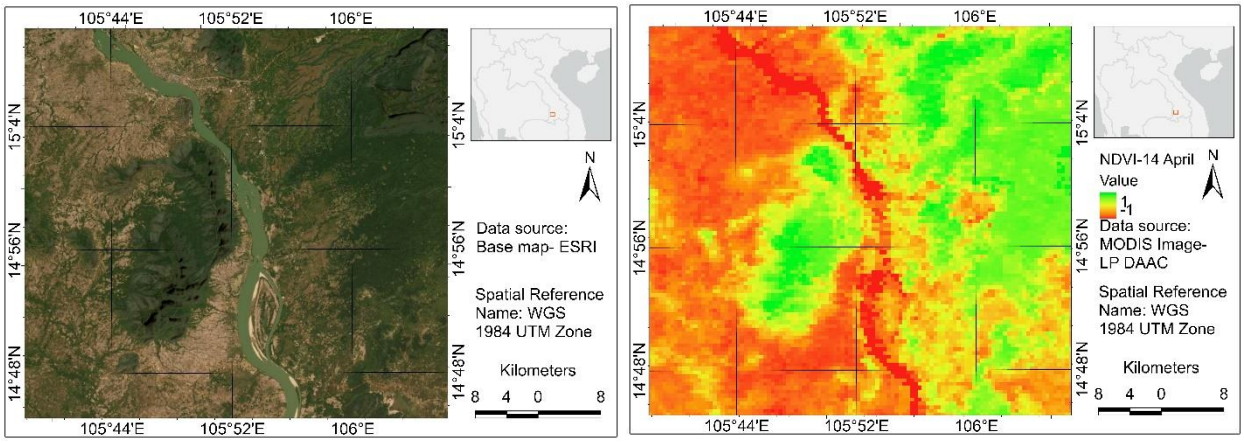

4.3.2 Enhanced Vegetation Index results

The Enhanced Vegetation Index (EVI) is the improved version of the NDVI. If compared with the NDVI above, the EVI represents the features better, for instance, the Mekong River or water is shown with the EVI better than what the NDVI can display. The reason for this is due to sensitivity to the effects of atmosphere, vegetation, and soil background, which were all removed. Similarly to the NDVI, the EVI is widely applied in crop yield estimates, and most likely this index offers an alternative to the NDVI for rice yield estimates given its lower sensitivity to the issues described above (Son et al. 2013). The application of the EVI in this study is crucial, for instance, in contributing to the detection of temporarily flooded areas of rice as well as the contribution to the finalisation of the rice yield forecasts. The EVI presents the Earth's surface in the ratio of -1 and +1. Also, Figure 12(b) illustrates how the EVI responds to the environment.

Figure 12. Response of the EVI to the environment

(a) The Earth's surface (b) EVI

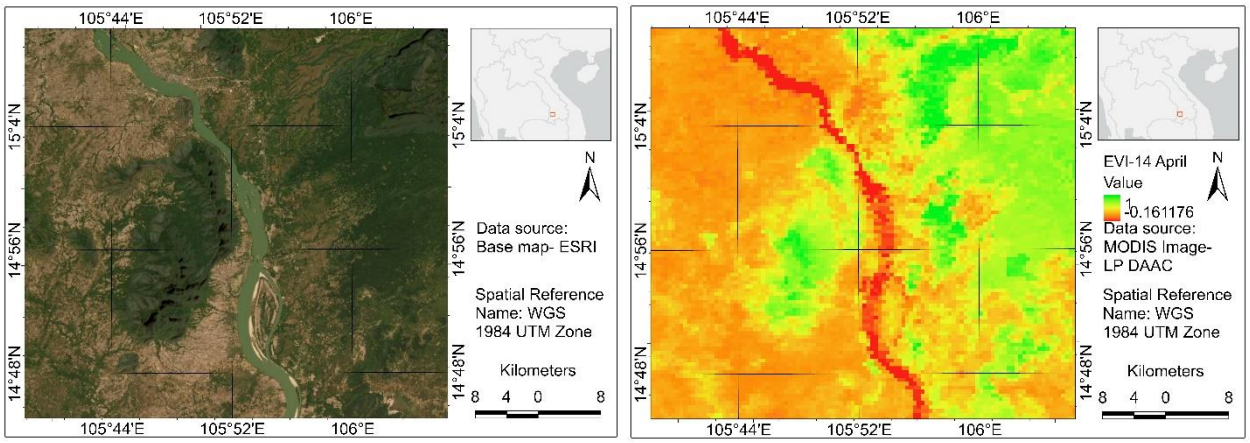

4.3.3 Land and Surface Water Index results

The Land Surface Water Index measures the moisture element of the vegetation canopy which interacts with sunlight (Gao, B-C 1996). Same as the other vegetation indices, the ratio of the liquid content of water or moisture ranges from -1 to +1. A low value in the LSWI indicates a low level of moisture in the vegetation while a higher value signals higher levels of moisture and bodies of water. Figure 13(b) illustrates how features on the Earth's surface interact with the sun's energy. Vegetation and rivers reflect high LSWI in blue while dry and bare soil reflects low moisture in yellow through to red.

Figure 13. Liquid water content of vegetation measured with LSWI

(a) The Earth's surface

(b) LSWI

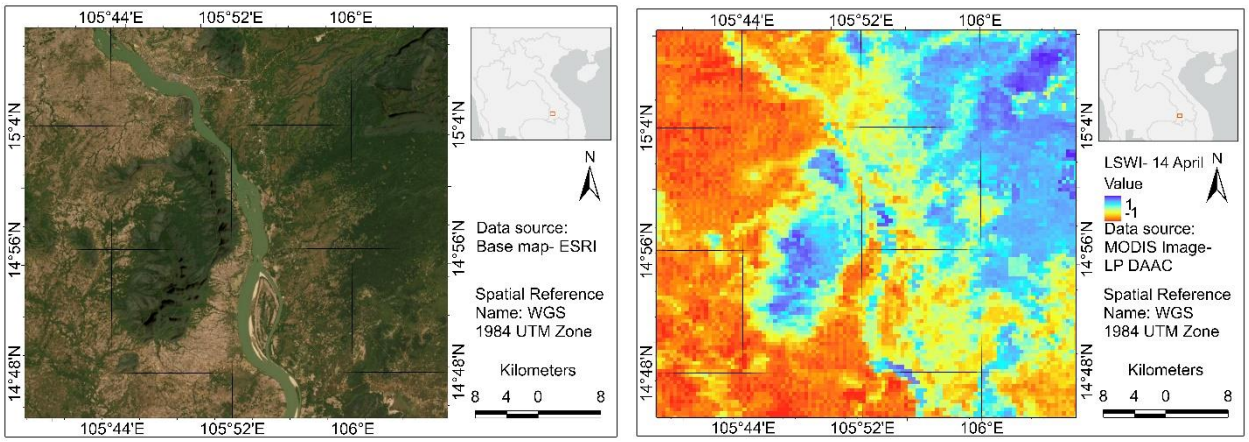

4.3.4 Results of temporarily flooded areas

The temporarily flooded areas from each image between July and August were summarised into one layer as the potential rice extent. This flooded area is the initial output of the extent of lowland rice. However, the temporarily flooded area needs more processing to eliminate non-rice areas, such as permanent water body, forest, and shrub pixels, and those pixels where water or moisture is higher than vegetation during this period. Figure 14 illustrates the temporarily flooded areas in the whole country. It found that a higher density of pixels is located where there are dams, rivers, and thick forest. Overall, the total of temporarily flooded areas is about 10,063,678 hectares. Hence, this area will be further processed as input for mapping the extent of rice in the following steps.

Figure 14. Temporary flooding areas

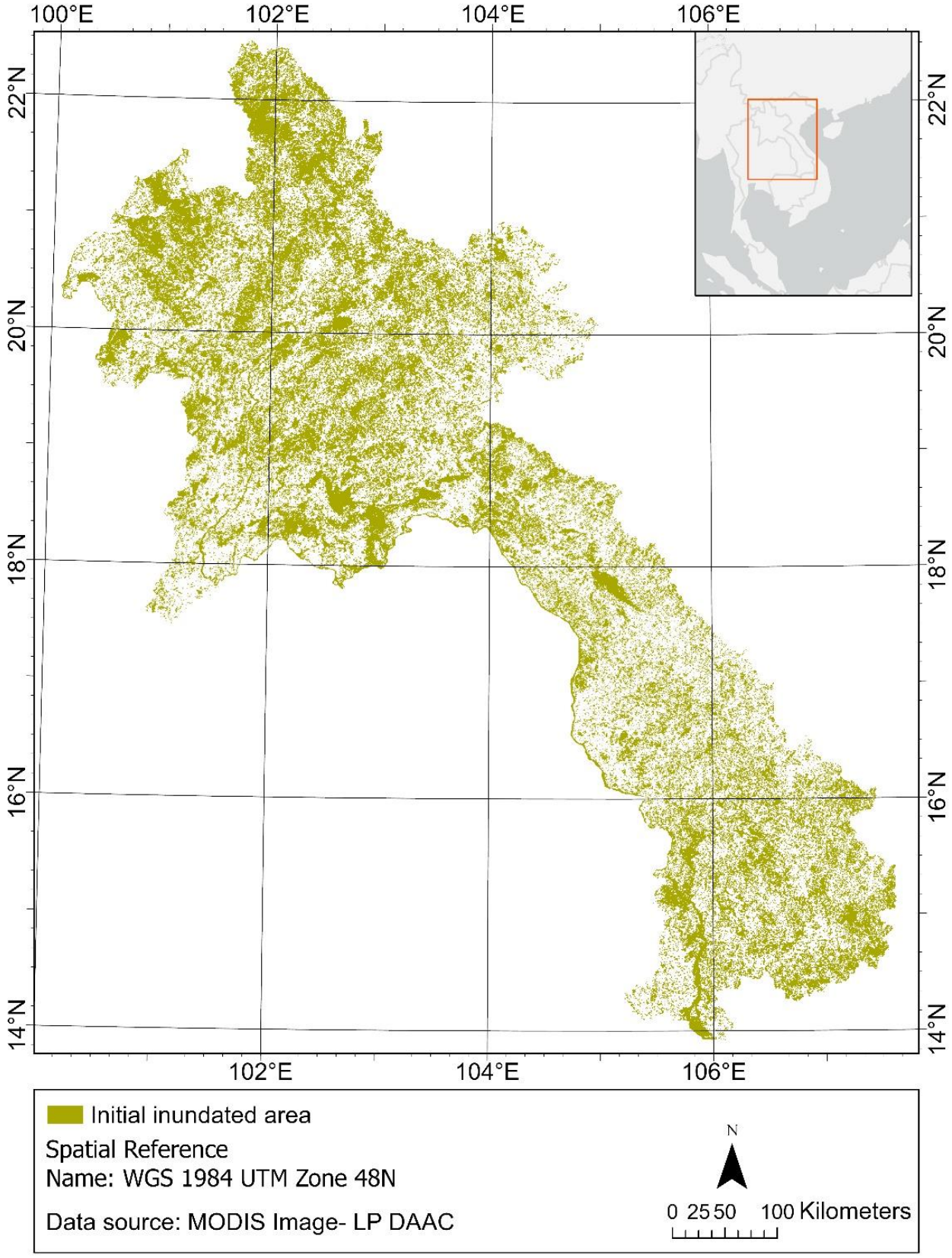

4.4 Results of the development of non-rice masking layers

4.4.1 Non-rice area masking

Non-rice areas such as permanent water, forest, and highly topographical areas where lowland rice is not commonly planted were excluded from the temporary flooding areas. Appendices 3, 4, and 5 display the permanent water layer, the forest or shrub layer, and steep sloping areas respectively. First, the permanent water illustrated in Appendix 3 is a combination of the water bodies derived from Global Land Cover and all the flooded areas – the combination of flooding from all the time-series images (that is, 46 time-series). The surface area of the water recorded totals approximately 304,670 hectares. Secondly, the forest layer was developed from the NDVI and LSWI, which have a high staple value throughout the year. Appendix 4 illustrates forest and shrubbery cover around 16,104,309 hectares. Also, the steep sloping terrain layer is displayed in Appendix 5. The highly topographical areas are mainly in the North and Eastern parts of the country, covering about 12,487,499 hectares.

4.4.2 Result for potential rice areas after non-rice areas are excluded

Potential rice areas following the exclusion of non-rice areas are provided in this section. The temporary flooding areas declined from 10,063,678 hectares to 1,028,804 hectares after all the non-rice areas were eliminated. It was found that most of the area, especially in the northern and eastern parts of the study area, were eliminated. This is consistent with the characteristics of the AEZs where the northern and eastern AEZs spreading from north to south are constrained with highly topographical conditions. However, this area will need further analysis to find the actual rice pixels by taking into account the differences of each AEZ and analysing its EVI. Below, Figure 15 displays this potential extent of rice.

Figure 15. Potential lowland rice areas

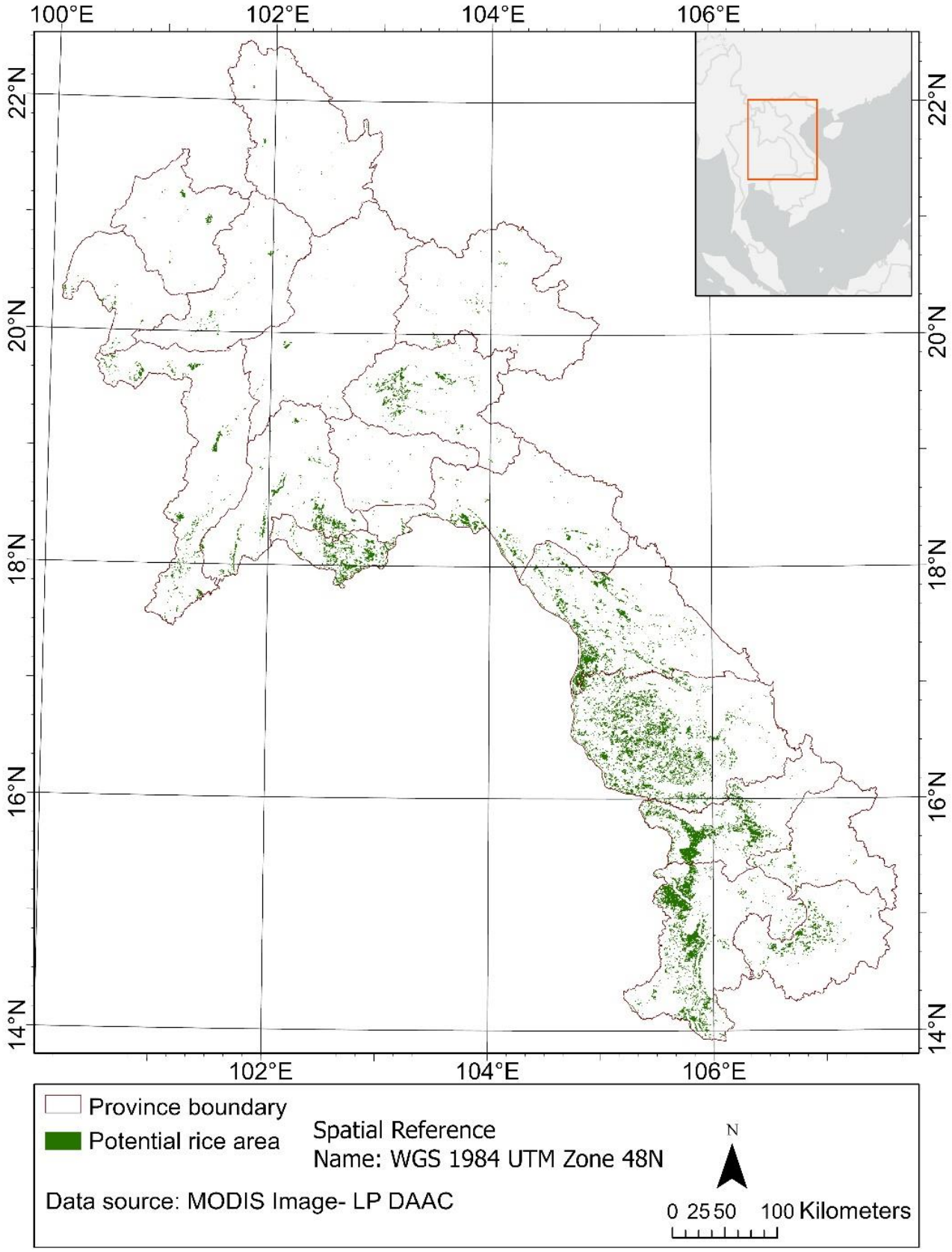

4.5 Results of the rice pixel estimation

4.5.1 Identification of rice transplanting dates by Agro-Ecological Zone

This section provides results for the finalised extent of lowland rice by taking AEZ character-specific information into account. First, the identification of rice transplanting dates is essential to estimate the extent of rice. The EVI was chosen instead of the NDVI for the change in 'greenness' analysis because the EVI has less sensitivity to noise than the NDVI. Figure 16 displays changes of the EVI and LSWI in the potential rice fields of the Vientiane Plain AEZ. It found that the EVI is lower than the water index on July 3, which is considered the date for transplanting rice in this AEZ. Thus, the rice pixel analysis using the EVI starts from this timeframe.

Figure 16. Identification of the rice transplanting date for the Vientiane Plain AEZ

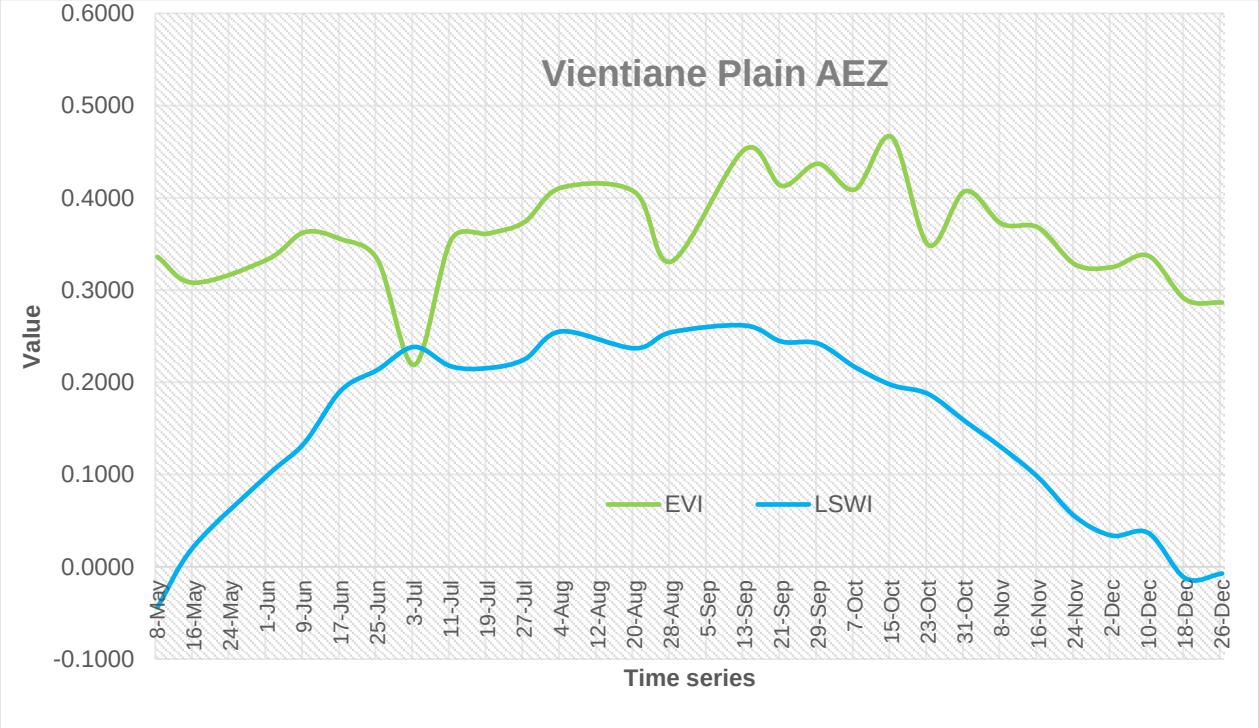

Figure 17 shows fluctuations in the EVI and LSWI in the Northern Lowlands AEZ. It shows that the moisture or water condition starts to increase above 0, which signals the onset of the rainy season, before it declines to the same level in early December, which is the end of the rainy season. In general, the EVI fluctuates higher than the water index throughout the year, however, the EVI is lower than the water index when farmers flood their rice fields for transplanting rice seedlings. The date of transplanting rice is found to be at the same time as with the Vientiane Plain AEZ (Figure 16), while the fluctuation of the EVI is slightly different.

Figure 17. Identification of the rice transplanting date for the Northern Lowlands AEZ

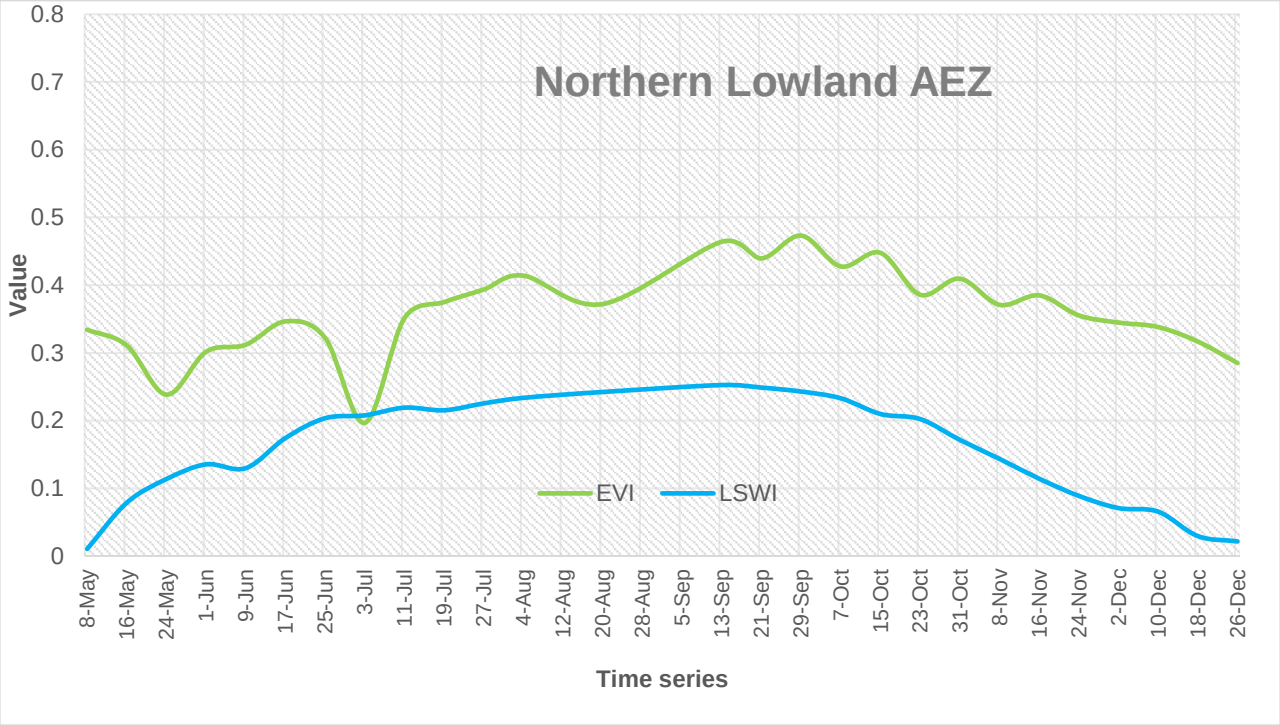

Identification of the transplanting date for rice crops in the Northern Highlands AEZ is displayed in Figure 18. Similarly, the transplanting date of rice is found to be at the same time as the Vientiane Plain and Northern Lowlands AEZs.

Figure 18. Identification of the rice transplanting date for the Northern Highlands AEZ

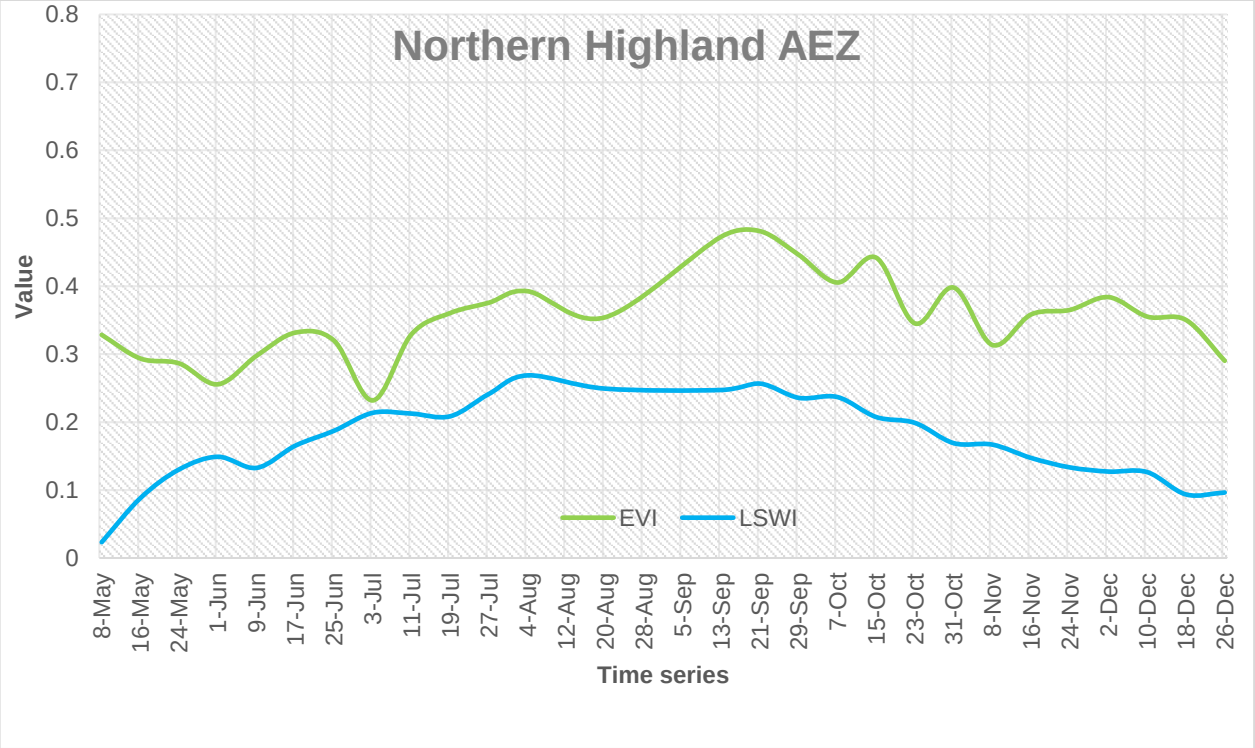

By contrast, it was discovered that the Mekong Corridor AEZ and the Central and Southern Highlands AEZ were different. The transplanting date was found to be later, in mid- to late August,

in the Mekong Corridor. The EVI is lower than the water index on August 20 in the Mekong Corridor (Figure 19), while the Central and Southern Highlands farmers transplanted their rice seedlings in mid-August (Figure 20).

Figure 19. Identification of the rice transplanting date for the Mekong Corridor AEZ

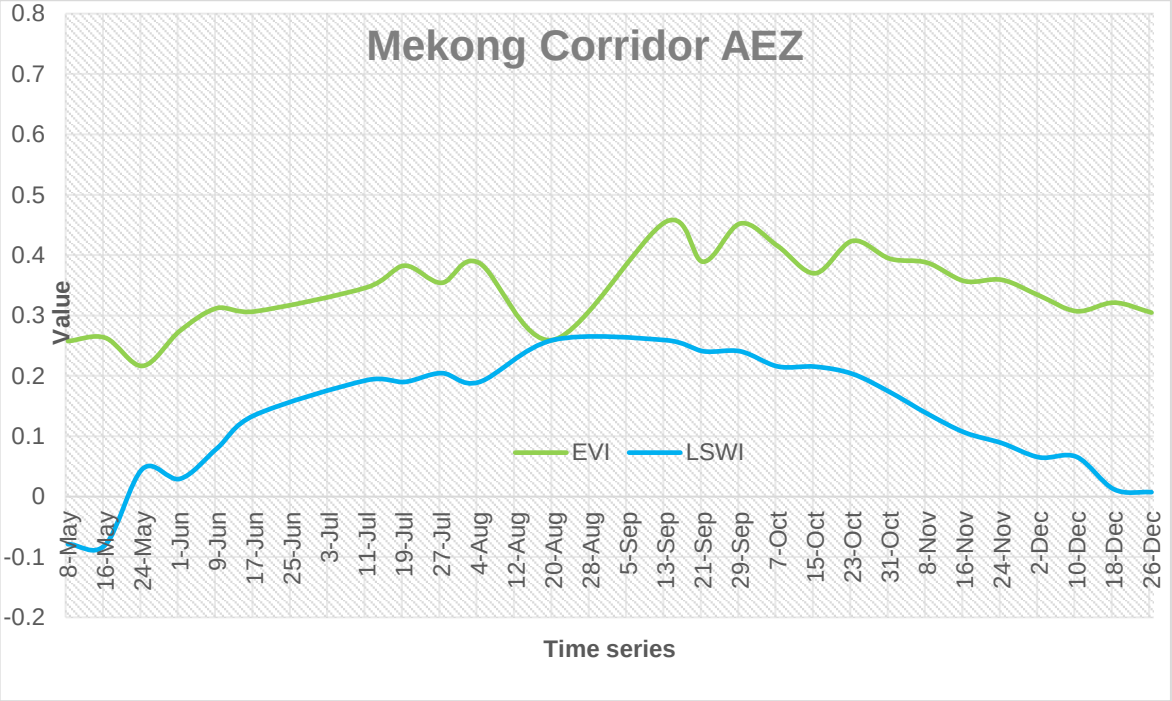

Figure 20. Identification of the rice transplanting date for the Central and Southern Highlands AEZ

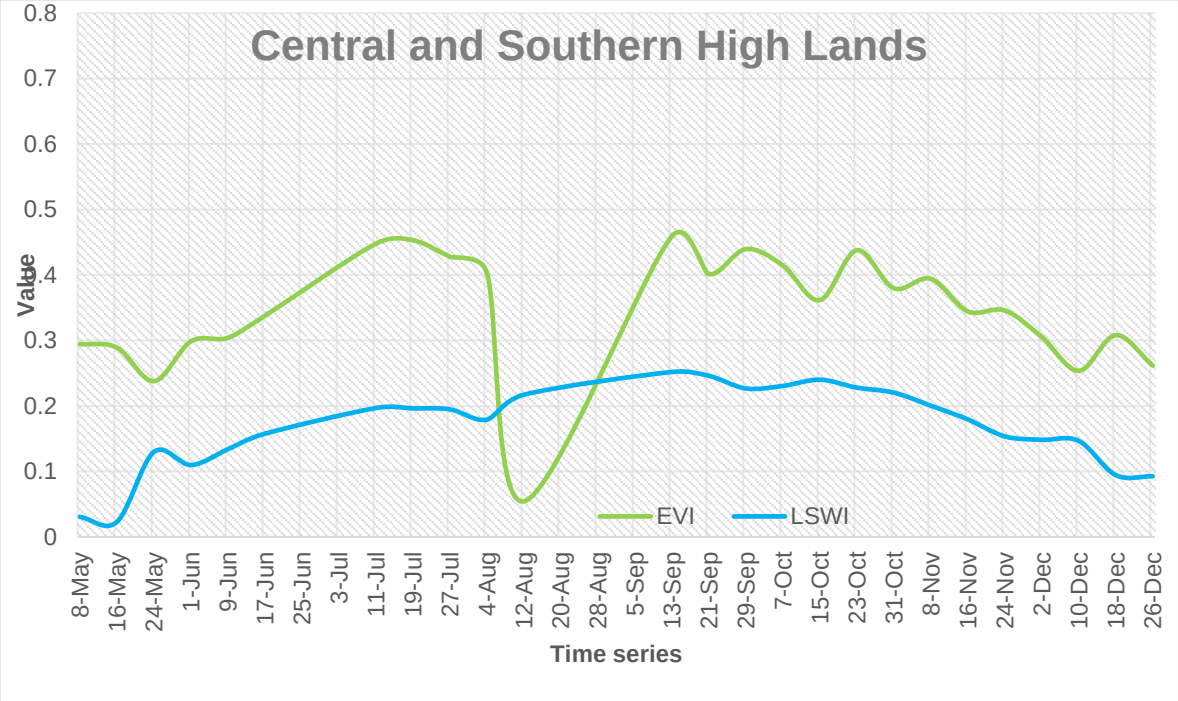

4.5.2 Result of the vegetation indices spot check

Validation of the temporal analysis of the vegetation indices which used MODIS imagery was carried out using the indices computed with a higher spatial resolution image or Landsat-8 imagery. Figure 21(a) shows the temporal changes of the NDVI and LSWI computed with Landsat-8 imagery in the Vientiane Plain AEZ while Figure 21(b) shows the phenological change of potential rice cropping in the Mekong Corridor AEZ. It was found that the trend of the vegetation and water index computed with Landsat-8 imagery is consistent with that computed using MODIS data. For instance, the NDVI was low and fluctuated close to the peak level of the LSWI in early July, which corresponds to the findings found for the same AEZ in Figure 16. Furthermore, the findings for the Mekong Corridor in Figure 21(b) are slightly different from the findings for the same AEZ in Figure 19. However, this difference is only seven days. Hence, the spot check using higher spatial resolution imagery can indicate the fluctuation of indices computed with coarse spatial resolution imagery like MODIS, which ensures that the trend of indices used to compute the extent of rice farming is reliable.

Figure 21. Vegetation index spot check

(a) Vientiane Plain AEZ

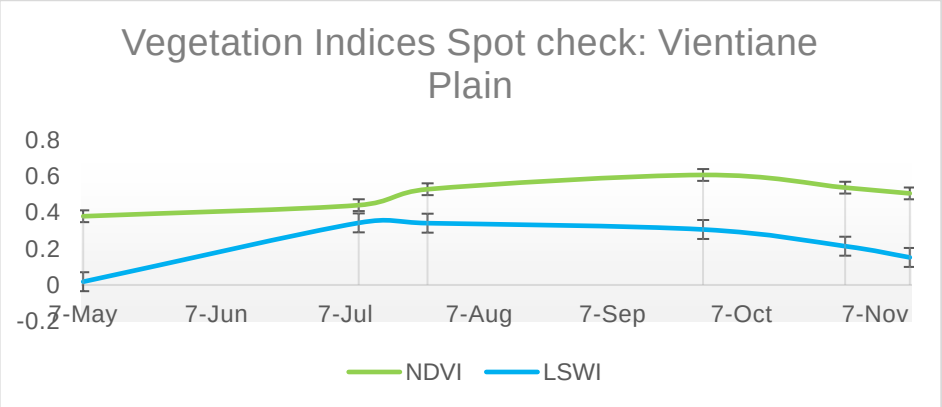

(b) Mekong Corridor AEZ

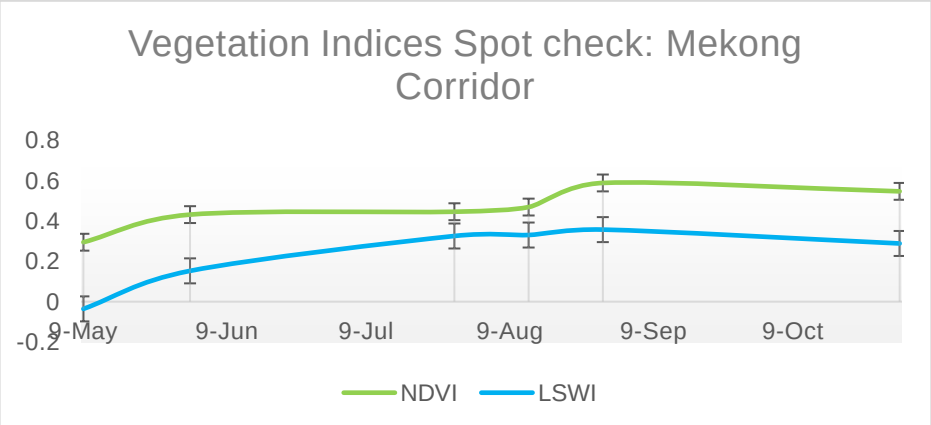

4.5.3 Result of the rice pixel estimation

Following the identification of the rice transplanting date in each Agro-Ecological Zone, it is possible to estimate the potential extent of rice farming. This section provides the output of the EVI temporal analysis for the potential rice fields. Figure 22(a) illustrates the estimated extent of rice after carrying out the EVI analysis for each AEZ. At this final stage, the temporary flooding area reduced to 29,368 pixels, which is equivalent to 688,009 hectares. Spatially, it looks similar to the previous map in Figure 15 after the non-rice areas were excluded. However, the area was actually about 33% per cent less than in Figure 15. Thus, this is the finalised extent of rice which could be used to forecast the rice yield. Refer to Appendix 5 for an improved visualisation of this finalised extent of rice farming.

Figure 22. Finalised extent of lowland rice

(a). Overall finalized rice extent

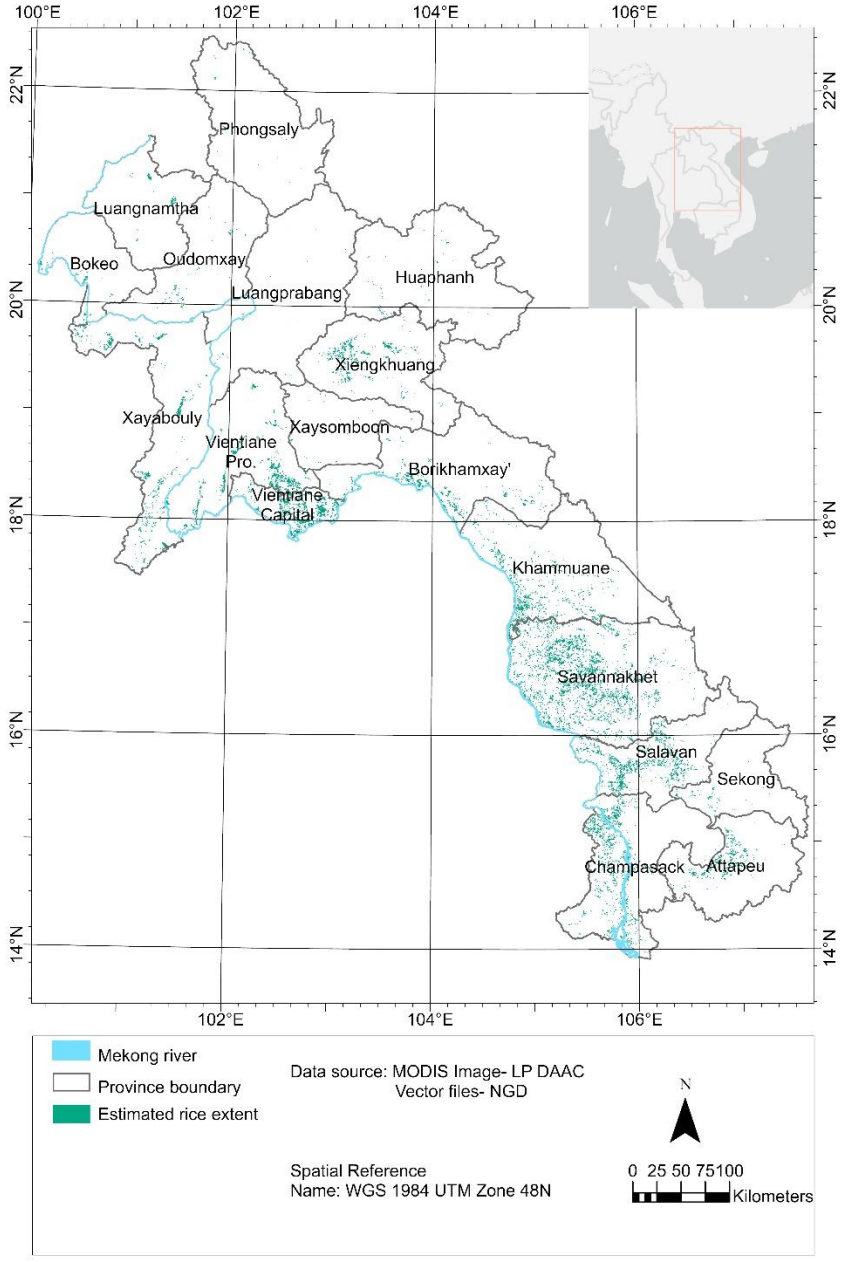

(b). High potential rice field

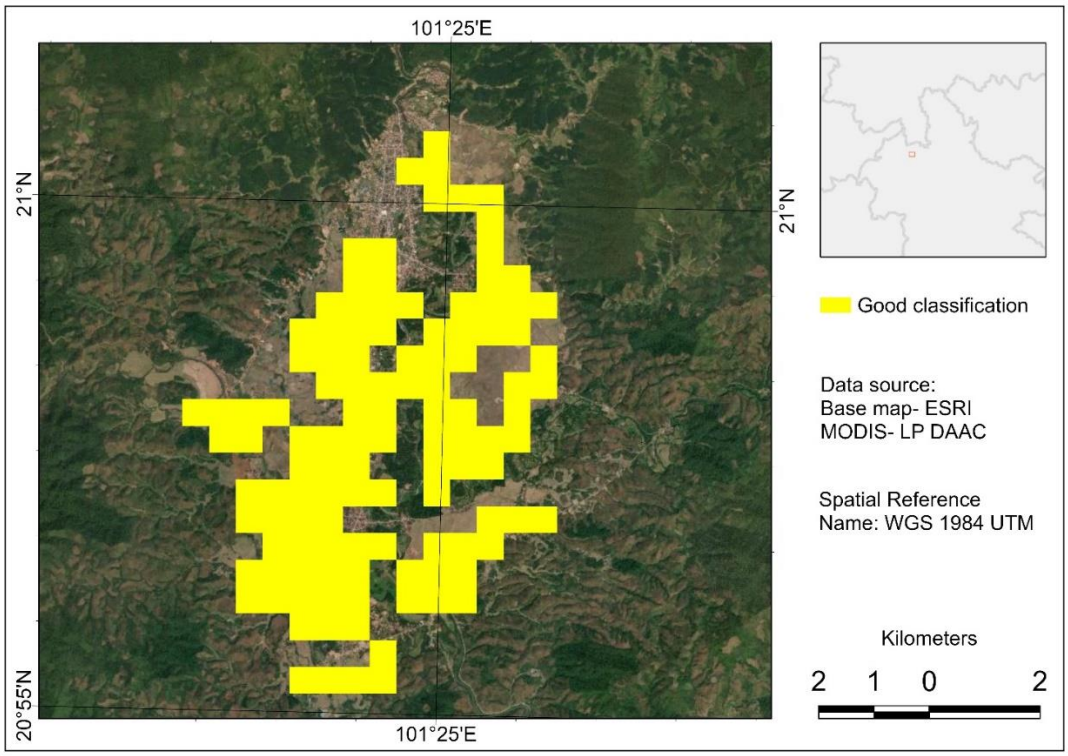

(c). Misclassification

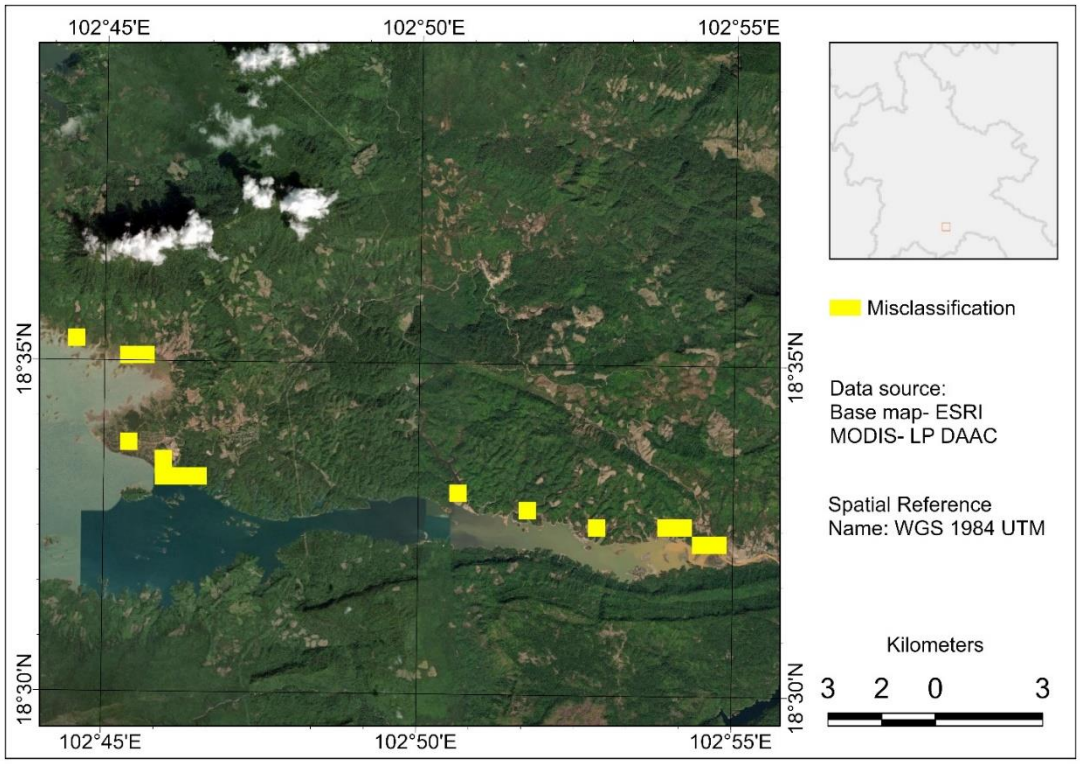

However, this result needs to be interpreted with caution since it contains both reasonable and some unreasonable estimates. The estimated extent of rice contains some suspicious rice areas. It was found that there are some odd pixels which were identified as rice areas, but these pixels are located in wetland areas or where there is a dam Figure 23(c). The dam and wetlands are uncommon locations for rice crops. This inaccuracy is caused by the similarity of the spectral profile of aquatic plants that grow in wetlands along the edge of water reservoirs. However, Figure 23(b) illustrates the area where there is a high possibility of rice fields being situated. Thus, the results of the estimation from this method may need to be applied and interpreted with a margin of error.

4.6 Results of district rice production estimations

4.6.1 Estimation of the rice yield for each AEZ

Despite the availability of rice yields at the provincial level, rice production at the district level is preferred for better planning and targeting in terms of food security and other program monitoring. Lao PDR has six Agro-Ecological Zones and each Zone has several subsequent provinces or districts of administration. Hence, the AEZ is the key to forecast district-level rice production accurately because rice yield is not determined by administrative boundaries, but climate and Agro-Climatic Zones do influence rice yield(Li, El Solh & Siddique 2019). Thus, this assumption was applied here with the rice yield estimation. Table1 shows the results of a simple linear regression model analysis which found that the coefficient which refers to rice yield ranges from 4.3 in the Northern Highlands AEZ to 4.8 in the Northern Lowlands AEZ. However, we must also consider the p-value which indicates a significant level of the yield estimate. The p-values of the estimates for the Northern Lowlands and Northern Highlands AEZs were higher than the significant level (0.05), while the correlation of rice yield and the independent variable (remotely-sensed extent of rice) were high for all estimates. Specifically, the Vientiane Plain AEZ and the Central and Southern Highlands AEZ are recorded as 0.96, while the lowest degree found in the Northern Highlands AEZ is 0.86. These results are useful for the estimation of rice yield in smaller spatial units.

Table 1. Summarised parameters of yield estimate by AEZ

Agro-Ecological Zone	R-square	Coefficient	P-value
Vientiane Plain	0.96	4.7	0.002967977
Northern Lowlands	0.92	4.8	2.17696E-07
Northern Highlands	0.86	4.3	1.42185E-05
Mekong Corridor	0.95	4.5	0.000137735
Central and Southern Highlands	0.96	4.5	0.000145006

Also, a strong correlation within each AEZ shows a consistent direction from all data points or provinces. Figure 23 illustrates some results of the correlation within each AEZ.

Figure 23. Scatter plots of the estimated area and provincial rice yield for each AEZ

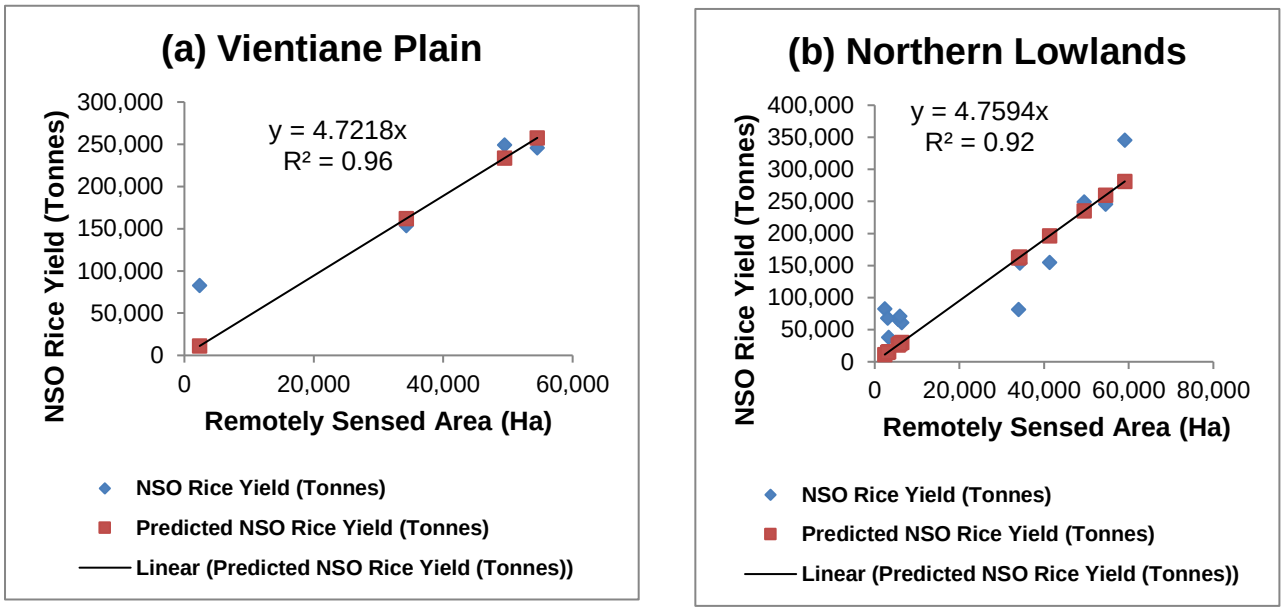

4.6.2 District rice production

This section provides the outputs from applying the GIS “Dasymetric mapping” technique to estimate rice production at the district level. Figures 24(a) and 24(b) present the estimated extent of rice and its production spatially using the pixel-based technique. It shows that higher rice yields, as well as the extent of lowland rice, is mostly distributed along the western side of the country, from the central down to the southern parts of the country. By contrast, the Northern and Eastern Districts were found to have fewer rice fields and so their production of rice is lower. Thus, the estimation of lowland rice at the district level could be useful to others, including food security program planners. Refer to Appendices 9 and 10 for more information.

Figure 24. Spatial distribution of estimated rice yields at the district level

(a) District rice extent

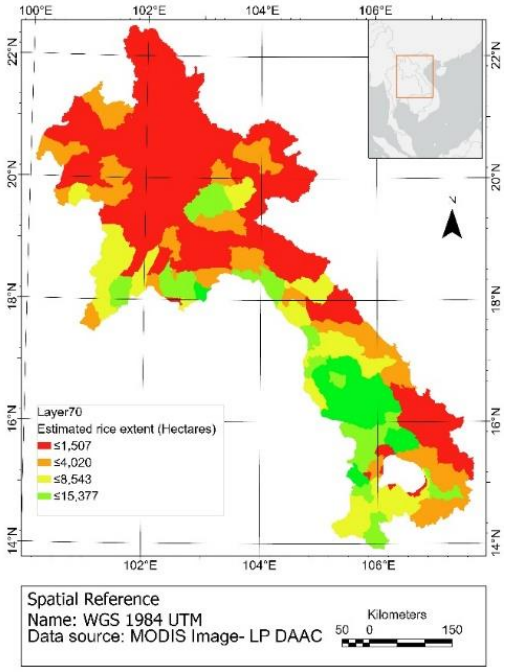

(b) District rice yield

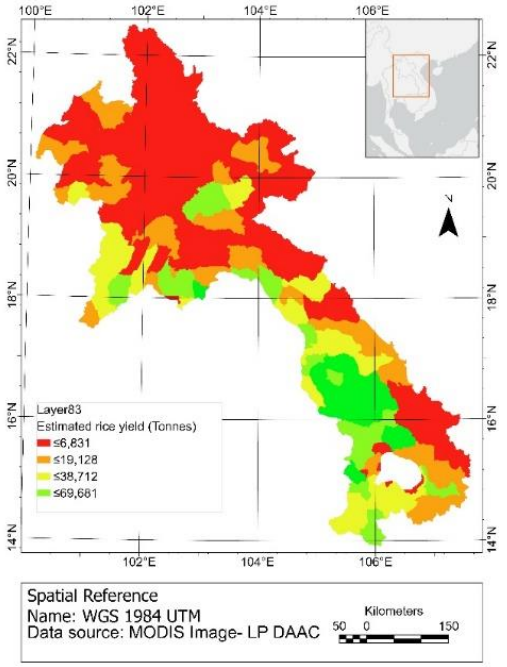

4.7 Accuracy assessment of the results

This section provides detailed results of the accuracy assessment of the method applied in the mapping of the extent of rice farming. With the absence of ground truth data and any independent auxiliary datasets, validation of this study was carried out by comparing the estimated rice extent with the official crop statistics from the Lao Statistics Bureau (LSB). Scatter plots were created using the estimated extent of lowland areas planted with rice crops in 2016 as inputs. Specifically, the validation was carried out within each AEZ as well as for the national average, as displayed in Figure 25(a-f). Overall, it was found that there is a strong relationship between the estimated extent of rice and the official statistics. In detail, the correlation value or R^2 in all the AEZs range from 0.85 to 0.95, and the national level is at 0.95. This proves that the remote sensing method produced results containing some level of consistency with the actual data, the census results.

The analysis discussed above indicates a degree of correlation between the estimated extent of rice and the actual number from official statistics. However, the magnitude of the difference between the estimations and the actual statistics is missing. Hence, the measurement of the root means square errors, as well as the mean absolute errors, needed to be conducted. Since the available rice statistics are at the provincial level only, the estimated extent of rice was summarised into the provincial level. Table 2 below shows details of the errors after comparing the estimated results with the official statistics. Overall, the total estimated rice area is 688,009 Ha. By contrast, the official statistic is 771,772 Ha. So, the mean absolute error is -83,763 and the RMSE is 14,687 Ha.

Figure 25. Scatter plots of the estimated areas and official figures

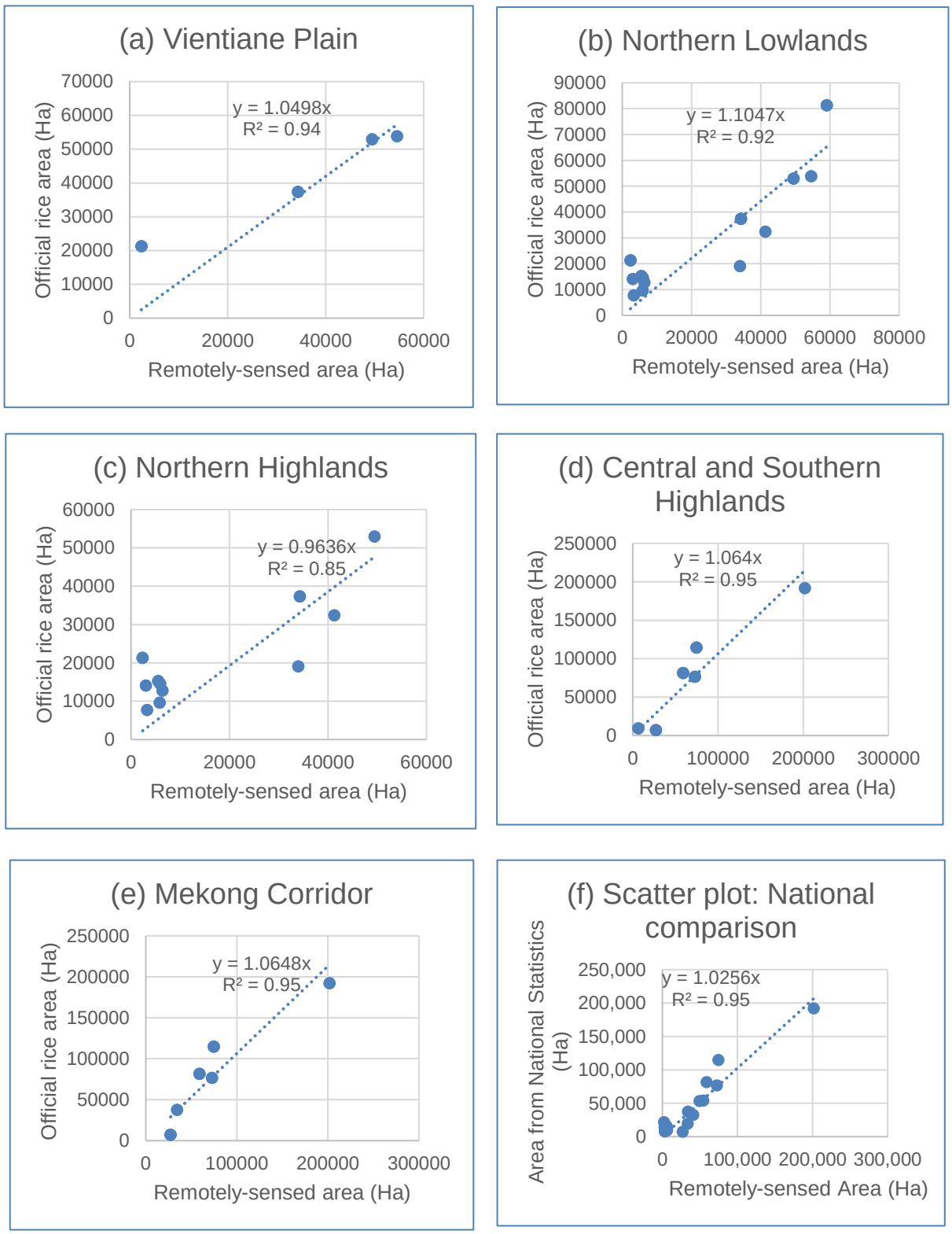

Furthermore, the absolute errors in each province range from 688 hectares in the Vientiane Capital to -40,011 hectares in Champasack province, as indicated in Table 2. The underestimation of the results tended to be in the northern provinces of Xaysomboon, Luangprabang, Oudomxay, Bokeo, Huaphanh, Phongsaly, and Luangnamtha respectively. Meanwhile, some significantly overestimated results were also observed in some provinces in the centre and south, such as Attapeu, Xiengkhuang, and Xayabouly. Nevertheless, there are some provinces in the Mekong Corridor AEZ which have an absolute error of less than 10%. These include the Vientiane Capital district, and the Salavan, Savannakhet, Vientiane, and Borikhamxay provinces. This is where the majority of rice is grown.

Table 2. Summary of errors as a result of comparing the estimated extent of rice with official crops statistics

Code	Provincial name	Estimated area Ha	NSO's rice area Ha	Absolute errors Ha	Percent of error %	Square error Ha squared	RMSE Ha
1	Vientiane Capital	54,538	53,850	688	1.3%	473,952	
2	Phongsaly	3,280	7,720	-4,440	-57.5%	19,715,348	
3	Luangnamtha	5,833	9,585	-3,752	-39.1%	14,074,771	
4	Oudomxay	5,529	15,282	-9,753	-63.8%	95,124,694	
5	Bokeo	5,927	14,565	-8,638	-59.3%	74,613,785	
6	Luangprabang	3,046	14,095	-11,049	-78.4%	122,090,754	
7	Huaphanh	6,372	12,770	-6,398	-50.1%	40,931,985	
8	Xayabouly	41,302	32,390	8,912	27.5%	79,425,399	
9	Xiengkhuang	33,993	19,060	14,933	78.3%	222,989,030	
10	Vientiane Pro.	49,478	52,950	-3,472	-6.6%	12,053,578	
11	Borikhamxay'	34,297	37,345	-3,048	-8.2%	9,288,046	
12	Khammuane	59,083	81,330	-22,247	-27.4%	494,915,149	
13	Savannakhet	201,802	191,940	9,862	5.1%	97,251,234	
14	Salavan	72,835	76,520	-3,685	-4.8%	13,578,800	
15	Sekong	6,442	9,250	-2,808	-30.4%	7,882,222	
16	Champasack	74,639	114,650	-40,011	-34.9%	1,600,884,168	
17	Attapeu	27,246	7,170	20,076	280.0%	403,037,486	
18	Xaysomboon	2,366	21,300	-18,934	-88.9%	358,490,914	
		688,009	771,772	-83,763	-10.9%	3,666,821,314	14,686.6

CHAPTER FIVE: DISCUSSION AND LIMITATIONS

This section aims to provide a dialogue aligned with the objectives and research question provided in chapter one. It discusses the main findings to provide a basis upon which chapter 6 can conclude whether the aim and objectives of the research have been met and satisfactorily addressed. There are three main points to be discussed, which are the performance of both the imagery and the method used to map the extent of rice farming and forecast rice production at the district level, the critical limitations encountered by the study, and possible solutions to any limitations.

5.1 Performance of optical imagery to map the extent of rice

5.1.1 Challenges of applying the method to map the extent of rice

Even if the study chose a better composite product than MODIS could provide, cloud cover and cloud shadow remain the critical issue, especially in this tropical monsoon region. As many studies have raised regarding the issue of cloud being persistent in optical satellite imagery, so this thesis project too encountered the severe effects of cloud contamination (Sun, H-s et al. 2009; Xiao et al. 2006). The impact is not just on the quality of the data but also on the availability of the vital time series that is necessary for temporal analysis of the rice areas. This study had to skip some time series from the analysis accordingly. With the missing essential time series, the imagery lost critical pixels or information, and this affected the amount of the rice area measured, which potentially resulted in the underestimation of rice yields in the study area. Furthermore, the cloud effect presented another bias for the results, for instance, overestimation. When cloud pixels remain in the dataset, for example, the cloud pixels around the edge of the cloud mask make the NDVI low – lower than the value of the water index even. As a result, unnecessary inundated areas were detected and counted as potential rice areas, as was the case for estimations in some areas in the north where clouds remained (Zhou et al. 2016).

Another challenge that affects the ability to correctly estimate the extent of rice using optical images is the temporal resolution of the available imagery. Despite the high dynamic of crop phenology, changes in the temporarily inundated areas of rice fields were significant too. This issue contributed to the underestimation of rice field area because the transplanting of rice fields started and finished at different times (Sun, H-s et al. 2009; Xiao et al. 2005). Hence, to ensure all potentially inundated areas can be detected when seedlings are transplanted, it is essential to have imagery with a high temporal resolution. Even if this study used the 8-day composite products of MODIS capable of avoiding cloud contamination, the cloud and cloud shadow are still critical (Xiao et al. 2005). Although some studies suggest that the daily product of MODIS may work better, the daily product will be even more affected (Sun, H-s et al. 2009). When rice crops are not transplanted at the same time, there is more opportunity to miss potential rice cropping areas. This incident can occur because the rice canopy can cover the water and saturated soil several weeks after transplanting.

Thus, despite the potential of the 8-day composite imagery, it could miss changes in rice crop development over this time period.

It is challenging to use MODIS data to detect the extent of rice in mountainous areas. Given the characteristics of the terrain, the size of rice fields is relatively smaller than the pixel size, which caused errors (Son et al. 2014; Sun, H-s et al. 2009; Xiao et al. 2006). Based on the results of this study, a relatively high error was recorded for many provinces, especially those located in the Northern Highlands AEZ and the upland areas in the eastern part of the country. The Northern Highlands AEZ has relatively steep and mountainous areas with altitudes of up to 2,500 metres above sea level (Li, El Solh & Siddique 2019). These highly topographical characteristics limit the opportunity for lowland rice cultivation. Consequently, some small areas that are suitable for lowland rice farming are located along the streams and in valleys. Thus, with a 500-metre spatial resolution MODIS image, the algorithm fails to capture small rice fields, which contributed to underestimated rice area data (Tingting & Chuang 2010).

Furthermore, the inclusion of non-rice areas in some pixels and the confusion for spectral pixels between rice crops and aquatic plants both caused results which were sometimes overestimated. Due to the large size of the pixels, there must be a mixture of rice and non-rice areas within some pixels. Unfortunately, such pixels were counted as rice for some positive values of the EVI and this increased the estimate of the extent of rice (Peng et al. 2011). Similarly, the similarity of the EVI value between rice pixels and those of aquatic plants or other similar crops can also cause errors of overestimation. According to Peña-Barragán et al. (2011), it is challenging to distinguish rice from other crops that have similar spectral profiles. This especially becomes an issue in cases where there is a similar environment to rice crops within the study area, for example, wetlands or dams where aquatic plants and other plants which appear similar to rice are grown (Zhang, G et al. 2015).

In addition, since the study area is large, different rice crops are grown in different areas within the AEZ, thereby posing difficulties in the rice crop temporal analysis. In Lao PDR, there are more than ten thousand rice varieties, including six per cent of unidentified varieties (Appa Rao et al. 2006; Basnayake et al. 2006; Rao et al. 2002). These rice varieties represent three different life spans of the rice crop – early, medium and late varieties – which are grown countrywide. Due to the diversity of rice and variations in the rice transplanting date, the trend of the vegetation index was quite noisy. These issues can lead to results which underestimate the extent of rice farming. For example, early rice varieties would be excluded because they were planted before the study timeframe or before the mapping stage took place (Sun, H-s et al. 2009). Because of this issue, some studies modified this algorithm to capture the different rice varieties using a detailed crop calendar (Bridhikitti & Overcamp 2012).

Also, utilisation of Landsat-8 OIL to verify some vegetation indices was found useful; however, level-1 data is challenging and can cause errors if misconduct on the pre-processing step was practiced.

As the imagery need atmospheric correction and it needs to apply for all relevant bands(Zanter 2016; Zhang, HK et al. 2018). Even more, when take time series into account, it would be a huge task and cost in time and resources of the project.

5.1.2 The opportunity to apply the method to map the extent of rice farming

The scale of mapping is another essential criterion to investigate the capacity of the optical image to estimate the extent of rice. The review has provided several sensors that have the capacity to cater to this scale, including AVHRR and SPOT VGT, which provide 10-kilometre and 1-kilometre spatial resolutions (Gumma et al. 2014). However, MODIS offers a better solution for providing the appropriate resolution. One tile of a MODIS image covers 1,200 x 1,200 kilometres, better allowing for a country-scale estimate, especially since this data has a better spatial resolution of 500 metres with daily and 8-day periods. This temporal resolution offers the potential to meet the objectives of this study. The study found that MODIS imagery and the method applied produce accurate results in the lowland areas where a large proportion of the rice cultivation is located. This means that MODIS provides the opportunity to map rice on a large scale in lowland areas, for instance, in the Vientiane Plain AEZ and the Mekong Corridor AEZ (Xiao et al. 2006; Xiao et al. 2005).

Another advantage of using MODIS imagery is that the data is both free and convenient to access. These characteristics make it the right choice for researchers and governments to use for further research, with the improved capacity for ground monitoring according to their needs (Elshorbagy 2013). Although other optical images are also free, finding cloud-free imagery with a high temporal resolution like MODIS is difficult. Thus, sustainable ground monitoring should not be limited in terms of access to data. Access to MODIS is not only a means of addressing the issue of cost but also those of the facility and convenience to access the information. MODIS has a professional team that maintains the system called the LPDAAC; they developed the product originally and provide ongoing support for ease of access to its information (Didan et al. 2015; Tingting & Chuang 2010; Vermote, FE, Kotchenova & Ray 2011).

In addition, the MOD09A1 provided radiometrically and geometrically corrected data. This quality is another advantage for the data analysis, which helped save time during the image processing stage. In most cases, such corrections cost time, especially when there are multiple data points or multitemporal images. Moreover, it was found that the data and the method applied in this study can help researchers save on resources (Elshorbagy 2013). One significant benefit that the study presents is the reduced reliance on data attained from field missions. The method is flexible in terms of accuracy assessment since it offers an alternative way to retrieve ground truth data by comparing estimates with the census data (Son et al. 2013; Sun, H-s et al. 2009; Xiao et al. 2006; Xiao et al. 2005). This increases the efficiency in terms of spending less in terms of monetary resources to conduct the mapping.

Also, MODIS and the method applied in this study showed a relatively high correlation with the census data, especially since there were only minor errors when compared with the actual data. According to Son et al. (2013), they considered the method consistent if the errors generated by the study are less than 10%. However, this thesis finds that the correlation of this study is 0.95 with an RMSE of 14,686 hectares (2%). Thus, when compared with the above comment, it is reasonable to assume that the overall method of the study is robust. This accuracy is further reinforced when compared to another similar study by Bridhikitti and Overcamp (2012) which reported a correlation of 0.93 for the r-square. Finally, the results from this study are slightly more accurate than the correlation found in Xiao et al. (2006) which was a similar study but for all of South East Asia, including Lao PDR. Their results yielded an R^2 of 0.79 and an RMSE of 45,000 hectares.

5.2 Performance of the technique used to forecast district level rice production

The method applied to forecast district level rice production is called ‘Dasymetric mapping’. This is a GIS technique which is commonly applied to interpolate population distribution spatially. The technique is based on the aggregated population density from the census with auxiliary datasets like the Land Use Map, which is in raster format (Su, M-D et al. 2010). Thus, in this study, the ancillary dataset is the MODIS dataset of the estimated extent of rice. The method assumed that, within each AEZ, rice yield is homogenous across the zone. The study shows that this method is simple and straightforward to apply. It does not need much information, just the aggregated information and some complementary datasets (Cai & Sharma 2010). The key is the aggregated data either by zone or by province. This type of data, that is, rice production statistics, is regularly produced and updated by the relevant government agencies.

Other similar products which are commonly generated by the government and can be used as inputs for Dasymetric modelling are choropleth and thematic maps. Since these maps do not spatially represent the data sought, the use of these maps requires extra attention as they could mislead the researcher in the interpretation of the data sought. They would be more beneficial if they allowed spatial analysis at smaller spatial units. Thus, by using the Dasymetric mapping technic, it is possible to offer analysis spatially. In turn, planners can see the information more accurately and be more effective in their planning accordingly (Bielecka 2005). Also, nowadays, auxiliary datasets such as the Global Land Cover map are becoming increasingly more accessible. This presents an opportunity to apply this method in regions or countries with a low capacity to typically research such information.

The only issue of this method is the control of the quality of the estimate. Since this method only facilitates the estimation stage of the process, it cannot influence the quality of the estimation. It is dependent on the spatial interpolation since the result of its estimation depends solely on the inputted data from the census and the ancillary dataset (Cai & Sharma 2010). Therefore, some

studies claim that the relationship, especially between the input from census and the ancillary data, should be assessed and quantified as well. Consequently, some studies propose later generations of Dasymetric modelling which take into account the uncertainties associated with the population data or the auxiliary datasets (Nagle et al. 2014).

5.3 Key limitations

This study did not have access to ground truth data and this is considered the main constraint of the study. Ground truth data is useful to check the accuracy of the rice field classification physically. However, the field mission and physical collection of field information could not be conducted. This issue was due to the timeframe of this study not allowing for ground truth data collection. Thus, it would be helpful to confirm the results rather than just relying on census figures which may still lack accuracy.

Furthermore, due to high cloud contamination, this study lacks high spatial resolution imagery for use as an independent dataset to capture the rice fields. Even if Landsat-8 OLI imagery was used, the repetitive rate of 16-day temporal resolution made it vulnerable to cloud during the monsoon season. Although Sentinel-2 data offers better output in terms of both spatial and temporal resolution, this data was limited by the same constraint. It was impossible to find a completed time series from these optical satellite images to fulfil the expectations of this study.

Another limitation of the study is the lack of an actual rice calendar for all the different rice varieties. The available crop calendar was quite broad, and it lacked the necessary information to distinguish the different rice varieties. This limitation made it difficult to interpret the pattern of different vegetation indices.

Also, the study lacks a detailed Land Cover Map of rice crops, especially in the lowland, rainfed rice areas. Although the global Land Cover map was useful for some water body mask development, it was unable to provide reliable data for such lowland, rainfed rice crops to satisfactorily undertake the accuracy assessment.

CHAPTER SIX: CONCLUSION AND RECOMMENDATIONS

6.1 Summary and conclusion

This study aimed to investigate and examine the capacity of optical imagery to map the extent of lowland, rainfed rice crops, which is necessary for the forecasting of district-level rice production. MOD09A1, the MODIS 8-day composite image product with a 500-metre spatial resolution acquired in 2016, was used to test all assumptions and hypotheses. The estimated extent of lowland, rainfed rice cropping was obtained based on the temporal, inundated areas of the rice crops, as estimated using the NDVI, EVI, and LSWI. While the AEZ plays a crucial role in determining the main livelihood of its citizens, it also directly influences the suitability of agricultural activities, including rice crops. Thus, the AEZ was used to guide the temporal analysis of the vegetation index for potential rice crops before the extent of rice cropping was estimated. Once the extent of rice became available at the pixel level, the Dasymetric modelling technique was used to spatially interpolate zonal rice yields at the district level.

The results of the research showed that cloud cover is the critical issue of the optical satellite imagery as it affects the quality of the estimates. Some essential time series were severely affected, and even if the 8-day temporal resolution imagery was used, the impact remained high. Another weakness of the method was the failure to capture the smaller sized rice fields, especially in the north and eastern provinces. Another challenge was that this method presents the issue of pixel confusion, failing to delineate rice crops in areas with high crop heterogeneity. Also, it was discovered that the large size of the pixels made it difficult to measure rice crop areas when there are non-rice areas mixed in with the same pixels. All these factors led to the study results having relatively high errors in the areas where there is high topography. While these issues persisted, the study offers some positive results too. For instance, the wide swath width of MODIS is suitable for mapping at the country level. The high temporal resolution of the data helps analysts access data better. When compared to other optical satellite imagery, MODIS data offers improved flexibility for avoiding cloud contamination. Also, it was found that this study is relatively efficient in terms of resources used. For instance, there was almost no cost associated with the data analysis.

In conclusion, despite the challenges in delineating the extent of rice from the non-rice areas, the optical satellite imagery and the method were shown to be a potential source of information for the mapping of rice areas. The study showed the potential for mapping rice in lowland areas where large scale rice cultivation is present. The results of the research indicate that large errors are found with estimating the extent of rice cropping in highly topographical areas while fewer errors were encountered in lowland areas. Thus, it may make more sense to apply this method for the Vientiane Plain AEZ and the Mekong Corridor AEZ. By contrast, the other Zones require more high spatial resolution imagery and other analysis techniques for mapping the extent of rice. Also,

the Dasymetric modelling technique is a potential tool to address gaps in spatial data, including rice crops. Therefore, the aim of this research yields mixed answers and further research in this field is required if the whole country is to be mapped again.

6.2 Recommendation

6.2.1 Further research on mapping the extent of rice cropping during the wet season

In terms of improving the availability of the imagery during the monsoon period, the application of active remote sensing, such as the Synthetic Aperture Radar (SAR), can be an alternative data source (Le Toan et al. 1997; Shao et al. 2001; Van Tricht et al. 2018). Despite the reliable performance of the long-wavelengths of SAR, for instance, the Phased Array type L-band SAR (PALSAR) from the Advanced Land Observation Satellite (Zhang, Y et al. 2009), the freely available C-band SAR imagery from Sentinel-1 could be a potential solution to fill this information gap (Mansaray et al. 2019). Sentinel-1 Synthetic Aperture RADAR (SAR) carries two C-band instruments, A and B. Launched by the European Spaceship Agency in 2014, it remains in orbit today. This can ensure the sustainability of the data source in the future. Also, with the high temporal resolution of up to 6 days, and a wide swath width of the image, this sensor has the potential to map rice at the whole country level. More specially, Sentinel-1 provides a high geometric resolution of 5 metres by 20 metres, which is capable of mapping small-sized rice fields in highly topographical regions (Mansaray et al. 2017; Zhang, Y et al. 2009).

Since MODIS and the applied method in this study are practical for the mapping of large rice-cultivated areas, this is favourable to map rice in the Vientiane Plain AEZ and along the Mekong Corridor AEZ. This study recommends experimenting with the daily product as well as adopting some new techniques. First, experimenting with the daily product instead of the composite product because the composite seem to selects only the minimal Blue band reflectance, which could skip some changes on crop (Xiao et al. 2005). Secondly, it is worthwhile to experiment with the second version of the LSWI because the MODIS product has two short-wave infrared bands that are sensitive to water. The longer wavelength band, which is the Short Wave Infrared Band (2,105–2,155 nanometres), could be more effective in detecting water (Xiao et al. 2005). Also, to better deal with the noise caused by cloud cover, after ensuring Quality Assurance from the product was enabled, gap-fill algorithms are necessary to smooth the trends of the indices. Some studies adopt the method “Empirical Mode Decomposition” (Son et al. 2013). In addition, it may be worthwhile to experiment with the Gaofen-4 satellite, which is a Chinese Earth Observation Satellite. The satellite provides a time series of optical images with a spatial resolution of 50 metres and a high temporal resolution (Xia et al. 2019; Zhang, T et al. 2018). This may be another solution in addition to using MODIS.

In addition, to address the issue of confusing the spectral profile of rice crops with non-rice crops, an object-based analysis may be a better solution to such an issue. Rather than using individual pixels as in this study, the object-based method uses groupings of the pixels and statistical parameters to segment similar pixels before analysing them and classifying any rice crops (Kontgis, Schneider & Ozdogan 2015; Peña-Barragán et al. 2011; Tingting & Chuang 2010). Also, in response to the absence of useful information for the accuracy assessment, it is recommended to adopt an alternative solution. It is recommended to find and acquire a higher spatial resolution dataset to classify as the land use map (Tingting & Chuang 2010). Once the reliable land cover map is available, the areas of interest (AOI) are randomly selected and an accuracy assessment may be conducted with Kapa, producer, and user indices. However, where fieldwork is feasible, it is best to physically inspect the classification of the study using GPS technology and local knowledge of rice areas (Gumma et al. 2011). Fieldwork needs to be conducted at around the same time as the mapping exercise to ensure the consistency of the fields and the modelling.

6.2.2 Mapping of the extent of rice upland

Although upland rice is not a part of this study, further research and experimentation are recommended regarding the best possible method for mapping the extent of upland rice cropping. Although this rice system accounts for only ten per cent of the nation's rice production, it plays a vital role in the food security of the rural communities and the poor (Heinimann et al. 2013; Krishnamurthy, Chong & Poungprom 2015; Linquist et al. 2006). The nature of upland rice cultivation is that it lacks surface water. Nevertheless, some studies use the same algorithm applied in this study. They still, however, experience a high degree of uncertainty and it is not recommended to use this algorithm with the mapping of upland rice (Tingting & Chuang 2010; Xiao et al. 2006). Given the nature of upland rice farming, cultivation involves slash and burn cultivation or shifting cultivation. Further research regarding detecting changes in land use is essential to delineate this rice ecosystem from other land cover classes (Hurni, Hett, Epprecht, et al. 2013).

6.2.3 Mapping the extent of irrigated rice

Based on the lessons learnt from this research, there is an issue with the mapping of small rice fields, especially in highly topographical areas. In general, irrigated rice is relatively smaller in terms of surface area than lowland, rainfed rice cultivation, so a high spatial resolution image is required to capture irrigated rice fields (Xiao et al. 2006). Fortunately, farmers in Lao PDR cultivate irrigation rice only in the dry season where cloud cover may not be as problematic as during the monsoon season. In this case, optical satellite imagery may be a potential source of data. Thus, it is worthwhile experimenting with free optical high-resolution imagery like Landsat-8 OLI and Sentinel-2. It is flexible as to which classification method is applied. Generally, both pixel and object-based methods are applied extensively. Zhou et al. (2016) use Landsat-8 OLI with a pixel or phenology-based method to map the rice fields, which has been found to yield a more accurate

result compared to object-based methods. However, Nguyen, TTH et al. (2012) used the NDVI to generate a hyper-temporal image time series using a ten-year time series of data. They used unsupervised ISODATA with a supplementary field trip and achieved 94% accuracy. Thus, the classifier is not as important as the spatial and temporal resolution of the image for mapping irrigated rice.

Appendix 1. Map of administration of Lao PDR

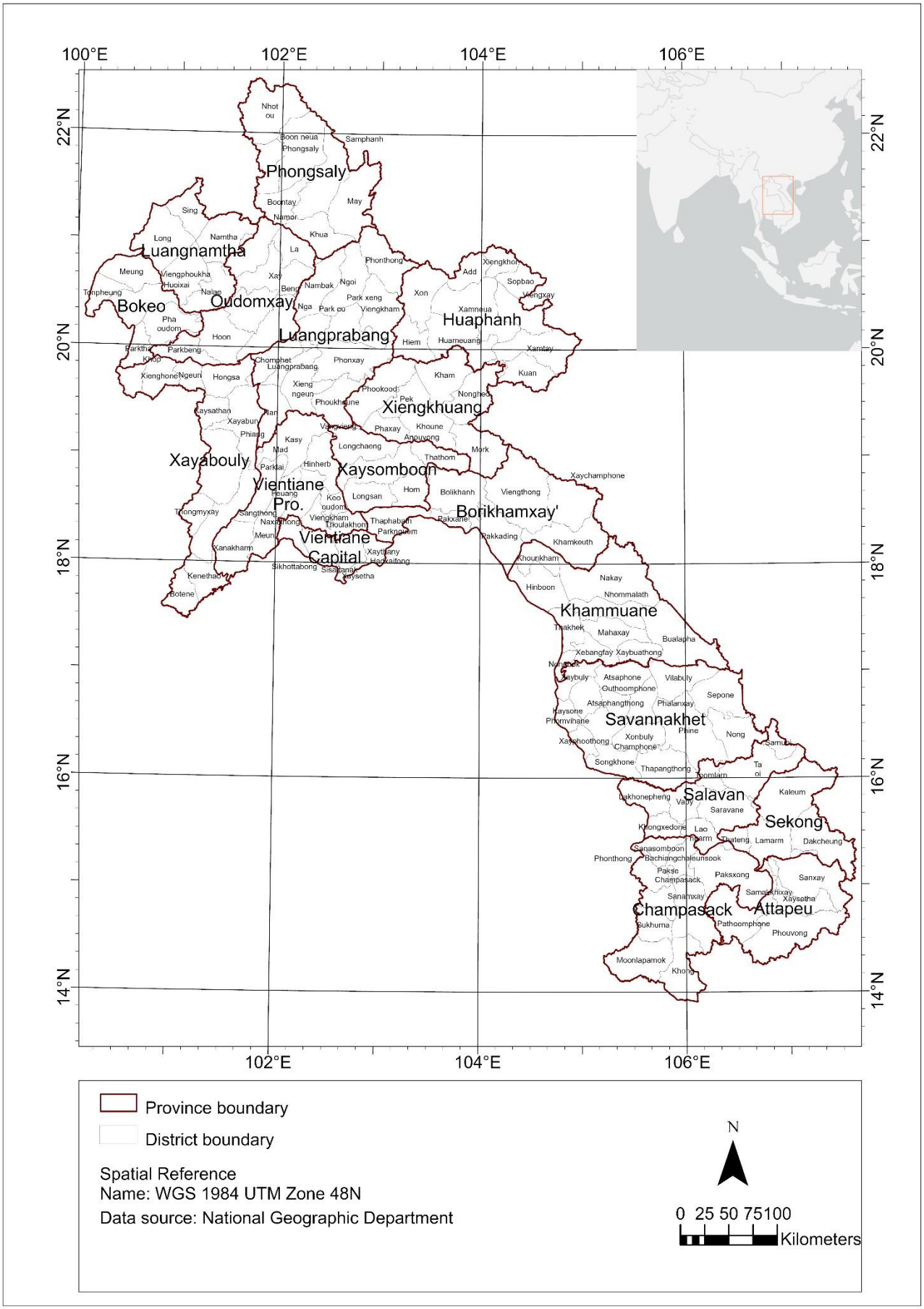

Appendix 2. Map of the Agro-Ecological Zones (AEZ)

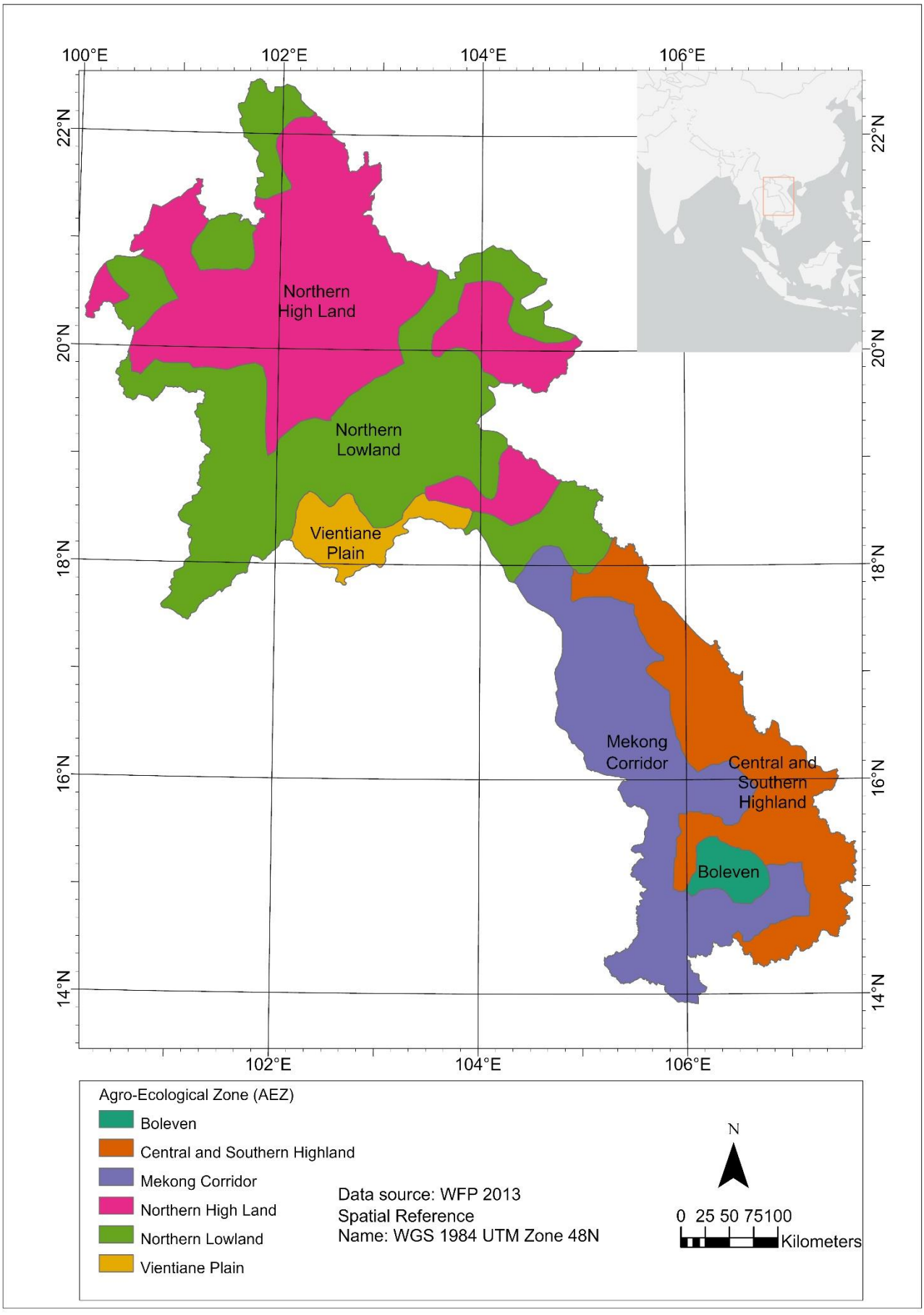

Appendix 3. Map of permanent water layer

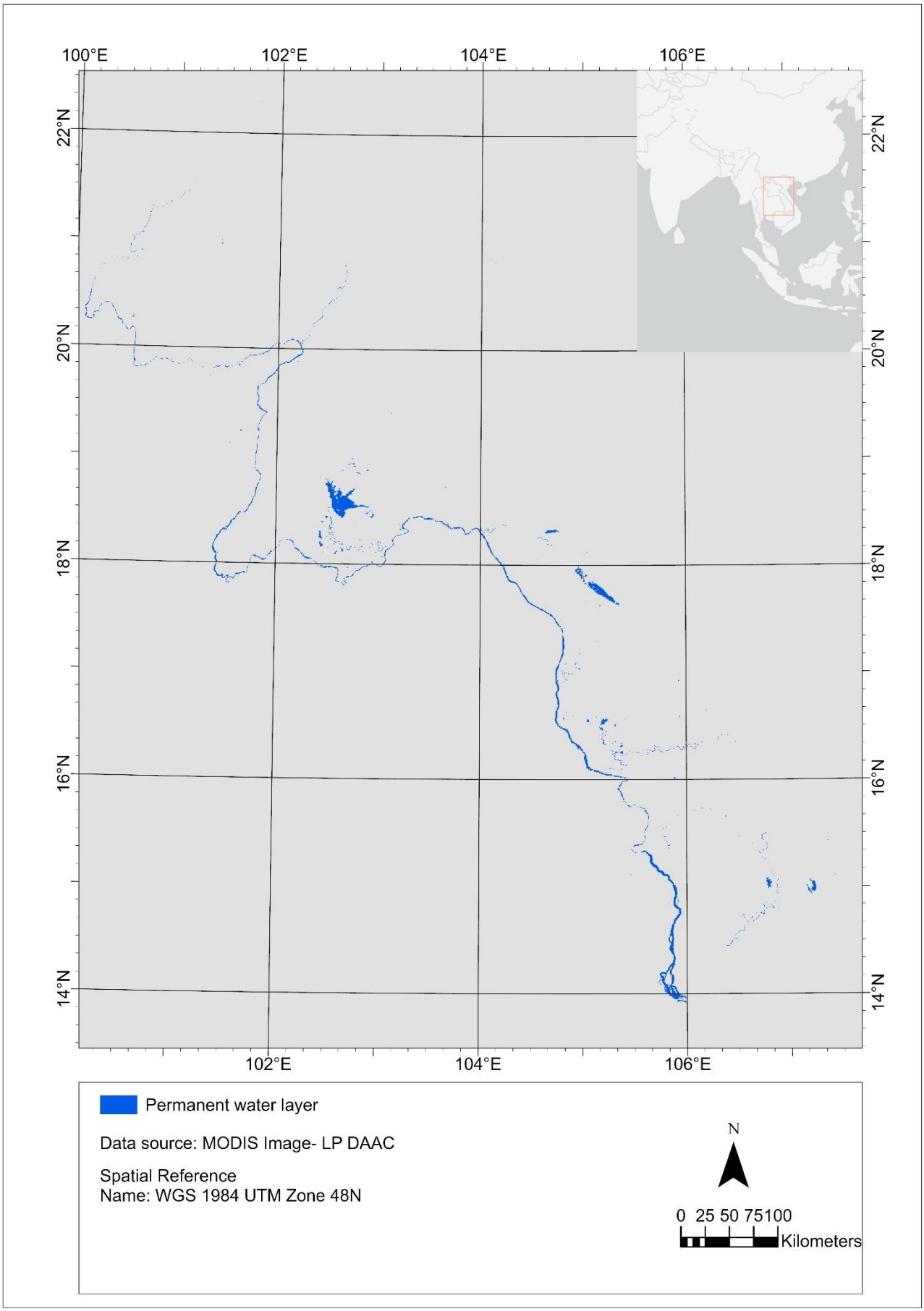

Appendix 4. Map of the forest layer

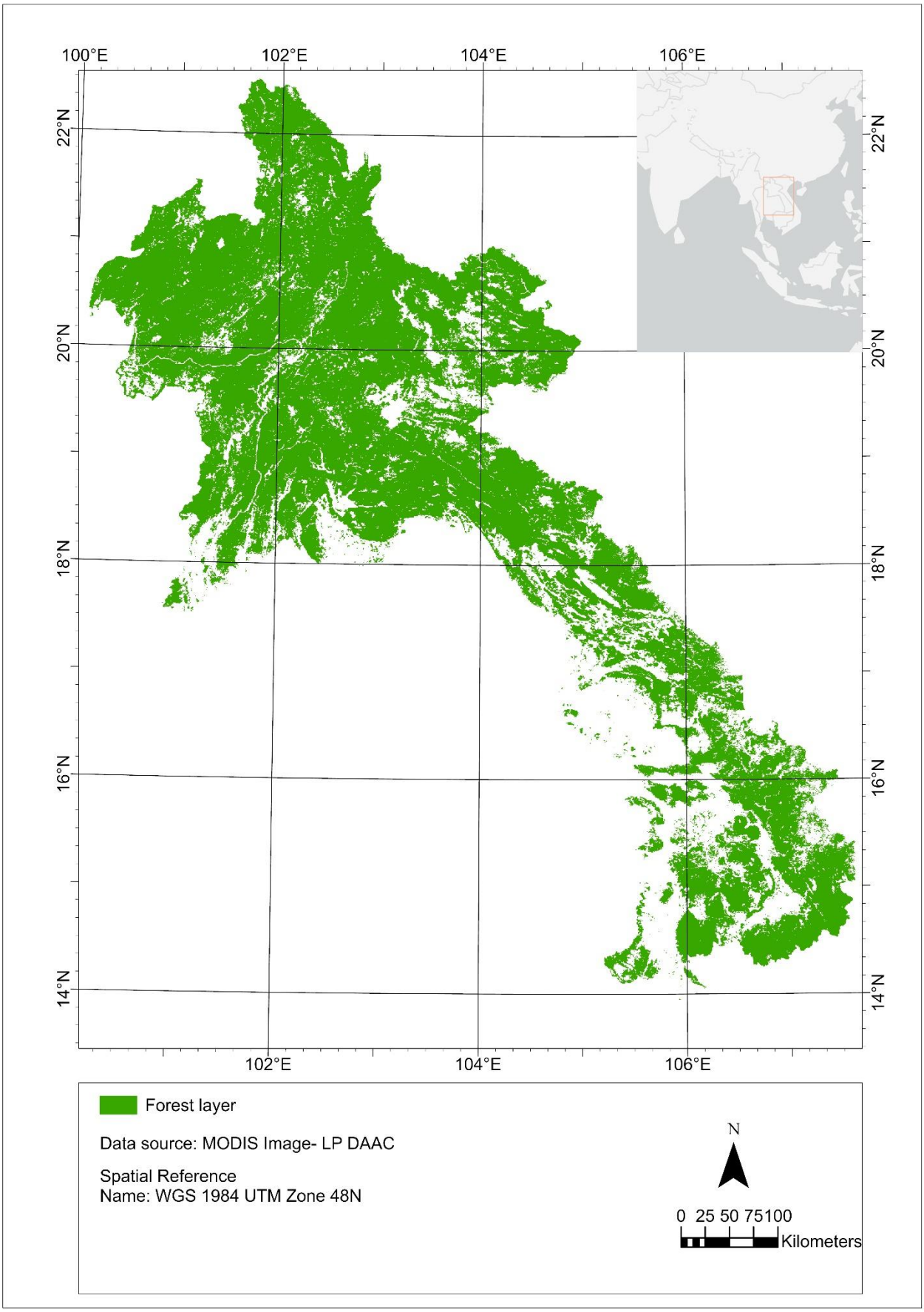

Appendix 5. Map of the slope layer

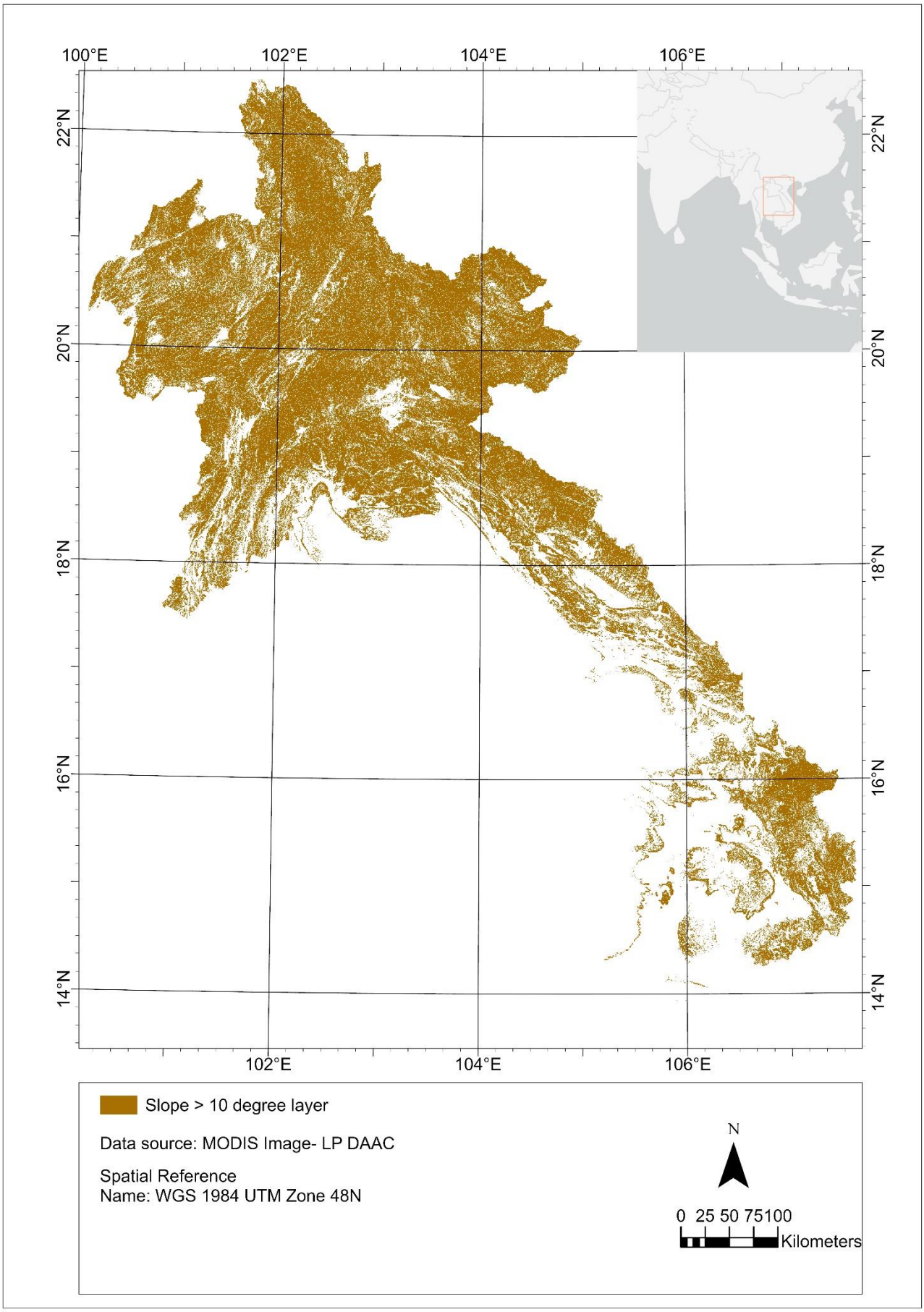

Appendix 6. Map of lowland rice extent

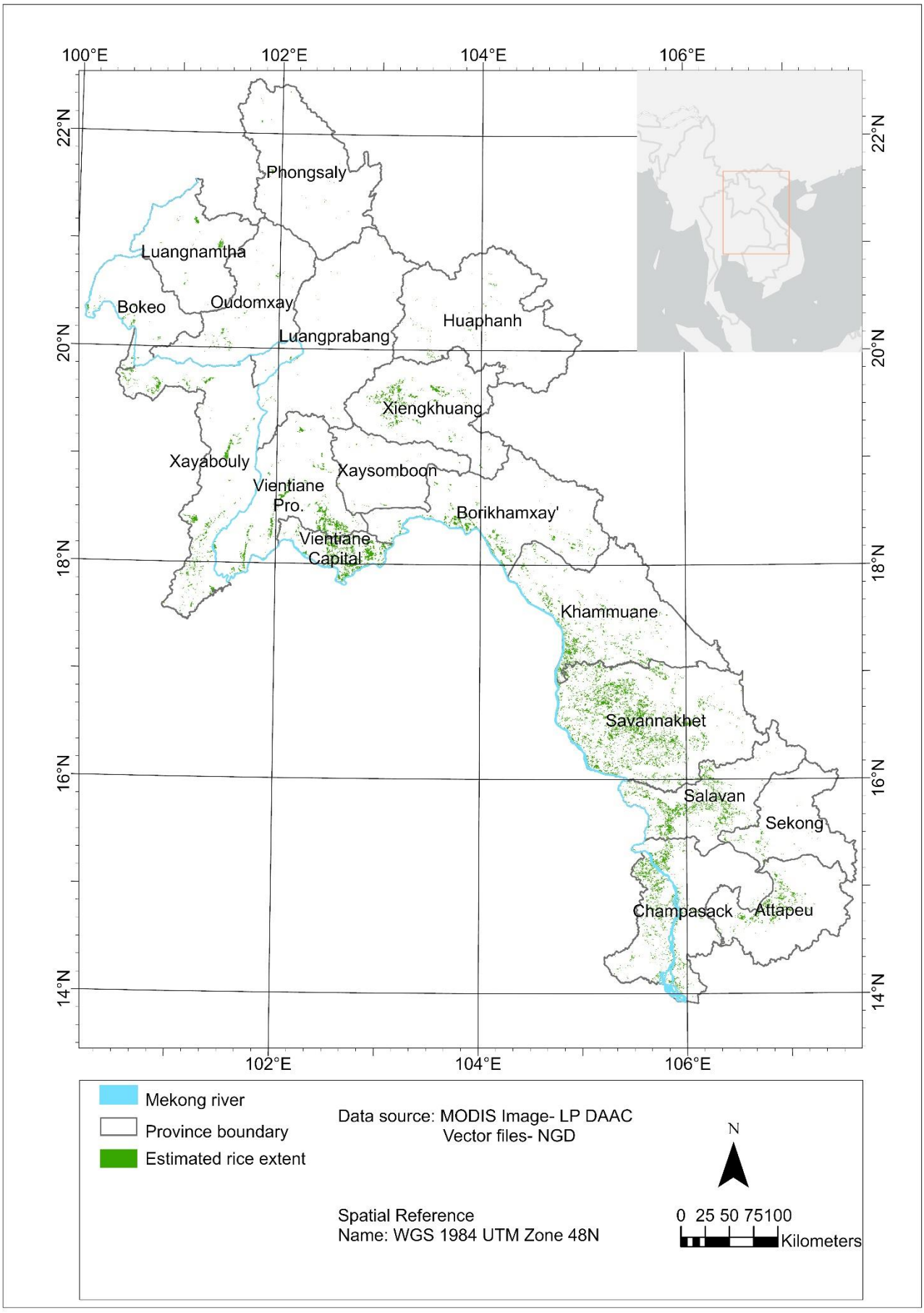

Appendix 7. LSB map of rice-planted areas by province

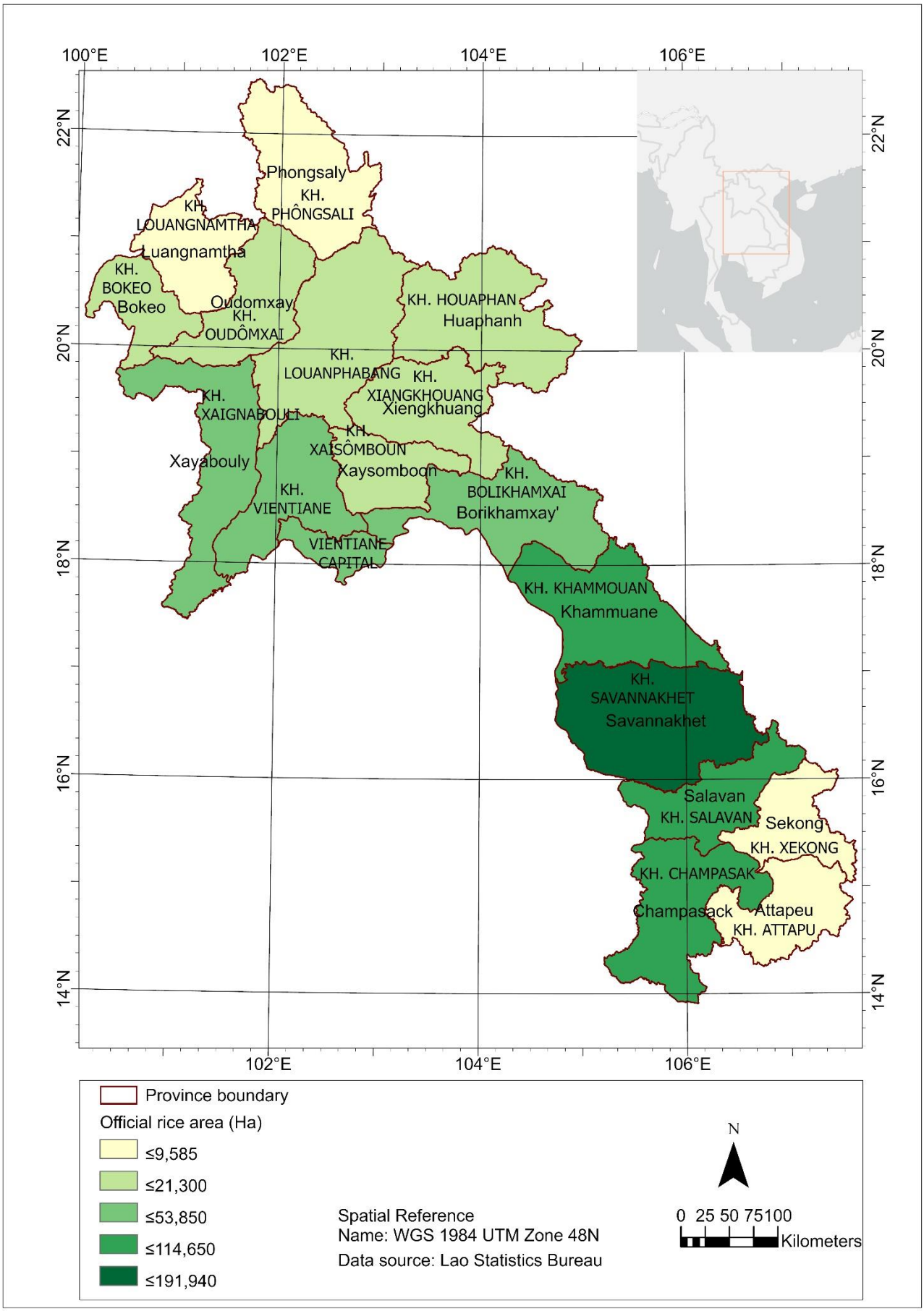

Appendix 8. LSB map of rice production by province

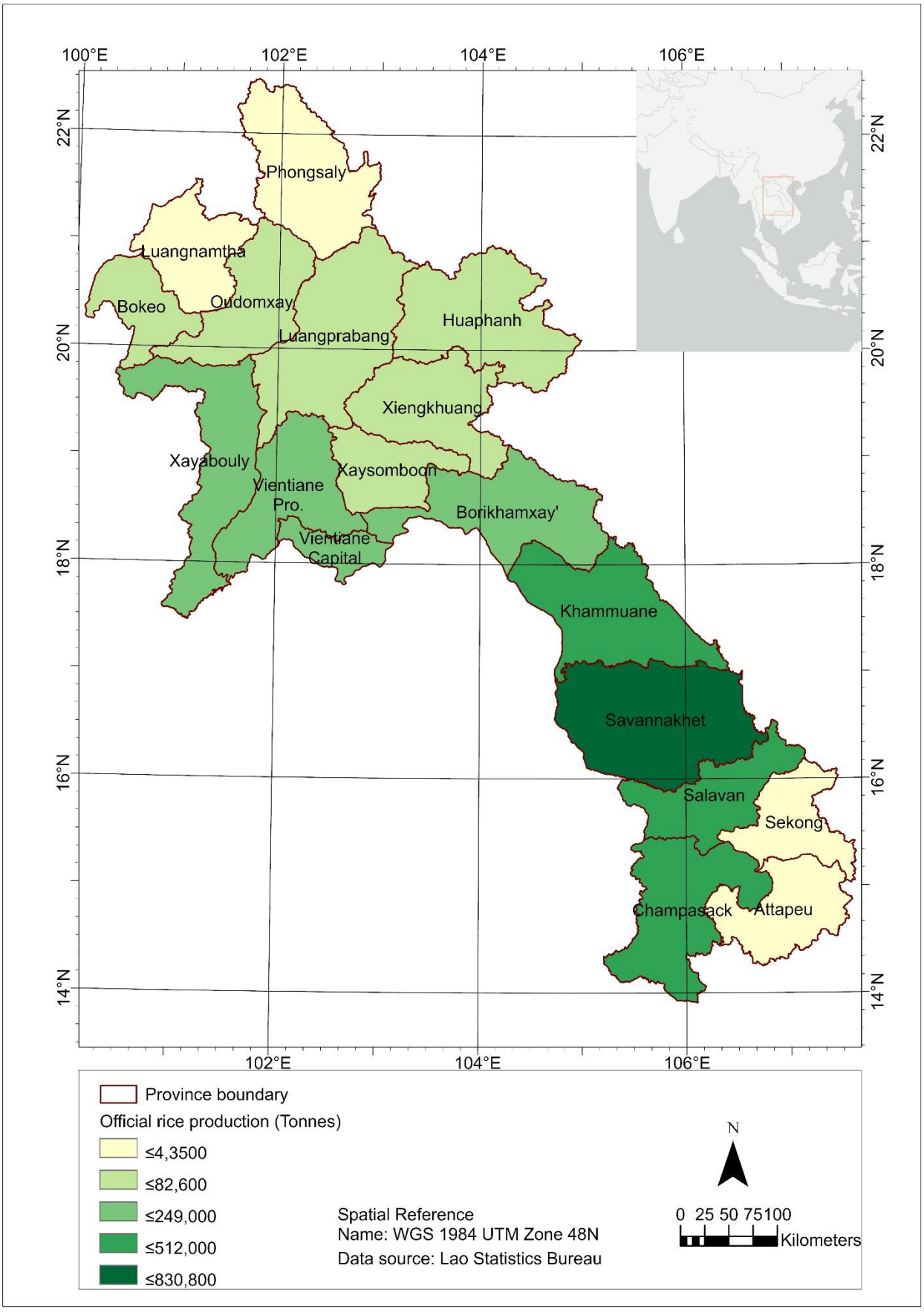

Appendix 9. Map of remotely-sensed extent of rice by district

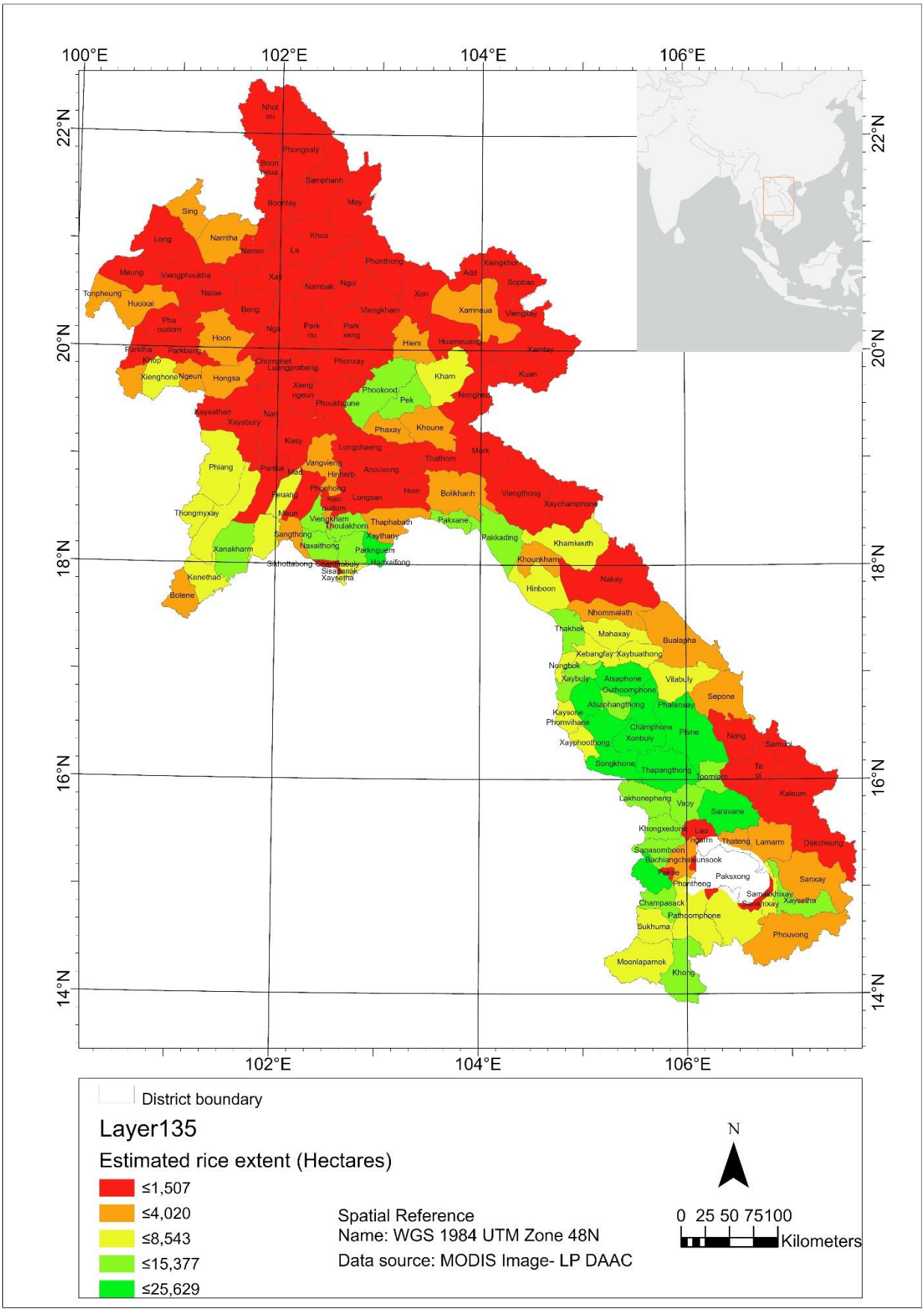

Appendix 10. Map of estimated rice production by district

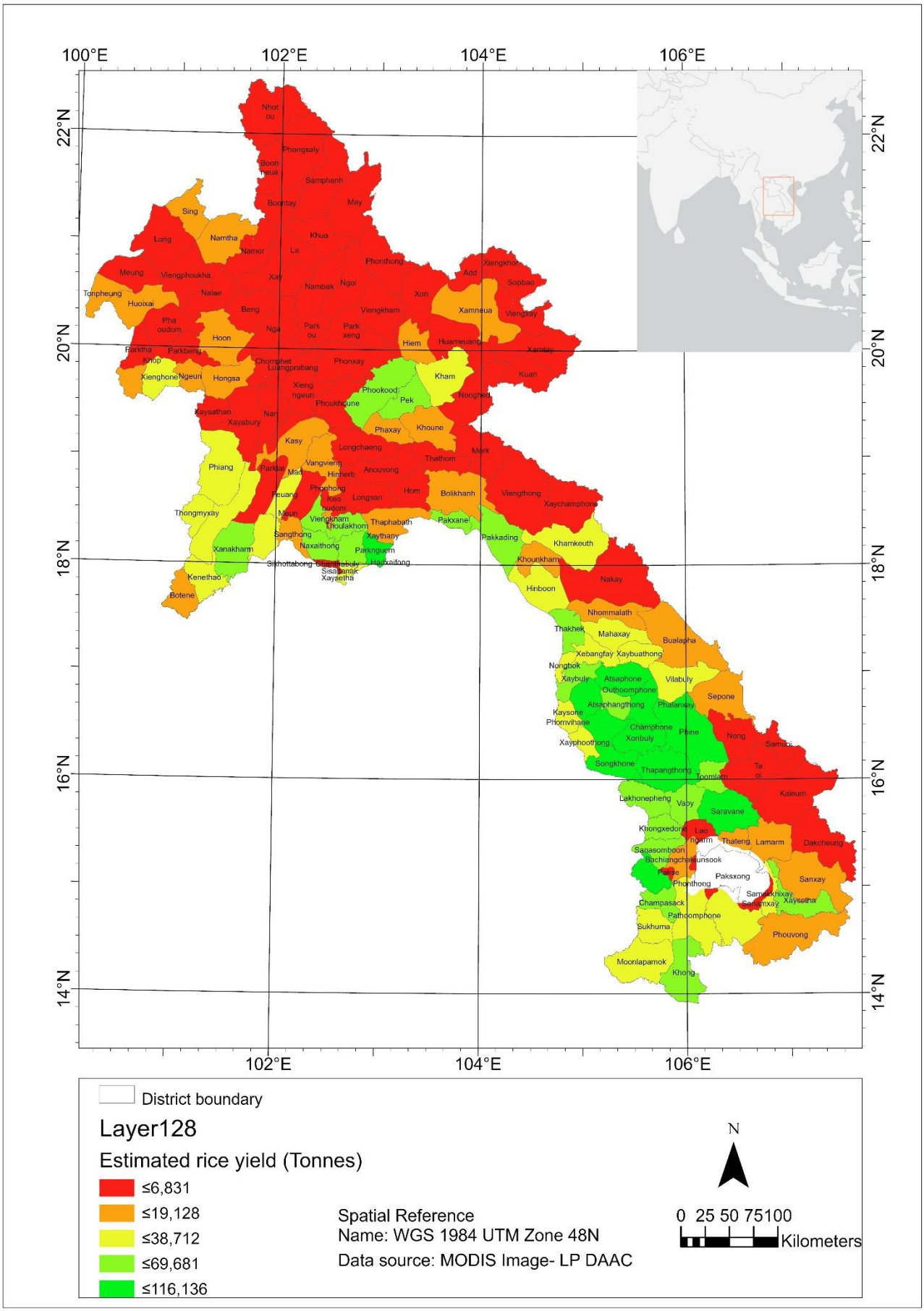

Appendix 11. Summary table of cloud contamination in the Vientiane Plain AEZ

No	Date	Pixel Count			Percentage		
		Cloud	Non-cloud	Total	Cloud	Non-cloud	Total
1	8-May	129	35,777	35,906	0%	100%	100%
2	16-May	3,328	32,578	35,906	9%	91%	100%
3	24-May	23,588	12,318	35,906	66%	34%	100%
4	1-Jun	5,289	30,617	35,906	15%	85%	100%
5	9-Jun	3,116	32,790	35,906	9%	91%	100%
6	17-Jun	2,642	33,264	35,906	7%	93%	100%
7	25-Jun	5,079	30,827	35,906	14%	86%	100%
8	3-Jul	14,729	21,177	35,906	41%	59%	100%
9	11-Jul	2,330	33,576	35,906	6%	94%	100%
10	19-Jul	949	34,957	35,906	3%	97%	100%
11	27-Jul	900	31,961	32,861	3%	97%	100%
12	4-Aug	276	32,585	32,861	1%	99%	100%
13	12-Aug	23,697	12,209	35,906	66%	34%	100%
14	20-Aug	5,173	30,733	35,906	14%	86%	100%
15	28-Aug	12,033	23,873	35,906	34%	66%	100%
16	5-Sep	30,346	5,560	35,906	85%	15%	100%
17	13-Sep	1,600	34,306	35,906	4%	96%	100%
18	21-Sep	1,605	34,301	35,906	4%	96%	100%
19	29-Sep	1,489	31,895	33,384	4%	96%	100%
20	7-Oct	1,548	34,358	35,906	4%	96%	100%
21	15-Oct	97	33,287	33,384	0%	100%	100%
22	23-Oct	2,898	33,008	35,906	8%	92%	100%
23	31-Oct	56	33,328	33,384	0%	100%	100%
24	8-Nov	1,133	34,773	35,906	3%	97%	100%
25	16-Nov	443	32,941	33,384	1%	99%	100%
26	24-Nov	3	35,903	35,906	0%	100%	100%
27	2-Dec	0	34,040	34,040	0%	100%	100%
28	10-Dec	0	34,040	34,040	0%	100%	100%
29	18-Dec	3	34,037	34,040	0%	100%	100%
30	26-Dec	6	34,037	34,043	0%	100%	100%

Appendix 12. Summary table of cloud contamination in the Northern Highlands AEZ

No	Date	Pixel Count			Cloud percentage		
		Cloud	Non-cloud	Total	Cloud	Non-cloud	Total
1	8-May	2,549	312,946	315,495	1%	99%	100%
2	16-May	45,322	270,173	315,495	14%	86%	100%
3	24-May	82,672	232,823	315,495	26%	74%	100%
4	1-Jun	93,355	222,140	315,495	30%	70%	100%
5	9-Jun	82,770	232,725	315,495	26%	74%	100%
6	17-Jun	46,785	268,710	315,495	15%	85%	100%
7	25-Jun	59,317	256,178	315,495	19%	81%	100%
8	3-Jul	126,992	188,503	315,495	40%	60%	100%
9	11-Jul	98,418	217,077	315,495	31%	69%	100%
10	19-Jul	66,275	249,220	315,495	21%	79%	100%
11	27-Jul	31,034	258,186	289,220	11%	89%	100%
12	4-Aug	6,069	283,151	289,220	2%	98%	100%
13	12-Aug	190,809	124,686	315,495	60%	40%	100%
14	20-Aug	83,713	231,782	315,495	27%	73%	100%
15	28-Aug	194,941	120,554	315,495	62%	38%	100%
16	5-Sep	203,348	112,147	315,495	64%	36%	100%
17	13-Sep	25,927	289,568	315,495	8%	92%	100%
18	21-Sep	33,217	260,412	293,629	11%	89%	100%
19	29-Sep	33,217	260,412	293,629	11%	89%	100%
20	7-Oct	73,767	241,728	315,495	23%	77%	100%
21	15-Oct	6,404	287,225	293,629	2%	98%	100%
22	23-Oct	65,210	250,285	315,495	21%	79%	100%
23	31-Oct	8,325	285,304	293,629	3%	97%	100%
24	8-Nov	71,300	244,195	315,495	23%	77%	100%
25	16-Nov	10,847	282,782	293,629	4%	96%	100%
26	24-Nov	20,770	294,725	315,495	7%	93%	100%
27	2-Dec	2,334	296,890	299,224	1%	99%	100%
28	10-Dec	2,204	313,291	315,495	1%	99%	100%
29	18-Dec	4,484	294,740	299,224	1%	99%	100%
30	26-Dec	34,895	280,600	315,495	11%	89%	100%

Appendix 13. Summary table of cloud contamination in the Northern Lowlands AEZ

No	Date	Pixel Count			Pixel Percent		
		Cloud	Non-cloud	Total	Cloud	Non-cloud	Total
1	8-May	7,355	334,862	342,217	2%	98%	100%
2	16-May	50,903	291,314	342,217	15%	85%	100%
3	24-May	147,427	194,790	342,217	43%	57%	100%
4	1-Jun	103,206	239,011	342,217	30%	70%	100%
5	9-Jun	87,212	255,005	342,217	25%	75%	100%
6	17-Jun	42,477	299,740	342,217	12%	88%	100%
7	25-Jun	74,859	267,358	342,217	22%	78%	100%
8	3-Jul	168,081	174,136	342,217	49%	51%	100%
9	11-Jul	68,157	274,060	342,217	20%	80%	100%
10	19-Jul	40,631	301,586	342,217	12%	88%	100%
11	27-Jul	25,760	288,016	313,776	8%	92%	100%
12	4-Aug	5,757	308,019	313,776	2%	98%	100%
13	12-Aug	253,482	88,735	342,217	74%	26%	100%
14	20-Aug	104,395	237,822	342,217	31%	69%	100%
15	28-Aug	191,805	150,412	342,217	56%	44%	100%
16	5-Sep	251,246	90,971	342,217	73%	27%	100%
17	13-Sep	34,315	307,902	342,217	10%	90%	100%
18	21-Sep	29,876	312,341	342,217	9%	91%	100%
19	29-Sep	42,268	276,143	318,411	13%	87%	100%
20	7-Oct	79,347	262,870	342,217	23%	77%	100%
21	15-Oct	8,248	310,163	318,411	3%	97%	100%
22	23-Oct	57,370	284,847	342,217	17%	83%	100%
23	31-Oct	10,952	307,459	318,411	3%	97%	100%
24	8-Nov	40,748	301,469	342,217	12%	88%	100%
25	16-Nov	4,740	313,671	318,411	1%	99%	100%
26	24-Nov	24,524	317,693	342,217	7%	93%	100%
27	2-Dec	1,783	322,935	324,718	1%	99%	100%
28	10-Dec	1,499	340,718	342,217	0%	100%	100%
29	18-Dec	3,324	321,394	324,718	1%	99%	100%
30	26-Dec	34,008	308,207	342,215	10%	90%	100%

Appendix 14. Summary table of cloud contamination along the Mekong Corridor AEZ

No	Date	Pixel Count			Cloud percentage		
		Cloud	Non-cloud	Total	Cloud	Non-cloud	Total
1	8-May	4,048	195,424	199,472	2%	98%	100%
2	16-May	10,220	189,252	199,472	5%	95%	100%
3	24-May	60,177	139,295	199,472	30%	70%	100%
4	1-Jun	31,355	168,117	199,472	16%	84%	100%
5	9-Jun	25,277	174,195	199,472	13%	87%	100%
6	17-Jun	29,560	169,912	199,472	15%	85%	100%
7	25-Jun	145,893	53,579	199,472	73%	27%	100%
8	3-Jul	89,790	109,682	199,472	45%	55%	100%
9	11-Jul	32,603	166,869	199,472	16%	84%	100%
10	19-Jul	10,941	188,531	199,472	5%	95%	100%
11	27-Jul	33,169	149,562	182,731	18%	82%	100%
12	4-Aug	9,301	173,431	182,732	5%	95%	100%
13	12-Aug	161,360	38,112	199,472	81%	19%	100%
14	20-Aug	93,389	106,083	199,472	47%	53%	100%
15	28-Aug	87,584	111,888	199,472	44%	56%	100%
16	5-Sep	122,185	77,287	199,472	61%	39%	100%
17	13-Sep	14,652	184,820	199,472	7%	93%	100%
18	21-Sep	23,334	176,138	199,472	12%	88%	100%
19	29-Sep	8,779	176,801	185,580	5%	95%	100%
20	7-Oct	33,724	165,748	199,472	17%	83%	100%
21	15-Oct	11,855	173,725	185,580	6%	94%	100%
22	23-Oct	179	199,293	199,472	0%	100%	100%
23	31-Oct	1,683	183,897	185,580	1%	99%	100%
24	8-Nov	0	199,472	199,472	0%	100%	100%
25	16-Nov	1,121	184,459	185,580	1%	99%	100%
26	24-Nov	75	199,397	199,472	0%	100%	100%
27	2-Dec	838	188,274	189,112	0%	100%	100%
28	10-Dec	14,248	185,224	199,472	7%	93%	100%
29	18-Dec	58	189,054	189,112	0%	100%	100%
30	26-Dec	3,141	196,331	199,472	2%	98%	100%

Appendix 15. Summary table of cloud contamination in the Central Southern Highlands AEZ

No	Date	Pixel Count			Cloud percentage		
		Cloud	Non-cloud	Total	Cloud	Non-cloud	Total
1	8-May	5,669	152,793	158,462	4%	96%	100%
2	16-May	15,926	142,536	158,462	10%	90%	100%
3	24-May	43,135	115,327	158,462	27%	73%	100%
4	1-Jun	30,837	127,625	158,462	19%	81%	100%
5	9-Jun	47,660	110,802	158,462	30%	70%	100%
6	17-Jun	24,360	134,102	158,462	15%	85%	100%
7	25-Jun	134,102	25,084	159,186	84%	16%	100%
8	3-Jul	96,883	61,579	158,462	61%	39%	100%
9	11-Jul	11,545	146,917	158,462	7%	93%	100%
10	19-Jul	4,495	153,967	158,462	3%	97%	100%
11	27-Jul	20,950	124,256	145,206	14%	86%	100%
12	4-Aug	21,977	123,229	145,206	15%	85%	100%
13	12-Aug	147,234	147,234	294,468	50%	50%	100%
14	20-Aug	91,364	67,098	158,462	58%	42%	100%
15	28-Aug	105,441	53,021	158,462	67%	33%	100%
16	5-Sep	92,831	65,631	158,462	59%	41%	100%
17	13-Sep	17,104	141,358	158,462	11%	89%	100%
18	21-Sep	16,368	142,094	158,462	10%	90%	100%
19	29-Sep	30,063	117,415	147,478	20%	80%	100%
20	7-Oct	47,859	110,603	158,462	30%	70%	100%
21	15-Oct	25,120	122,358	147,478	17%	83%	100%
22	23-Oct	4,475	153,987	158,462	3%	97%	100%
23	31-Oct	20,552	126,926	147,478	14%	86%	100%
24	8-Nov	2,567	155,895	158,462	2%	98%	100%
25	16-Nov	10,557	136,921	147,478	7%	93%	100%
26	24-Nov	30,230	128,232	158,462	19%	81%	100%
27	2-Dec	31,693	118,566	150,259	21%	79%	100%
28	10-Dec	21,463	128,796	150,259	14%	86%	100%
29	18-Dec	21,463	128,796	150,259	14%	86%	100%
30	26-Dec	58,469	99,993	158,462	37%	63%	100%

Appendix 16. Table of rice crop statistics, 2016 derived from the LSB

Code	Province Name	Planted area (Ha)	Production (Tonnes)
1	Vientiane Capital	53,850	245,600
2	Phongsaly	7,720	38,100
3	Luangnamtha	9,585	43,500
4	Oudomxay	15,282	66,200
5	Bokeo	14,565	71,200
6	Luangprabang	14,095	68,000
7	Huaphanh	12,770	61,000
8	Xayabouly	32,390	155,000
9	Xiengkhuang	19,060	81,500
10	Vientiane Pro.	52,950	249,000
11	Borikhamxay'	37,345	153,800
12	Khammuane	81,330	345,300
13	Savannakhet	191,940	830,800
14	Salavan	76,520	358,000
15	Sekong	9,250	40,400
16	Champasack	114,650	512,000
17	Attapeu	7,170	26,000
18	Xaysomboon	21,300	82,600
	Total	771,772	3,428,000

REFERENCES

Ackerman, SA, Strabala, KI, Menzel, WP, Frey, RA, Moeller, CC & Gumley, LE 1998, 'Discriminating clear sky from clouds with MODIS', *Journal of Geophysical Research: Atmospheres*, vol. 103, no. D24, pp. 32141-57.

Ahmadi, N, Dzido, J-L, Vales, M, Rakotoarisoa, J & Chabanne, A 2004, 'Upland rice for highlands: New varieties and sustainable cropping systems for food security promising prospects for the global challenges of rice production the world will face in the coming years?', in.

Appa Rao, S, Bounphanousay, C, Schiller, J, Jackson, M, Inthapanya, P & Doungsila, K 2006, 'The aromatic rice of Laos', in J Schiller, M Chanphengxay, B Linquist & S Appa Rao (eds), *Rice in Lao PDR*, International Rice Resreach Institute, Manila, Philippines, pp. 150 - 74.

Armstrong, J & Ramasawmy, S 2012, *Food security in Lao PDR: A trend analysis* Lao Statistics Bureau (LSB), Forestry Agriculture Organization (FAO), and European Union (EU), Vientiane, Lao PDR.

Basnayake, J, Inthavong, T, Kham, S, Fukai, S, Schiller, J & Chanphengxay, M 2006, 'Climatic diversity within the rice environments in Laos', in J Schiller, M Chanphengxay, B Linquist & S Appa Rao (eds), *Rice in Laos*, IRRI, Makati City, Philipines, pp. 46-61.

Bielecka, E 2005, 'A dasymetric population density map of Poland', in *Proceedings of the 22nd International Cartographic Conference*, vol. 9, p. 15.

2016, *Strategic review of food and nutrition security in Lao People's Democratic Republic* by Bouapao, L, Insouvanh, C, Pholsena, M, Armstrong, J & Staab, M.

2020, *Poverty in Lao PDR : Key findings from the Lao Expenditure and Consumption Survey, 2018-2019*, by Boupha, S, Ministry of Planning and Investment.

Bridhikitti, A & Overcamp, TJ 2012, 'Estimation of Southeast Asian rice paddy areas with different ecosystems from moderate-resolution satellite imagery', *Agriculture, ecosystems & environment*, vol. 146, no. 1, pp. 113-20.

Bruniquel, J & Lopes, A 1997, 'Multi-variate optimal speckle reduction in SAR imagery', *International journal of remote sensing*, vol. 18, no. 3, pp. 603-27.

Cai, X & Sharma, BR 2010, 'Integrating remote sensing, census and weather data for an assessment of rice yield, water consumption and water productivity in the Indo-Gangetic river basin', *Agricultural Water Management*, vol. 97, no. 2, pp. 309-16.

Chandrasekar, K, Sesha Sai, M, Roy, P & Dwevedi, R 2010, 'Land Surface Water Index (LSWI) response to rainfall and NDVI using the MODIS Vegetation Index product', *International journal of remote sensing*, vol. 31, no. 15, pp. 3987-4005.

Chang, K-W, Shen, Y & Lo, J-C 2005, 'Predicting rice yield using canopy reflectance measured at booting stage', *Agronomy Journal*, vol. 97, no. 3, pp. 872-8.

Chen, C, Quilang, E, Alosnos, E & Finnigan, J 2011, 'Rice area mapping, yield, and production forecast for the province of Nueva Ecija using RADARSAT imagery', *Canadian Journal of Remote Sensing*, vol. 37, no. 1, pp. 1-16.

Chen, CF, Son, N, Chang, L & Chen, C 2011, 'Classification of rice cropping systems by empirical mode decomposition and linear mixture model for time-series MODIS 250 m NDVI data in the Mekong Delta, Vietnam', *International journal of remote sensing*, vol. 32, no. 18, pp. 5115-34.

Cheng, Q, Shen, H, Zhang, L, Yuan, Q & Zeng, C 2014, 'Cloud removal for remotely sensed images by similar pixel replacement guided with a spatio-temporal MRF model', *ISPRS Journal of photogrammetry and remote sensing*, vol. 92, pp. 54-68.

Clauss, K, Ottinger, M & Künzer, C 2017, 'Mapping rice areas with Sentinel-1 time series and superpixel segmentation', *International journal of remote sensing*, vol. 39, no. 5, pp. 1399-420.

Clauss, K, Ottinger, M, Leinenkugel, P & Kuenzer, C 2018, 'Estimating rice production in the Mekong Delta, Vietnam, utilising time series of Sentinel-1 SAR data', *International Journal of Applied Earth Observation and Geoinformation*, vol. 73, pp. 574-85.

Dao, PD & Liou, Y-A 2015, 'Object-based flood mapping and affected rice field estimation with Landsat 8 OLI and MODIS data', *Remote Sensing*, vol. 7, no. 5, pp. 5077-97.

Deus, D & Gloaguen, R 2013, 'Remote sensing analysis of lake dynamics in semi-arid regions: implication for water resource management. Lake Manyara, East African Rift, Northern Tanzania', *Water*, vol. 5, no. 2, pp. 698-727.

Didan, K, Munoz, AB, Solano, R & Huete, A 2015, *MODIS Vegetation Index User's Guide*, <https://vip.arizona.edu/documents/MODIS/MODIS_VI_UsersGuide_June_2015_C6.pdf>.

Dong, J & Xiao, X 2016, 'Evolution of regional to global paddy rice mapping methods: A review', *ISPRS Journal of photogrammetry and remote sensing*, vol. 119, pp. 214-27.

Eliste, P & Santos, N 2012, *Lao People's Democratic Republic Rice Policy Study*, IRRI, MAF,WB,FAO, Rome, Italy.

Elshorbagy, AMA 2013, 'A low-cost rice mapping remote sensing based algorithm'.

ESA 2000-2020, *Sentinel-1 SAR user guide*, <https://sentinel.esa.int/web/sentinel/user-guides/sentinel-1-sar>.

2020, *Special Report - 2019 FAO/WFP Crop and Food Security Assessment Mission to the Lao People's Democratic Republic*, by FAO, FAO, WFP.

Forkuor, G, Conrad, C, Thiel, M, Ullmann, T & Zoungrana, E 2014, 'Integration of optical and Synthetic Aperture Radar imagery for improving crop mapping in Northwestern Benin, West Africa', *Remote Sensing*, vol. 6, no. 7, pp. 6472-99.

Fukai, S 1999, 'Phenology in rainfed lowland rice', *Field Crops Research*, vol. 64, no. 1-2, pp. 51-60.

Gao, B-C 1996, 'NDWI—A normalized difference water index for remote sensing of vegetation liquid water from space', *Remote Sensing of Environment*, vol. 58, no. 3, pp. 257-66.

Gao, B, Yang, P, Han, W, Li, R & Wiscombe, W 2002, *An algorithm using visible and 1.38-µm channels to retrieve cirrus cloud reflectances from aircraft and satellite data, IEEE T. Geosci. Remote, 40, 1659–1668*.

Gesch, B, Muller, J & Farr, TG 2006, 'The shuttle radar topography mission-Data validation and applications', *Photogrammetric engineering and remote sensing*, vol. 72, no. 3, p. 233.

2013, *FAO Country Programming Framework for Lao PDR 2013-2015*, by GoL & FAO, Food and Agriculture Organization of the United Nations and Ministry of Agriculture and Forestry , Government of Lao PDR.

González-Márquez, LC, Torres-Bejarano, FM, Torregroza-Espinosa, AC, Hansen-Rodríguez, IR & Rodríguez-Gallegos, HB 2018, 'Use of landsat 8 images for depth and water quality assessment of El Guájaro reservoir, Colombia', vol. 82, pp. 231-8.

Groten, S 1993, 'NDVI—crop monitoring and early yield assessment of Burkina Faso', *TitleREMOTE SENSING*, vol. 14, no. 8, pp. 1495-515.

Gumma, MK, Nelson, A, Thenkabail, PS & Singh, AN 2011, 'Mapping rice areas of South Asia using MODIS multitemporal data', *Journal of Applied Remote Sensing*, vol. 5, no. 1, p. 053547.

Gumma, MK, Thenkabail, PS, Maunahan, A, Islam, S & Nelson, A 2014, 'Mapping seasonal rice cropland extent and area in the high cropping intensity environment of Bangladesh using MODIS 500 m data for the year 2010', *ISPRS Journal of photogrammetry and remote sensing*, vol. 91, pp. 98-113.

Gupta, PC & O'Toole, JC 1986, *Upland rice: a global perspective*, Int. Rice Res. Inst.

Hattori, Y, Nagai, K & Ashikari, M 2011, 'Rice growth adapting to deepwater', *Current opinion in plant biology*, vol. 14, no. 1, pp. 100-5.

Heinimann, A, Hett, C, Hurni, K, Messerli, P, Epprecht, M, Jørgensen, L & Breu, T 2013, 'Socio-economic perspectives on shifting cultivation landscapes in Northern Laos', *Human Ecology*, vol. 41, no. 1, pp. 51-62.

Huang, J, Wang, X, Li, X, Tian, H & Pan, Z 2013, 'Remotely sensed rice yield prediction using multi-temporal NDVI data derived from NOAA's-AVHRR', *PloS one*, vol. 8, no. 8, p. e70816.

Huete, A, Didan, K, Miura, T, Rodriguez, EP, Gao, X & Ferreira, LG 2002, 'Overview of the radiometric and biophysical performance of the MODIS vegetation indices', *Remote Sensing of Environment*, vol. 83, no. 1-2, pp. 195-213.

Huete, A, Liu, H, Batchily, K & Van Leeuwen, W 1997, 'A comparison of vegetation indices over a global set of TM images for EOS-MODIS', *Remote Sensing of Environment*, vol. 59, no. 3, pp. 440-51.

Hurni, K, Hett, C, Epprecht, M, Messerli, P & Heinimann, A 2013, 'A texture-based land cover classification for the delineation of a shifting cultivation landscape in the Lao PDR using landscape metrics', *Remote Sensing*, vol. 5, no. 7, pp. 3377-96.

Hurni, K, Hett, C, Heinimann, A, Messerli, P & Wiesmann, U 2013, 'Dynamics of shifting cultivation landscapes in Northern Lao PDR between 2000 and 2009 based on an analysis of MODIS time series and Landsat images', *Human Ecology*, vol. 41, no. 1, pp. 21-36.

Ikeura, H, Phongchanmixay, S, Phonsangone, S, Xaypanya, P, Inkhamseng, S & Soubat, S 2016, 'Factors affecting differences in the rainy season rice yield in a lowland area of a mountainous village in Lao PDR', *Paddy and water environment*, vol. 14, no. 2, pp. 343-53.

IRRI, LB 1975, 'Major research in upland rice', *Major research in upland rice.*

Ishimaru, T, Xaiyalath, S, Nallathambi, J, Sathishraj, R, Yoshimoto, M, Phoudalay, L, Samson, B, Hasegawa, T, Hayashi, K & Arumugam, G 2016, 'Quantifying rice spikelet sterility in potential heat-vulnerable regions: Field surveys in Laos and southern India', *Field Crops Research*, vol. 190, pp. 3-9.

Jackson, TJ, Chen, D, Cosh, M, Li, F, Anderson, M, Walthall, C, Doriaswamy, P & Hunt, ER 2004, 'Vegetation water content mapping using Landsat data derived normalized difference water index for corn and soybeans', *Remote Sensing of Environment*, vol. 92, no. 4, pp. 475-82.

Jamali, S, Seaquist, J, Ardö, J & Eklundh, L 2011, 'Investigating temporal relationships between rainfall, soil moisture and MODIS-derived NDVI and EVI for six sites in Africa', *Savanna*, vol. 21, no. 547550, p. 38.

Jensen, JR 2007, 'Remote sensing of vegetation', in 2nd (ed.), *Remote sensing of the environment: An earth resource perspective*, Pearson Prentice Hall, Upper Saddle River, New Jork, pp. 355-408.

Kanemaru, K, Muhammad, R & Hirota, I 2014, 'Analysis of monsoon climate variability for swidden agriculture in northern Laos', in *Integrated studies of social and natural environmental transition in Laos*, Springer, pp. 85-97.

Khorram, S, Koch, FH, van der Wiele, CF & Nelson, SA 2012, *Remote sensing*, Springer Science & Business Media.

Khorram, S, Van Der Wiele, CF, Koch, FH, Nelson, SA & Potts, MD 2016, *Principles of applied remote sensing*, Springer.

Kim, H-O & Yeom, J-M 2014, 'Effect of red-edge and texture features for object-based paddy rice crop classification using RapidEye multi-spectral satellite image data', *International journal of remote sensing*, vol. 35, no. 19, pp. 7046-68.

Kirches, G, Brockmann, C, Boettcher, M, Peters, M, Bontemps, S, Lamarche, C, Schlerf, M, Santoro, M & Defourny, P 2017, *Land cover cci-product user guide version 2.0. ESA Public Document CCI-LC-PUG*.

Kittikhoun, A 2009, 'Small state, big revolution: geography and the revolution in Laos', *Theory and society*, vol. 38, no. 1, pp. 25-55.

Kogan, F 1990, 'Remote sensing of weather impacts on vegetation in non-homogeneous areas', *International journal of remote sensing*, vol. 11, no. 8, pp. 1405-19.

Kontgis, C, Schneider, A & Ozdogan, M 2015, 'Mapping rice paddy extent and intensification in the Vietnamese Mekong River Delta with dense time stacks of Landsat data', *Remote Sensing of Environment*, vol. 169, pp. 255-69.

Krishnamurthy, K, Chong, A & Poungprom, R 2015, *Consolidated livelihood exercise for analysing resilience (CLEAR)*, Disaster Management and Climate Change (DDMCC) and the World Food Programme (WFP), Vientiane, Laos.

Kuenzer, C & Knauer, K 2013, 'Remote sensing of rice crop areas', *International journal of remote sensing*, vol. 34, no. 6, pp. 2101-39.

Lasko, K, Vadrevu, KP, Tran, VT & Justice, C 2018, 'Mapping double and single crop paddy rice with Sentinel-1A at varying spatial scales and polarizations in Hanoi, Vietnam', *IEEE Journal of Selected Topics in Applied Earth Observations and Remote Sensing*, vol. 11, no. 2, pp. 498-512.

Le Toan, T, Ribbes, F, Wang, L-F, Floury, N, Ding, K-H, Kong, JA, Fujita, M & Kurosu, T 1997, 'Rice crop mapping and monitoring using ERS-1 data based on experiment and modeling results', *IEEE Transactions on Geoscience and Remote Sensing*, vol. 35, no. 1, pp. 41-56.

Li, X, El Solh, M & Siddique, K 2019, *Mountain Agriculture: Opportunities for Harnessing Zero Hunger in Asia*, Food and Agriculture Organization of the United Nations (FAO).

Linquist, B, Keoboualapha, B, Sipaseuth, P & Inthapanya, P 2006, 'Rice production systems of Laos', in J Schiller, M Chanphengxay, B Linquist & S Appa Rao (eds), *Rice in Laos*, IRRI, Manila,

Philippines, pp. 29-45.

Liu, J, Xu, Z, Chen, F, Chen, F & Zhang, L 2019, 'Flood hazard mapping and assessment on the Angkor world heritage site, Cambodia', *Remote Sensing*, vol. 11, no. 1, p. 98.

Lopes, A, Nezry, E, Touzi, R & Laur, H 1993, 'Structure detection and statistical adaptive speckle filtering in SAR images', *International journal of remote sensing*, vol. 14, no. 9, pp. 1735-58.

Lopes, A, Touzi, R & Nezry, E 1990, 'Adaptive speckle filters and scene heterogeneity', *IEEE Transactions on Geoscience and Remote Sensing*, vol. 28, no. 6, pp. 992-1000.

LSB 2019, *LAOSIS*, <https://laosis.lsb.gov.la/tblInfo/TblInfoList.do;jsessionid=3c1VPiVLmr6NzNgyp4H3N4jgezZY3Rz8qZK8GRFZ.laosis-web>.

2018, *Lao Social Indicator Survey II 2017, Survey Findings Report*, by LSB & UNICEF, Lao Statistics Bureau and UNICEF.

Manivong, V, Cramb, R & Newby, J 2014, 'Rice and remittances: crop intensification versus labour migration in Southern Laos', *Human Ecology*, vol. 42, no. 3, pp. 367-79.

Mansaray, LR, Huang, W, Zhang, D, Huang, J & Li, J 2017, 'Mapping rice fields in urban Shanghai, southeast China, using Sentinel-1A and Landsat 8 datasets', *Remote Sensing*, vol. 9, no. 3, p. 257.

Mansaray, LR, Wang, F, Huang, J, Yang, L & Kanu, AS 2019, 'Accuracies of support vector machine and random forest in rice mapping with Sentinel-1A, Landsat-8 and Sentinel-2A datasets', *Geocarto International*, pp. 1-21.

Mohanty, S, Wailes, E & Chavez, E 2010, 'The global rice supply and demand outlook: the need for greater productivity growth to keep rice affordable', *Rice in the Global Economy: Strategic Research and Policy Issues for Food Security. International Rice Research Institute, Los Baños*.

Moldenhauer, K & Slaton, N 2001, 'Rice growth and development', in *Rice production handbook*, vol. 192, pp. 7-14.

Mosleh, M, Hassan, Q & Chowdhury, E 2015, 'Application of remote sensors in mapping rice area and forecasting its production: A review', *Sensors*, vol. 15, no. 1, pp. 769-91.

Mosleh, MK, Hassan, QK & Chowdhury, EH 2015, 'Application of remote sensors in mapping rice area and forecasting its production: A review', *Sensors*, vol. 15, no. 1, pp. 769-91.

Nagle, NN, Buttenfield, BP, Leyk, S & Spielman, S 2014, 'Dasymetric modeling and uncertainty', *Annals of the Association of American Geographers*, vol. 104, no. 1, pp. 80-95.

Nelson, A, Setiyono, T, Rala, AB, Quicho, ED, Raviz, JV, Abonete, PJ, Maunahan, AA, Garcia, CA, Bhatti, HZM & Villano, LS 2014, 'Towards an operational SAR-based rice monitoring system in Asia: Examples from 13 demonstration sites across Asia in the RIICE project', *Remote Sensing*, vol. 6, no. 11, pp. 10773-812.

Nguyen, DB, Gruber, A & Wagner, W 2016, 'Mapping rice extent and cropping scheme in the Mekong Delta using Sentinel-1A data', *Remote Sensing Letters*, vol. 7, no. 12, pp. 1209-18.

Nguyen, TTH, De Bie, C, Ali, A, Smaling, E & Chu, TH 2012, 'Mapping the irrigated rice cropping patterns of the Mekong delta, Vietnam, through hyper-temporal SPOT NDVI image analysis', *International journal of remote sensing*, vol. 33, no. 2, pp. 415-34.

Noureldin, N, Aboelghar, M, Saudy, H & Ali, A 2013, 'Rice yield forecasting models using satellite

imagery in Egypt', *The Egyptian Journal of Remote Sensing and Space Science*, vol. 16, no. 1, pp. 125-31.

Oza, S, Panigrahy, S & Parihar, JS 2008, 'Concurrent use of active and passive microwave remote sensing data for monitoring of rice crop', *International Journal of Applied Earth Observation and Geoinformation*, vol. 10, no. 3, pp. 296-304.

Peña-Barragán, JM, Ngugi, MK, Plant, RE & Six, J 2011, 'Object-based crop identification using multiple vegetation indices, textural features and crop phenology', *Remote Sensing of Environment*, vol. 115, no. 6, pp. 1301-16.

Peng, D, Huete, AR, Huang, J, Wang, F & Sun, H 2011, 'Detection and estimation of mixed paddy rice cropping patterns with MODIS data', *International Journal of Applied Earth Observation and Geoinformation*, vol. 13, no. 1, pp. 13-23.

Petrov, A 2012, 'One hundred years of dasymetric mapping: back to the origin', *The Cartographic Journal*, vol. 49, no. 3, pp. 256-64.

Pozhamkandath, V, Nampanya, S & Ishihara, N 2014, *Lao Census of Agriculture 2010/11: Aalayis of selected themes* MAF, FAO, SDC, Vientiane, Lao PDR.

Rao, SA, Bounphanousay, C, Schiller, J, Alcantara, A & Jackson, M 2002, 'Naming of traditional rice varieties by farmers in the Lao PDR', *Genetic Resources and Crop Evolution*, vol. 49, no. 1, pp. 83-8.

Reiche, J, Hamunyela, E, Verbesselt, J, Hoekman, D & Herold, M 2018, 'Improving near-real time deforestation monitoring in tropical dry forests by combining dense Sentinel-1 time series with Landsat and ALOS-2 PALSAR-2', *Remote Sensing of Environment*, vol. 204, pp. 147-61.

Rosenqvist, A, Shimada, M, Ito, N & Watanabe, M 2007, 'ALOS PALSAR: A pathfinder mission for global-scale monitoring of the environment', *IEEE Transactions on Geoscience and Remote Sensing*, vol. 45, no. 11, pp. 3307-16.

Saito, K, Linquist, B, Keobualapha, B, Shiraiwa, T & Horie, T 2006, 'Farmers' knowledge of soils in relation to cropping practices: A case study of farmers in upland rice based slash-and-burn systems of northern Laos', *Geoderma*, vol. 136, no. 1-2, pp. 64-74.

Sakamoto, T, Van Nguyen, N, Ohno, H, Ishitsuka, N & Yokozawa, M 2006, 'Spatio–temporal distribution of rice phenology and cropping systems in the Mekong Delta with special reference to the seasonal water flow of the Mekong and Bassac rivers', *Remote Sensing of Environment*, vol. 100, no. 1, pp. 1-16.

2018, *Post-disaster needs assessment, 2018 floods, LAO PDR*, by Saysompheng, K, Government of Lao People’s Democratic Republic.

Schiller, J, Chanphengxay, M, Linquist, B & Appa Rao, S 2006, *Rice in Laos*, International Rice Research Institute, Manila, Philippines.

Schiller, J, Linquist, B, Douangsila, K, Inthapanya, P, Douang Boupha, B, Inthavong, S & Sengxua, P 2001, *Constraints to rice production systems in Laos*.

Shao, Y, Fan, X, Liu, H, Xiao, J, Ross, S, Brisco, B, Brown, R & Staples, G 2001, 'Rice monitoring and production estimation using multitemporal RADARSAT', *Remote Sensing of Environment*, vol. 76, no. 3, pp. 310-25.

Singha, M, Wu, B & Zhang, M 2016, 'An object-based paddy rice classification using multi-spectral data and crop phenology in Assam, Northeast India', *Remote Sensing*, vol. 8, no. 6, p. 479.

Skakun, S, Vermote, E, Roger, J-C & Franch, B 2017, 'Combined use of Landsat-8 and Sentinel-2A images for winter crop mapping and winter wheat yield assessment at regional scale', *AIMS geosciences*, vol. 3, no. 2, p. 163.

Slagter, B, Tsendbazar, N-E, Vollrath, A & Reiche, J 2020, 'Mapping wetland characteristics using temporally dense Sentinel-1 and Sentinel-2 data: A case study in the St. Lucia wetlands, South Africa', *International Journal of Applied Earth Observation and Geoinformation*, vol. 86, p. 102009.

Son, N, Chen, C, Chen, C, Chang, L, Duc, H & Nguyen, L 2013, 'Prediction of rice crop yield using MODIS EVI− LAI data in the Mekong Delta, Vietnam', *International journal of remote sensing*, vol. 34, no. 20, pp. 7275-92.

Son, N, Chen, C, Chen, C, Minh, V & Trung, N 2014, 'A comparative analysis of multitemporal MODIS EVI and NDVI data for large-scale rice yield estimation', *Agricultural and Forest Meteorology*, vol. 197, pp. 52-64.

Sozzi, M, Marinello, F, Pezzuolo, A & Sartori, L 2018, 'Benchmark of satellites image services for precision agricultural use', in *Proceedings of the AgEng Conference, Wageningen, The Netherlands*, pp. 8-11.

Su, M-D, Lin, M-C, Hsieh, H-I, Tsai, B-W & Lin, C-H 2010, 'Multi-layer multi-class dasymetric mapping to estimate population distribution', *Science of the total environment*, vol. 408, no. 20, pp. 4807-16.

Su, X, Yan, X & Tsai, CL 2012, 'Linear regression', *Wiley Interdisciplinary Reviews: Computational Statistics*, vol. 4, no. 3, pp. 275-94.

Suepa, T 2013, 'Satellite time-series data for vegetation phenology detection and environmental assessment in Southeast Asia', Doctor of Philosophy thesis, Michigan State University.

Sun, C, Bian, Y, Zhou, T & Pan, J 2019, 'Using of multi-source and multi-temporal remote sensing data improves crop-type mapping in the subtropical agriculture region', *Sensors*, vol. 19, no. 10, p. 2401.

Sun, H-s, Huang, J-f, Huete, AR, Peng, D-l & Zhang, F 2009, 'Mapping paddy rice with multi-date moderate-resolution imaging spectroradiometer (MODIS) data in China', *Journal of Zhejiang University-SCIENCE A*, vol. 10, no. 10, pp. 1509-22.

Sun, P, Zhang, J, Zhu, X, Pan, Y & Liu, H 2017, 'A highly efficient temporal-spatial probability synthesized model from multi-temporal remote sensing for paddy rice identification', *European Journal of Remote Sensing*, vol. 50, no. 1, pp. 98-110.

Tan, C-P, Koay, J-Y, Lim, K-S, Ewe, H-T & Chuah, H-T 2007, 'Classification of multi-temporal SAR images for rice crops using combined entropy decomposition and support vector machine technique', *Progress In Electromagnetics Research*, vol. 71, pp. 19-39.

Tian, H, Wu, M, Wang, L & Niu, Z 2018, 'Mapping early, middle and late rice extent using sentinel-1A and Landsat-8 data in the poyang lake plain, China', *Sensors*, vol. 18, no. 1, p. 185.

Tingting, L & Chuang, L 2010, 'Study on extraction of crop information using time-series MODIS data in the Chao Phraya Basin of Thailand', *Advances in Space Research*, vol. 45, no. 6, pp. 775-84.

Torbick, N, Chowdhury, D, Salas, W & Qi, J 2017, 'Monitoring rice agriculture across myanmar using time series Sentinel-1 assisted by Landsat-8 and PALSAR-2', *Remote Sensing*, vol. 9, no. 2, p. 119.

UN 2019, *2018 progress report: Lao PDR- United Nations Partnership Frame Work 2017-2021, A partnership for Sustainable Development*.

Van Tricht, K, Gobin, A, Gilliams, S & Piccard, I 2018, 'Synergistic use of radar Sentinel-1 and optical Sentinel-2 imagery for crop mapping: A case study for Belgium', *Remote Sensing*, vol. 10, no. 10, p. 1642.

Vermote, EF, Roger, JC & Ray, JP 2015, *MODIS Surface Reflectance User's Guide*, <https://lpdaac.usgs.gov/documents/306/MOD09_User_Guide_V6.pdf>.

Vermote, FE, Kotchenova, SY & Ray, JP 2011, *MODIS surface reflectance user's guide*, <http://modis-sr.ltdri.org/guide/MOD09_UserGuide_v1_3.pdf>.

Wardlow, BD, Egbert, SL & Kastens, JH 2007, 'Analysis of time-series MODIS 250 m vegetation index data for crop classification in the US Central Great Plains', *Remote Sensing of Environment*, vol. 108, no. 3, pp. 290-310.

WFP 2013, *Food and nutrition security Atlas of Lao PDR* United Nations World Food Programme, and
Federal Ministry for Economic Cooperation and Development Vientian, Lao PDR.

Willmott, CJ & Matsuura, K 2005, 'Advantages of the mean absolute error (MAE) over the root mean square error (RMSE) in assessing average model performance', *Climate research*, vol. 30, no. 1, pp. 79-82.

Wulder, MA, White, JC, Hay, GJ & Castilla, G 2008, 'Towards automated segmentation of forest inventory polygons on high spatial resolution satellite imagery', *The Forestry Chronicle*, vol. 84, no. 2, pp. 221-30.

Xia, Z, Peng, Y, Liu, S, Liu, Z, Wang, G, Zhu, A & Hu, Y 2019, 'The Optimal Image Date Selection for Evaluating Cultivated Land Quality Based on Gaofen-1 Images', *Sensors*, vol. 19, no. 22, p. 4937.

Xiao, X, Boles, S, Frolking, S, Li, C, Babu, JY, Salas, W & Moore III, B 2006, 'Mapping paddy rice agriculture in South and Southeast Asia using multi-temporal MODIS images', *Remote Sensing of Environment*, vol. 100, no. 1, pp. 95-113.

Xiao, X, Boles, S, Frolking, S, Salas, W, Moore Iii, B, Li, C, He, L & Zhao, R 2002, 'Observation of flooding and rice transplanting of paddy rice fields at the site to landscape scales in China using VEGETATION sensor data', *International journal of remote sensing*, vol. 23, no. 15, pp. 3009-22.

Xiao, X, Boles, S, Liu, J, Zhuang, D, Frolking, S, Li, C, Salas, W & Moore III, B 2005, 'Mapping paddy rice agriculture in southern China using multi-temporal MODIS images', *Remote Sensing of Environment*, vol. 95, no. 4, pp. 480-92.

Xiao, X, He, L, Salas, W, Li, C, Moore Iii, B, Zhao, R, Frolking, S & Boles, S 2002, 'Quantitative relationships between field-measured leaf area index and vegetation index derived from VEGETATION images for paddy rice fields', *International journal of remote sensing*, vol. 23, no. 18, pp. 3595-604.

Zanter, K 2016, 'Landsat 8 (L8) data users handbook', *Landsat Science Official Website*.

Zhang, G, Xiao, X, Dong, J, Kou, W, Jin, C, Qin, Y, Zhou, Y, Wang, J, Menarguez, MA & Biradar, C 2015, 'Mapping paddy rice planting areas through time series analysis of MODIS land surface temperature and vegetation index data', *ISPRS Journal of photogrammetry and remote sensing*, vol. 106, pp. 157-71.

Zhang, HK, Roy, DP, Yan, L, Li, Z, Huang, H, Vermote, E, Skakun, S & Roger, J-C 2018, 'Characterization of Sentinel-2A and Landsat-8 top of atmosphere, surface, and nadir BRDF adjusted reflectance and NDVI differences', *Remote Sensing of Environment*, vol. 215, pp. 482-94.

Zhang, P 2007, 'Remotely-sensed vegetation metrics for real-time crop monitoring and yield estimation', Doctor of Philosophy thesis, BOSTON UNIVERSITY.

Zhang, T, Ren, H, Qin, Q & Sun, Y 2018, 'Snow Cover Monitoring with Chinese Gaofen-4 PMS Imagery and the Restored Snow Index (RSI) Method: Case Studies', *Remote Sensing*, vol. 10, no. 12, p. 1871.

Zhang, Y, Wang, C, Wu, J, Qi, J & Salas, WA 2009, 'Mapping paddy rice with multitemporal ALOS/PALSAR imagery in southeast China', *International journal of remote sensing*, vol. 30, no. 23, pp. 6301-15.

Zhang, Y, Yan, W, Yang, B, Yang, T & Liu, X 2020, 'Estimation of rice yield from a C-band radar remote sensing image by integrating a physical scattering model and an optimization algorithm', *Precision Agriculture*, vol. 21, no. 2, pp. 245-63.

Zhou, Y, Xiao, X, Qin, Y, Dong, J, Zhang, G, Kou, W, Jin, C, Wang, J & Li, X 2016, 'Mapping paddy rice planting area in rice-wetland coexistent areas through analysis of Landsat 8 OLI and MODIS images', *International Journal of Applied Earth Observation and Geoinformation*, vol. 46, pp. 1-12.

Zhu, Z, Wang, S & Woodcock, CE 2015, 'Improvement and expansion of the Fmask algorithm: Cloud, cloud shadow, and snow detection for Landsats 4–7, 8, and Sentinel 2 images', *Remote Sensing of Environment*, vol. 159, pp. 269-77.

Zhu, Z & Woodcock, CE 2012, 'Object-based cloud and cloud shadow detection in Landsat imagery', *Remote Sensing of Environment*, vol. 118, pp. 83-94.